Math and the Fountain of Youth

by

Mehrshad Sadria

A thesis
presented to the University of Waterloo
in fulfillment of the
thesis requirement for the degree of
Master of Mathematics
in
Applied Mathematics

Waterloo, Ontario, Canada, 2020

AUTHOR'S DECLARATION

I hereby declare that I am the sole author of this thesis. This is a true copy of the thesis, including any required final revisions, as accepted by my examiners.

I understand that my thesis may be made electronically available to the public.

Abstract

Ageing is associated with impairments in a number of regulatory processes, including in energy dysregulation that affects multiple metabolic pathways and in the circadian rhythms. In the management of metabolic stress and ageing mechanisms, key proteins such as mTORC, AMPK, and sirtuins are known to play an essential role. An impairment in these mechanisms is commonly associated with cellular ageing and degenerative diseases. To understand the complex interactions of ageing-related signalling pathways and environmental signals, and the impacts on lifespan and health-span, we developed a computational model of metabolic signalling pathways. The model includes (i) the insulin/IGF-1 pathway, which couples energy and nutrient abundance to the execution of cell growth and division, (ii) mTORC1 and amino acid sensors, (iii) the Preiss-Handler and salvage pathways, which regulate the metabolism of NAD+ and the NAD+-consuming factor SIRT1, (iv) the energy sensor AMPK, and (v) transcription factors FOXO and PGC-1α. The model can be used as an essential component to simulate gene manipulation, therapies (e.g., rapamycin and wortmannin), calorie restrictions, and chronic stress, and to assess their functional implications on longevity and ageing-related diseases.

Another goal of this research project is to unravel the complex interactions among ageing, metabolism, and the circadian clock. We seek to identify key factors that inform the liver circadian clock of cellular energy status, and to reveal the mechanisms by which variations in food intake may disrupt the clock. To address these questions, we develop a comprehensive mathematical model that represents the circadian pathway in the mouse liver, together with the insulin/IGF-1 pathway, mTORC1, AMPK, NAD+ and the NAD+-consuming factor SIRT1. The model is age-specific and can simulate the liver of a young mouse or an aged mouse. Simulation results suggest that the reduced NAD+ and SIRT1 bioavailability may explain the shortened circadian period in aged rodents. Importantly, the model identifies the dosing schedules for maximizing the efficacy of some anti-ageing medications.

Acknowledgment

I would like to express my sincere gratitude to my advisor Prof. Anita Layton for her continuous support of my Master's study and research. In particular, for allowing me to grow as an independent research scientist and giving me the opportunity to work on a topic outside of her research expertise. Her guidance helped me in all the time of research and writing of this thesis and it was impossible to finish it without her guidance. Like many people around the world, I lost my beloved grandparents because of covid-19. I want to thank Prof. Layton for supporting me not only as a great supervisor but also as a good friend.

I am also grateful for the financial support provided by University of Waterloo, the Applied Mathematics Department and Prof. Layton, which allowed me to attend a number of national and international conferences and present my work.

Finally, I would like to thank my family, especially my mom for being my best friend. She has been an everlasting source of encouragement and support. I could not have reached this point without her.

Dedication

I dedicate my thesis to my beloved grandparents

who sadly passed away in October 2020 because of Covid-19.

Table of Contents

List of Figures

List of Tables

Chapter 1

Background

1.1 Motivation

Recent medical advances have dramatically increased life expectancy. By 2050 the world's population aged 60 years and older is expected to total 2 billion, up from 900 million in 2015 (45). However, the prevalence of age-related diseases such as cancer, diabetes, and neurodegenerative and cardiovascular diseases has risen accordingly. Ageing is a multifactorial process characterized by a gradual decline of physiological functions. A series of mechanisms are involved at the molecular, cellular, and tissue levels, which include deregulated autophagy, mitochondrial dysfunction, telomere shortening, oxidative stress, systemic inflammation, and metabolism dysfunction (149). The dysregulation of these pathways gives rise to cellular senescence, which contributes to ageing phenotype and, eventually, age-related diseases. However, despite intense research, the molecular basis of the ageing processes has remained incompletely understood. The principal goal of this thesis is to utilize mathematical modeling and computer simulations to unravel biological processes that contribute to or affected by ageing and ways to stop this process which is not generally classified as a disease.

1.2 Ageing over time

Achieving immortality or at least increasing lifespan has been one of the greatest challenges facing mankind. One can even say the ultimate dream of humankind. This endeavor appears in different forms in many cultures and religions. While the symbols or the stories may be different, they all share a common theme: Immortality. For example, one of the fundamental and common mythemes in many religions or philosophical traditions is the Tree of Life. This tree has been known as a connection between the ephemeral life in earth and the source of life. Also, it symbolizes wisdom, strength and beauty (117). Various trees of life have been mentioned over time. In the Persian empire, Iranians believed in sacred plants related to perpetuity and life. They believed that a tree called Homa was planted by god and possessed miraculous curative powers and bestowed the gift of immortality (71). In Chinese mythology, a Tree of Life is depicted with a phoenix and a dragon; the dragon often represents immortality and every three thousand years the tree produces a fruit which grants immortality to the one who eats it. This concept can be found in different religions too. In Islam, there is a tree in Eden called tree of immortality which doesn't decay. It is represented in many artistic paintings or carpets (Quran 14:24). The book of Genesis and the book of Revelation address the Tree of Life too; the tree is considered a reward for those who obey the commandments

(Revelation 2:7). In the book of Proverbs, the Tree of Life is associated with wisdom and calmness (Proverbs 3:13-18). In art, the effect of life can be seen in many paintings or movies. For instance, this famous tree can be seen in 17th centuries paintings of Iranian artists and in the famous symbolic work of Gustav Klimt in 1909. Beside art works, many movies have been made about immortality. In 2006, Darren Arnofsky produced The Fountain, which tells a story of a researcher who seeks for a cure for his dying wife. In 2009, Alex Proyas directed Knowing, about two young protagonists whose search is toward the Tree of Life.

Historically, ageing has been thought to be an inevitable process: unless one dies young, one would gradually weaken over the years, suffer from more and more age-related diseases, and eventually die. However, the distinction between an inevitable process and a (preventable) disease often evolves over time. New scientific and technological developments may lead to a reconsideration of these classification and switching between those two groups. For example, osteoporosis wasn't classified as a disease until 1994 by the World Health Organization (90). Recently, scientists have started challenging some popular beliefs regarding ageing. Should ageing be considered a disease? If so, perhaps efforts can be invested to combat this "disease". For the past 25 years scientists have sought to answer this question by conducting experiments in different model organisms such as yeast, flies, rodents, fish and etc. (8). Some of these efforts were successful and it was shown that life span can be increased by tenfold in C. elegans and by 60% in killifish (177). These results support the idea that ageing should be considered a disease, a concept that has the benefit of potentially increasing funding for ageing research studies (29). However, thus far methods which lead to longevity are limited to the following: calorie restriction, mimic drugs, gene manipulation, senolytics, stem cells therapy and heterochronic parabiosis (14, 82, 193).

1.3 Ageing and metabolism

The challenges in fully elucidating and, eventually, combating the ageing process may be attributed, in part, to the multitude of molecular and cellular processes involved. In particular, the insulin/IGF-1 (Insulin-like Growth Factor 1) signaling pathway are known to regulate lifespan, and is coupled to the mammalian target of rapamycin (mTOR) pathway. mTOR is a highly conserved serine/threonine protein kinase that controls cell growth, cell proliferation, cell motility, cell survival, protein and lipid synthesis, glucose metabolism, mitochondrial function and transcription in response to nutrient and hormonal signals. It is a catalytic subunit of two distinct complexes known as mTORC1 and mTORC2. mTORC2 consists of mTOR, Rictor (Avo3 homolog) and mLST8, whereas mTORC1 consists of mTOR, Raptor

and mLST8 (also known as GβL (197)). The two complexes have different functions. mTORC1 integrates information about nutritional abundance and environmental status to balance anabolism and catabolism in the cell, while mTORC2 focuses on cytoskeletal behavior and activates several pro-survival pathways, especially in caner.

mTORC1 controls cellular entry into an anabolic state that requires energy and macromolecules, which means its activation only occurs when amino acids, insulin/growth factors, ATP and oxygen are all available. In the presence of growth factors and insulin, Rheb is GTP loaded and act as a kinase activator of mTORC1, but only if mTORC1 is on the lysosomal surface. mTORC1 localization to the lysosomal surface in response to nutrient levels, specifically amino acids and glucose is controlled by the active Rag. Rag GTPases consist of a constitutive heterodimer of RagA or RagB bound to RagC or RagD (163). When there are enough nutrients, RagA/B is GTP loaded and RagC/D is GDP loaded. This active form of Rag GTPases promotes the translocation of mTORC1 to the lysosomal surface, where it may come into contact with its kinase activator, Rheb in the loaded form. mTORC2 is also regulated by growth factors and nutrient availability, and its activation affects insulin signalling pathways, especially AKT. It is not clear where mTORC2 activation occurs, however MAPK signalling pathway might recruit mTORC2 to the plasma membrane. This interaction between MAPK pathway and mTOR signalling plays a pivotal role in cancer which leads to hyperactivation of mTOR signalling up to 80% (116, 187) (Fig. 1).

mTORC1 protein synthesis process starts by phosphorylating the eukaryotic initiation factor 4E (eIF4E)-binding protein 1 (4E-BP1) and the ribosomal S6 kinase 1 (S6K1). The phosphorylation of 4E-BP1 inhibits its binding to eIF4E, enabling eIF4E to stimulate cap-dependent translation (148). In its unphosphorylated state, 4E-BP1 suppresses translation by binding and sequestering eukaryotic translation initiation factor 4E (eIF4E), an essential component of the eIF4F cap-binding complex but when mTORC1 is in its active form it remains at the mRNA 5′-cap, where it is well positioned to phosphorylate 4E-BP1 resulting in its dissociation from eIF4E and the recruitment of eIF4G to the 5′-cap, which allows cap-dependent translation process to continue (142).

Moreover, mTORC1 can suppress autophagy inside the cell through phosphorylation of ULK1 and ATG13, which are the major initiator of catabolism process inside the cell (73). mTORC1 phosphorylation of ULK1 and ATG13 blocks this process, causing the accumulation rather than the recycling of damaged proteins. mTORC1 inhibits autophagosome maturation and the conversion of endosomes into lysosomes, thereby acting as a check on both the early and late stages of autophagy (94).

During periods of starvation or energy stress, the mTORC1 molecular switch is turned off, restoring autophagosome initiation and permitting nuclear translocation of both the transcription factor

EB (TFEB) and the related transcription factor E3 (TFE3). Then, the new lysosomes break down proteins and release amino acids back to the cytoplasm to regenerate the pool of cellular amino acids, enabling reactivation of the mTORC1 pathway after starvation. This feedback between mTORC1 activation and autophagy by lysosome is essential in conditions including a number of tumors. Similar to mTORC1, mTORC2 affects cellular metabolism. It phosphorylates other AGC family kinases, including several classes of PKCs (79), the ion transport regulator serum- and glucocorticoid-induced protein kinase 1 (SGK1) and the Akt (158). This interconnection between AKT and mTORC2 is one of the main regulators of cellular metabolism in response to nutrient availability and growth. Within the signaling pathway, AKT is located at the nexus of mTORC1 and mTORC2, and can deactive TSC1_TSC2 inhibition of mTORC1. Moreover, AKT is one of the most frequently mutated signaling nodes in cancer cells. AKT also governs the activity of glycogen synthase kinase 3b (GSK3b) to suppress apoptosis and modulate glucose homeostasis (110). This suppression of apoptosis is done in another way by AKT. Activation of AKT disturbs the balance of cell survival and apoptosis by promoting pro-survival transcription factors and inhibiting the FOXO3a pro-apoptotic transcription factor (25). FOXO3a has a pivotal role in both oncogenesis and tumor suppression; thus, the inhibition of FOXO30a causes diseases and is known as a biomarker of oncogenesis (65).

Inhibition of this nutrient response pathway extends lifespan in several model organisms and ameliorates age-related pathologies. The presence of nutrients and growth factors increases mTORC1 activity and reduces autophagy initiation, whereas the caloric restriction or inactivation of mTORC1 increases autophagy contributing to cellular longevity. Insulin/IGF-1 activates mTORC1 by AKT (also known as protein kinase B), while mTORC1 inhibits insulin/IGF-1 through S6K by inhibiting insulin receptor substrate (IRS). mTORC1 is also regulated by a multitude of amino acid sensors, including the sestrin family, the CASTOR family, and the lysosomal amino acid transporter SLC38A9.

Also important in the ageing process is the sirtuin family, which consists of highly conserved protein deacetylases found nearly in all organisms studied. In mammals, seven silent information regulator (SIRT) proteins (SIRT1-7) exist, with SIRT1 being the most extensively studied in the context of ageing and is known as one of the main mediators in calorie restriction. SIRT1 senses changes in intracellular nicotinamide adenine dinucleotide (NAD+) levels, which reflect energy level, and uses this information to adapt the cellular energy output. SIRT1 also enhances DNA repair, cell survival, mitochondrial function and reduces ageing inflammatory/immune responses (34).

Connecting the sirtuin family to the mTOR pathway is AMPK, a key regulator in energy balance in the cells. During periods of cellular energy stress or changes in the ratio between ATP to AMP, AMPK is activated and it phosphorylates a number of proteins in various pathways to return the cell to the stable condition by favoring catabolism and suppressing anabolism by autophagy. Also, AMPK promotes mitochondrial health by promoting mitochondrial fission and biogenesis. One of the mechanisms known to reduce cancer growth rate is through AMPK. Its direct phosphorylation of the tumour suppressor TSC2 and the mTORC1 subunit Raptor blocks mTORC1 from phosphorylating its substrates, thereby preventing tumor growth. Furthermore, AMPK has received much attention as a potential target for treating metabolic diseases e.g., diabetes. Metformin, a widely used drug for treatment of type 2 diabetes, activates AMPK and leads to induction of the expression of glucose transporters (GLUT4), mimicking the effects of extensive exercise training. Metformin increases AMPK phosphorylation of acetyl-CoA carboxylases, which contributes to changes in lipid synthesis and appears to have a direct impact on insulin sensitivity and glucose absorption (205). Additionally, studies on model organisms have revealed that mammalian AMPK plays a crucial role in the regulation of lifespan (156). Overexpression of AMPK by metformin may extend lifespan in some species, e.g., C. elegans and Drosophila (56). Other studies have revealed that the decline in AMPK activation and sensitivity during ageing (147) can activate mTORC1 and lead to chronic tissue inflammation.

In the past decade, high-throughput genomic and proteomic technologies have generated a wealth of data in ageing. Despite the increasing availability of data, some of the molecular mechanisms that mediate key ageing effects have yet to be elucidated. The difficulty lies in the complexity of ageing: Not only are a large number of genes involved in the ageing process, many with competing roles, but their interactions are complex and often incompletely characterized. Indeed, due to the multiple feedback loops and regulatory mechanisms, a main challenge in interpreting gene-expression data is to understand the biological consequences of gene-expression changes. A promising methodology for interpreting data and untangling the interactions among signaling pathways is computational biology. One such approach is to describe regulatory interactions using ordinary differential equations (ODEs), which relate changes in the expressions of model variables to other quantities. The insulin/IGF-1 pathway has been the subject of modeling and analysis by a series of previous studies (3, 4, 39, 40, 101, 132, 133, 166). For instance, omics technologies have been applied to investigate the mTOR network (164) and ribosome profiling has been used to produce a map of the mTOR targets, which are translationally regulated in different diseases (76). Also, In cancer biology and oncology, mathematical models are used to uncover the progression of oncogenesis in time and space. That information may be used to identify personalized and precision

therapeutics (151). A variety of mathematical methods have been used to model the mTOR signalling pathway, including fuzzy logic, ODE, PDEs, and Boolean techniques (15, 170). A Boolean model uses 0 or 1, respectively, to represent active and inactive forms in biological pathways (182). A fuzzy logic model, which considers a range of activity values from 0 to 1, was built by Kriete et al. to study the interconnection between mTORC1, ROS and NF-KB in ageing (99). Borisov and colleague showed the connection between MAPK and mTOR the two main Signalling pathways in cell growth using ODEs (19). In 2016 a mathematical model was proposed by de Pezze and co-workers to investigate the connection between AMPK and mTOR signalling pathways (40).

Unlike the insulin/IGF-1 and mTOR pathways, theoretical effort in modeling the arguably equally important regulators NAD+ and SIRT1 is much more limited (an exception is (16)). Thus, in Chapter 2 we develop a state-of-the-art computational model that couples these and other critical signaling pathways in growth, ageing, metabolism, and disease in mammals. In Chapter 3, we conduct model simulations and analyze the interactions among key players in ageing and metabolism: mTORC, AMPK, and SIRT1. A dynamic model of mTOR was proposed to find better therapeutic ways for inhibiting mTOR by considering mTOR signaling interaction with Akt.

1.4 Circadian rhythms and metabolism

From bacteria to humans, organisms possess a network of molecular reactions and pathways, the interactions of which form an internal biological clock, known as a circadian clock, which generates biochemical oscillations with a near 24-hour period (46). The mammalian circadian system can be divided into two interacting components: the central clock in the suprachiasmatic nucleus (SCN) of the hypothalamus and the peripheral clocks that reside in various tissues throughout the body. The peripheral clocks play an integral and unique role in each of their respective tissues, driving the circadian expression of specific genes involved in a variety of physiological functions. As a whole, the circadian system drives daily oscillation in most physiological functions, including circulating hormones (48, 95), cardiac and circulatory function (119, 125), and core body temperature (145). The circadian clock can synchronize the timing of physiological processes with cyclic changes in the external environment (called “zeitgebers”), to the advantage of the organism. Light is a major zeitgeber, especially for the SCN; its importance is evinced by the ubiquitous presence of an anticipatory system linking physiology with the light/dark cycle in all species. Other key zeitgebers include temperature, food intake, and exercise. Feeding is a particularly potent zeitgeber for the peripheral circadian clocks such as the liver clock.

The control of the circadian clock over a variety of cellular and circulating metabolites and fuels is well documented. However, that link is more complex than the rhythm simply controlling metabolism. Indeed, studies have pointed to a cyclic relationship wherein the rhythm impacts metabolic activity and metabolism feeds back to impinge upon the rhythm(152). Perhaps the best test case to evaluate the link between metabolism and circadian rhythms is the liver, an organ that is critically involved in the primary food response. Cellular metabolism in the liver is markedly affected by changes in feeding status and therefore fluctuates as a function of the day/night cycle in rodents (89, 150). To complete the cycle of influence, restricted feeding is also known to significantly alter the circadian phase in the liver (42, 169). In fact, liver should be considered as one of the main factors in research related to circadian rhythmicity and metabolism. As it displays robust oscillations in circadian output genes as well as in genes related to the hepatic system (2) especially with metabolism and food intake. Although, SCN lesions generally perturb circadian rhythmicity in many organs such as the liver metabolites and strong transcriptional activators, such as the glucocorticoid receptor, can return about 60% of rhythmicity to gene expression made arrhythmic by SCN lesions (144).

Nowadays, there is a dramatic increase in metabolic disorders in a number of societies. This unfortunate phenomenon is observed even among children and adolescents due to high fat foods and sedentary life style. Not only can zeitgebers affect the circadian clock, they can also perturb our metabolism. For example, it has been shown that circadian disturbance, cardiovascular disease, increased body mass, and elevated plasma glucose and lipid levels all are common among nighttime shift workers (91, 178). Many metabolites that control food intake, including insulin, glucagon, some peptides, NAMPT, corticosterone, leptin, and ghrelin, etc. depend on energy status or oscillate in a mostly tissue-specific circadian manner. Therefore, our feeding and metabolism cycle are affected by the circadian clock. Early lesion studies identified the SCN's contribution to circadian rhythmicity in eating and drinking. As ablation of the SCN perturbs rhythmicity in both eating and drinking cycle in our body (179). SCN in the brain is not the only tissue that can perturb the metabolic cycle (137). Rhythmicity in gene expression within tissues is generally unique, in a cell dependent manner. Even the brain itself shows tissue-specific oscillations in gene expression, which can be independent of SCN rhythmicity(60). Desynchrony between SCN and tissues specific clock rhythm can cause various problems.

A concern with this internal and external desynchrony is that the levels of diseases like coronary artery diseases like coronary artery disease associated are rising among shift workers (47). To better understand the mechanism behind this desynchronization, experiments in rodents have been designed to

demonstrate the health difference between night shift workers and the control group. In one study, a wheel-running task was imposed on nocturnal rats either during their normal sleep or wake phase. Plasma glucose oscillation was lost in rodents that were awake during their sleep phase, and serum triglyceride (TAG) levels were reversed from those of control animals, with peaks occurring during the sleep phase (155). After a month of sleep-phase work, rats subjected to work during the sleep phase gained more weight than controls, supporting human studies that show a similar profile of adiposity and weight gain in shift workers.

Impairments in circadian rhythms in sleep and behaviors (98) are known to occur in ageing, although the underlying mechanisms are not well understood. Ageing is a multifactorial process characterized by a gradual decline of physiological functions. A series of mechanisms are involved at the molecular, cellular, and tissue levels, which include dysregulated autophagy, mitochondrial dysfunction, telomere shortening, oxidative stress, systemic inflammation, and metabolism dysfunction (149). Furthermore, ageing is associated with a reduction in the cellular concentration of nicotinamide adenine dinucleotide (NAD+), a critical coenzyme for enzymes that fuel reduction-oxidation, and with a decline in the expression of SIRT1, a member of the sirtuin family for which NAD+ is a co-substrate, at the transcriptional and translational levels. Additionally, ageing is associated with energy deregulation which affects many pathways such as pyruvate metabolism, the tricarboxylic acid cycle, and insulin.

The interactions among ageing, metabolism, and circadian clock are difficult to unravel. Despite the wealth of ageing-related data generated by high-throughput genomic and proteomic technologies, some of the molecular mechanisms in these systems have yet to be elucidated. The difficulty lies in the complexity of these processes. Previously, models have been developed in order to analyze this complex system of interactions inside the cell and try to answer questions related to the circadian clock in our body in different specious. These models range from minimal models that can just reproduce one behavior to detailed ones that can describe precise mechanisms. The Goodwin model is the first oscillatory model that describes the oscillation based on feedback loops from the clock mRNA to its protein and from the repressor to mRNA. This model can produce limit cycle oscillation or damped oscillation based on the parameters. Further, new detailed models appeared based on the fact that new pathways, proteins and genes related to circadian clock discovered. They use many types of models such as Michaelis-Menten equation, Hill function or protein sequestration (140). Since it has been shown that for the Goodwin model to produce a limit cycle oscillation the hill coefficient should be above 8 (61). So, it motivated many scientists to model this system with other methods (38, 207). In 2003 Goldbeter developed two

basic and extended models based on the interconnected negative and positive regulating feedbacks, including *Bmal1, Clock, Per* and *Cry* genes which one has 16 ODEs and the latter model has 19 ODEs. Both models showed the autonomous circadian oscillations of *Per* and *Bmal1* during the night in an antiphase manner. Forger and Peskin also proposed a model that contained detailed regulation model of the mammalian circadian clock (51). They fitted the model based on optimization methods to find a set of parameters for which the model can describe experimental data reported before well. Also, they developed another model which was based on stochastic modeling and they compared the behavior of deterministic models and the stochastic one (52). They showed in different case scenarios that the stochastic model and deterministic model can show different things. For example, one can oscillate while the other one doesn't predict that. There were efforts to reduce the size of the models without losing information. Cometa et al. paper can be named as one of these attempts (36). The model developed by Forger and Peskin got extended more by Kim and Forger (93) to explain and show more complicated processes in the circadian clock pathway. In 2016 Woller et al. built a mathematical model that contains metabolic sensors such as SIRT1, AMPK and circadian clock proteins and genes in liver.

In Chapter 4, we present such a model that couples the metabolism model (Chapter 2) to a model of core circadian clock genes. In Chapter 5, we conduct model simulations to predict how perturbation in one model parameter or variable (or a set of parameters and variables), can affect other variables and overall system behaviors.

Chapter 2

Mathematical Model of Metabolic Pathways

2.1 Introduction

In this chapter we present a comprehensive model that includes (i) the insulin/IGF-1 pathway, which couples energy and nutrient abundance to the execution of cell growth and division, (ii) mTORC1 and the amino acid (AA) sensors, (iii) the Preiss-Handler and salvage pathways, which regulate the metabolism of NAD+ and the NAD+-consuming factor SIRT1, (iv) the energy sensor adenosine monophosphate-activated protein kinase (AMPK), and (v) transcription factors forkhead box O (FOXO) and peroxisome proliferator-activated receptor gamma coactivator 1-α (PGC-1α), the overexpression or mutation of which affects lifespan. In the next chapter, we apply the model to investigate the synergy among regulators of nutrients, energy, metabolism, and autophagy, and to identify novel therapeutic targets. The model can be used to aid in the interpretation of genomic and proteomic data, and to provide an integrated understanding of the mechanisms that lead the cell to senescence and how this process contributes to metabolic disorders and age-related diseases.

2.2 Model description

Main model components include the insulin/IGF-1 or mTOR signaling pathway (103), the Preiss-Handler and salvage pathways (43), energy sensor AMPK, and transcription factor FOXO and PGC-1α, in the mouse C2C12 cell. The dynamics of the signaling pathways is modeled as a system of ODEs; Figs. 1 and A1 depict the pathways and protein interactions. The reactions and associated parameters are presented in Table S1 and the Excel file. Model parameters are taken from published studies which were able to capture the biochemical interaction rates (16, 40, 192) and fitted to experimental data (39, 109, 135, 165, 192) using the interior point optimization method in fmincon() in MATLAB, with parameter ranges set to physiologically realistic values.

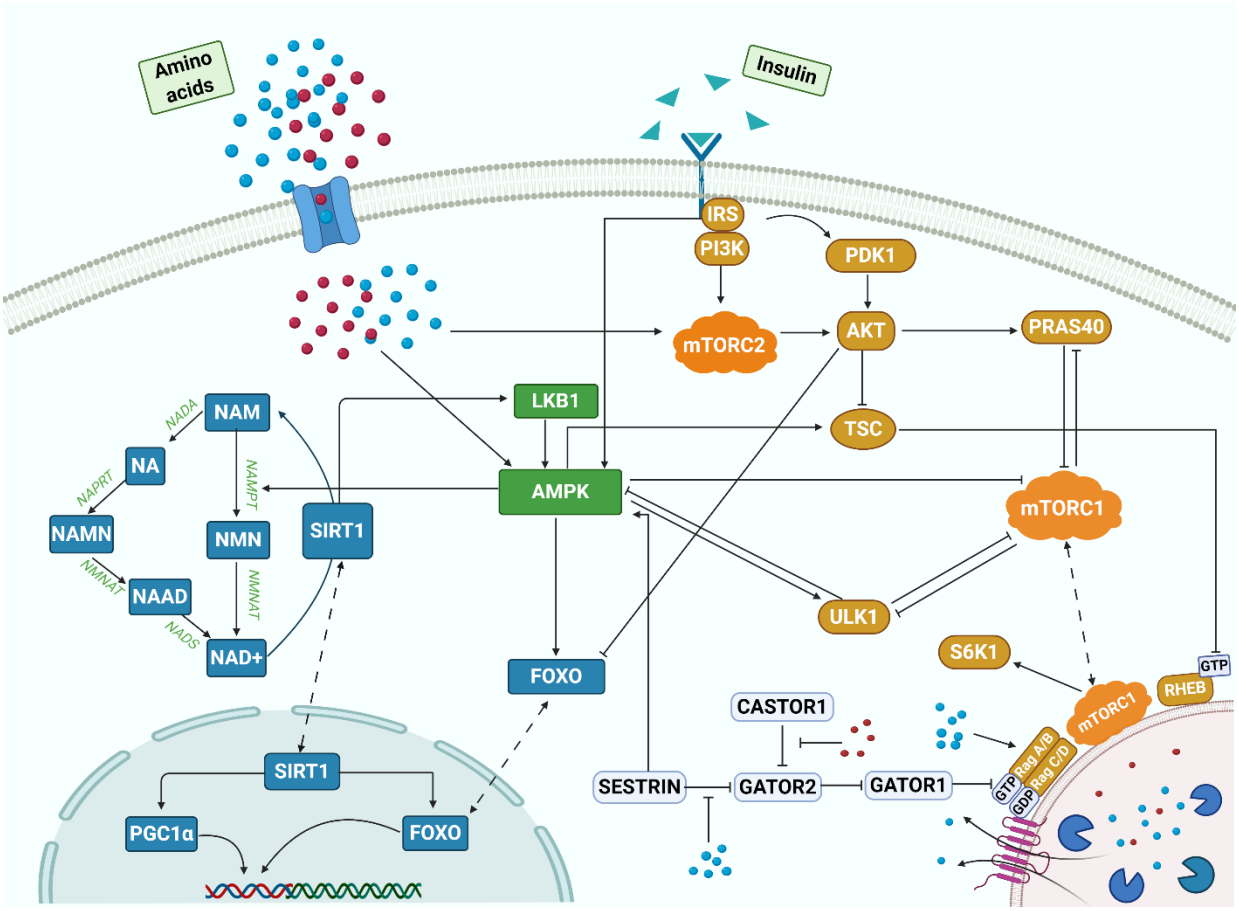

Figure 1. Pathway representation of network model, some components of which may be activated by amino acids, such as leucine (blue circles) and arginine (red circles), and insulin (green triangles0. The model represents three distinct areas in the cell: the cytoplasm, lysosome, and the nucleus.

Within the insulin/IGF-1 signaling and mTOR pathways, insulin activates the insulin receptor (IR), which triggers the IRS and PI3K, resulting in the phosphorylation of PDK1 and mTORC2, respectively. mTORC2 phosphorylates AKT on the S473 and T308 residues, whereas PDK1 activates AKT. Active AKT phosphorylates a variety of proteins, including FOXOs, TSC1_TSC2 and PRAS40. Phosphorylation of TSC1_TSC2 by AKT inactivates the TSC complex, thereby activating mTORC1 and resulting in a number of downstream effects. These include (i) inhibition of ULK1 by phosphorylating ULK1 on Ser 757; the ULK1 complex is a key contributor to the initiation of autophagy; (ii) phosphorylation of PRAS40, which attenuates the inhibition of mTORC1; (iii) phosphorylation of p70S6K on T229 and T389, which initiates a negative feedback loop via IRS.

An important novel aspect of our model is the explicit representation of the role of sestrin2 and leucine in the regulation of mTORC1. Sestrin2 deactivates mTORC1, via its effects on protein complexes GATOR1 and GATOR2. GATOR1 inhibits mTORC1, whereas GATOR2 inhibits GATOR1. Sestrin2 inhibits GATOR2, enhancing the activation of GATOR1, and eventually suppressing mTORC1. This process is modulated by leucine, which binds to sestrin2 and impeding its inhibitory effect on mTORC1 (187). Thus, mTORC1 activation depends, among other factors, on the concentration of sestrin2 and leucine. To illustrate that dependence, we consider the mTORC1 activation rate:

$$\frac{d}{dt}[\text{mTORC1\_pS2448}] = -k_{\text{TSC}}[\text{mTORC1\_pS2448}]([\text{TSC1\_TSC2}] + [\text{TSC1\_TSC2\_pS1387}]) + k_{\text{AA}}[\text{mTORC1}_{tot}][\text{AA}]\left(\frac{V_{\max}([\text{L}] + c_{\text{LS}})}{[\text{S}] + [\text{L}] + c_{\text{LS}}}\right) - f_1([\text{PRAS40}]) - f_2([\text{Act ULK1}]) \quad (1)$$

where [AA], [L], and [S] denote the amino acid, leucine, and sestrin2 concentrations, respectively; and $\text{mTORC1}_{\text{tot}}$ denotes total mTORC1. Act ULK1 denotes the activated form of ULK1. The first term on the right describes the inhibition of mTORC1 by the TSC1_TSC2 complexes; the second term describes the effects of leucine and sestrin2 on mTORC1; the third and fourth terms describe the contributions from PRAS40 and activated ULK1. respectively. The expression for f_1 and f_2 can be found in the Appendix.

The model simulates the dynamics of another key player in metabolism, NAD+, which is produced through the *de novo*, Preiss-Handler and salvage pathways. The major source of NAD+ in mammals is the salvage pathway, which recycles NAM produced by enzymes utilizing NAD+. The first step in the salvage pathway involves the rate-limiting enzyme NAMPT, which facilitates the conversion of NAM to NMN and whose activity is increased by AMPK, and the expression and/or activity of which when reduced is associated with ageing and poor health. (81) The second step converts NMN to NAD+ via the NMNAT enzymatic reaction. NAD+ thus produced activates substrates including SIRT1 and is consumed in the process. Albeit less important for NAD+ biosynthesis in mammals, the Preiss-Handler pathway is also represented. The pathway begins with the conversion of NAM to NA, followed by the conversion to NAMN, catalyzed respectively by NADA and NAPRT. Like the salvage pathway, NMNAT in Preiss-Handler pathway also catalyzes the process of production of NAAD from NAMN. Finally, the reamidation of NAAD by NADS yields NAD+. The Preiss-Handler pathway is more energy and ATP consuming than the salvage pathway.

Connecting the mTORC1 and NAD+ pathways is AMPK, a master regulator of cellular energy that is activated under starvation or hypoxia. AMPK can be stimulated by sestrin, IRS, and liver kinase B1 (LKB1) which deacetylated by SIRT1. Activated AMPK promotes autophagy by directly phosphorylating and activating ULK1. As such, there is a competition between mTORC1 and AMPK to phosphorylate different residues of ULK1 to decide cells fate. ULK1 in turn inhibits AMPK and mTORC1 in a negative feedback loop, whereas leucine activates them.

Therapeutic treatments and dietary conditions are simulated by changing selected model parameters (see below). For a given set of parameters, a steady-state solution can be computed by integrated the model equations for a sufficiently long time. For simulations that involve a change in model parameters, model variables are initialized to the steady-state solution corresponding to the parameter values at the initial time. Such initial conditions are realistic and avoid an abrupt change in solution at the initial time.

Chapter 3

Interactions among mTORC, AMPK, and SIRT: A Computational Model for Cell Energy Balance and Metabolism

3.1 Introduction

In Chapter 2 we describe a state-of-the-art computational model for investigating signaling pathways in growth, ageing, metabolism, and disease in mammals. Major model components include the insulin/IGF-1 or mTOR signaling pathway (103), the Preiss-Handler and salvage pathways (43), energy sensor AMPK, and transcription factors FOXO and PGC-1α. The mTOR signaling pathway couples energy and nutrient abundance to the execution of cell growth and division, whereas the Preiss-Handler and salvage pathways regulate the metabolism of NAD+ as well as NAD+-consuming proteins such as sirtuins.

In this chapter, we conduct model simulations to (1) compare different means of pharmacologically suppressing mTORC1, often done to control tumor growth, (2) interrogate the interplay between amino acid leucine and its sensor, sestrin2, and the effect on mTORC1 activity, (3) analyze the interactions between arginine and leucine during protein deprivation, which predicts a signal that reactivates mTORC1 and downregulates autophagy, and (4) examine the pharmacological activation of SIRT1 and its regulation of autophagy.

3.2 Pharmacological suppression of mTORC1.

Given the role of mTORC1 in metabolic diseases, there is great interest in developing drugs to suppress this enzyme. Rapamycin, a potent and selective inhibitor of mTORC1, has emerged as an FDA-approved immunosuppressant and anti-cancer agent. We conduct simulations to investigate the molecular mechanisms underlying the effects of rapamycin and its interactions with other mTORC1 inhibitors (87).

How do nutritional levels affect the actions of mTORC1 inhibitors? Because hyperactivation of mTORC1 disrupts cellular homeostasis, mTORC1 is regulated by a number of mechanisms, some of which are included in the present model. Both TSC1_TSC2 and its S1387-phosphorylated form deactivate mTORC1, as does the (dephosphorylated) proline-rich AKT substrate of 40 kDa (PRAS40). Compared to TSC1_TSC2, the regulation by PRAS40 of mTORC1 is less well studied; in fact, PRAS40's

effect on mTORC1 was not represented in a recent detailed mTORC pathway model (40). Located at the crossroad of the insulin/IGF-1 pathway, PRAS40 is phosphorylated by growth factors or other stimuli, and in turn regulates the activation of these signaling pathways. PRAS40 plays an important role in metabolic disorders and multiple cancers, and is known to be an insulin-regulated inhibitor of mTORC1 (157). To assess how that regulation is altered by nutritional levels and pharmacological interventions, we develop the first metabolism model that includes the actions of PRAS40. In these simulations, the model is initialized at the fasting state with a low insulin level (10% of baseline level). At t = 40 min, insulin level is returned to baseline and maintained at that level.

The inhibitory effect of PRAS40 is contingent on the nutritional level. With sufficient insulin and no drug treatment (i.e., control; administration of rapamycin will be considered below), PRAS40 inhibition of mTORC1 has only a minor impact on mTORC1, lowering its steady-state phosphorylated level by 18% (compare Fig. 2a, left and right panels, black curves, t > 40 min). The effects of PRAS40 on other proteins are similarly minor (Figs. 3 and 4). In contrast, at low insulin level, PRAS40 inhibition of mTORC1 results in a substantially lower phosphorylated mTORC1 level (1.00 versus 3.94; compare Fig. 2a panels, black curves, t < 40 min). A lower insulin level decreases AKT_pT308_S473 (Fig. 3b) and thus phosphorylated mTORC1; both changes reduce the phosphorylation rate of PRAS40 (Fig. 2c). The resulting higher unphosphorylated PRAS40 level reduces mTORC1 phosphorylation rate. The predicted profiles are consistent with experimental data in (40), measured by the L_2 norm of the difference between data and predicted values.

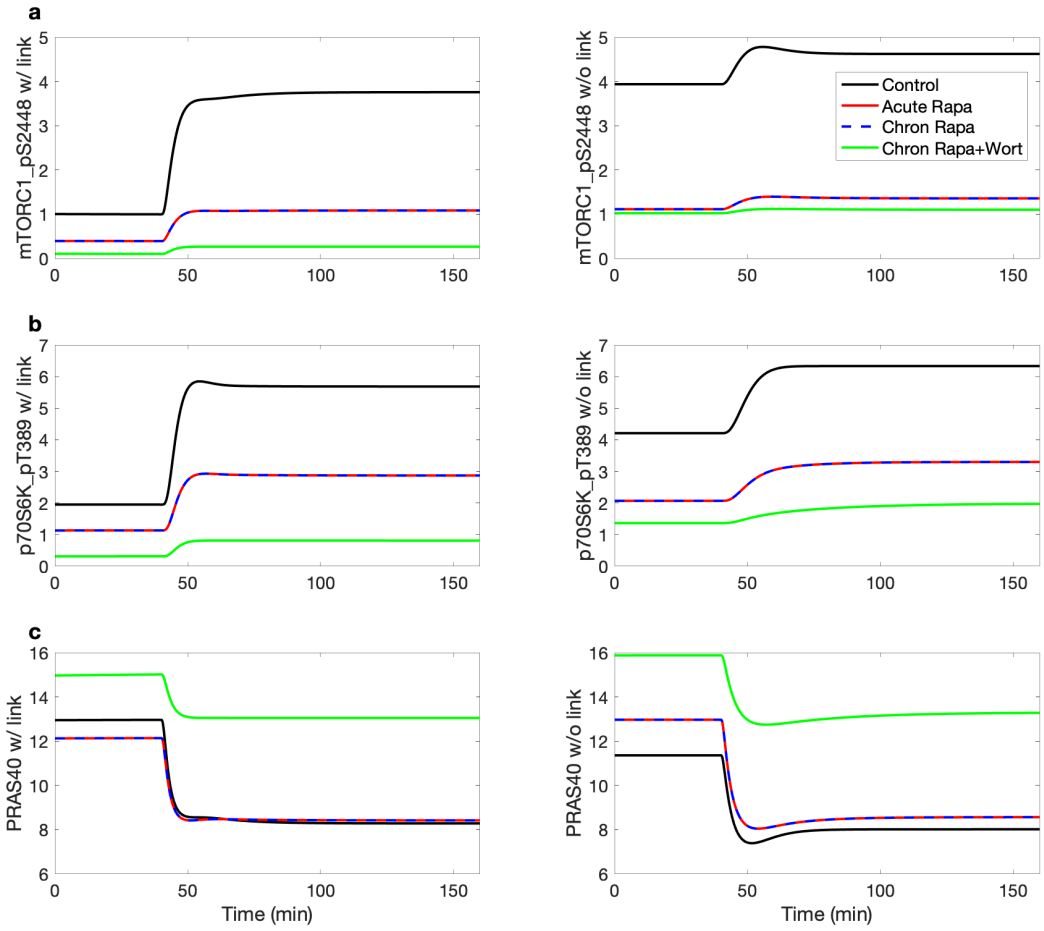

Figure 2. Effects of insulin, rapamycin, and wortmannin on key proteins and their interactions. Insulin was lowered to 10% of its baseline level for the initial 40 min of the simulation, and subsequently returned to baseline level. Simulations are conducted for control, acute and chronic administration of rapamycin, chronic administration of rapamycin with wortmannin. The inhibition of PRAS40 of mTORC1 is represented in the left panels but not the right ones. Model predicts that PRAS40 substantially lowers mTORC1 level under low insulin conditions. That effect is the most prominent under chronic administration of rapamycin and wortmannin.

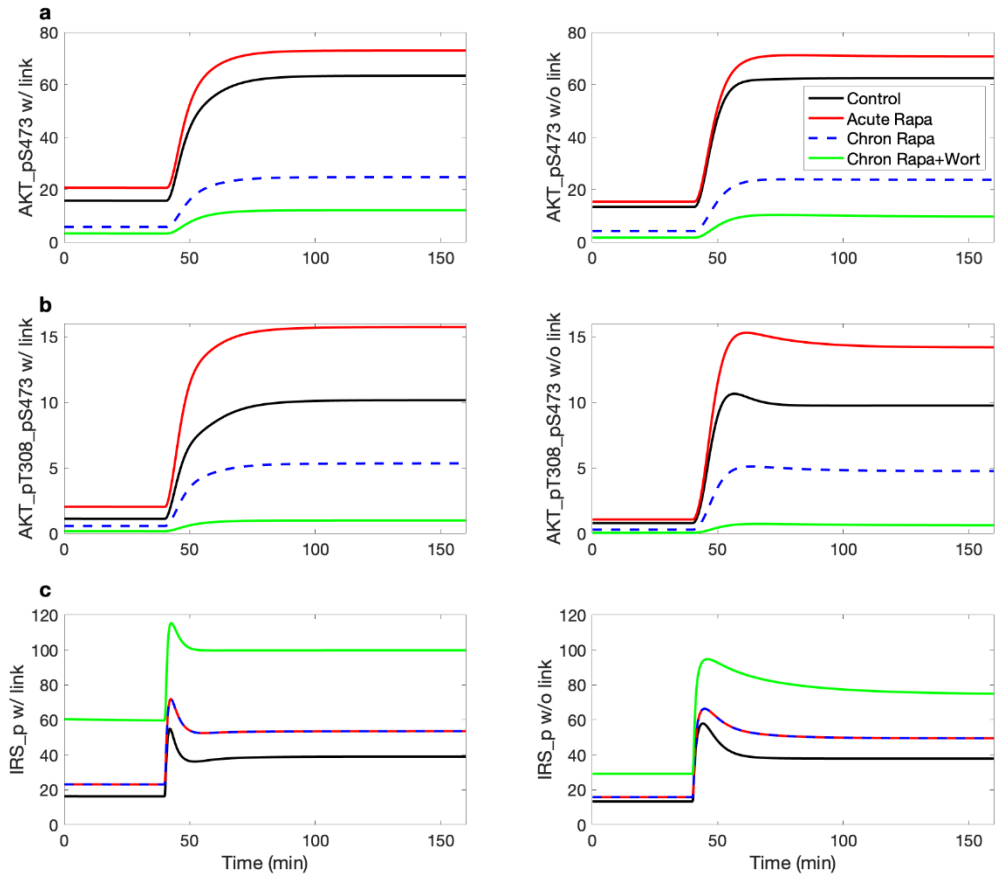

Figure 3. Effects of insulin, rapamycin, and wortmannin on key proteins and their interactions. Notations are analogous to Fig. 1.

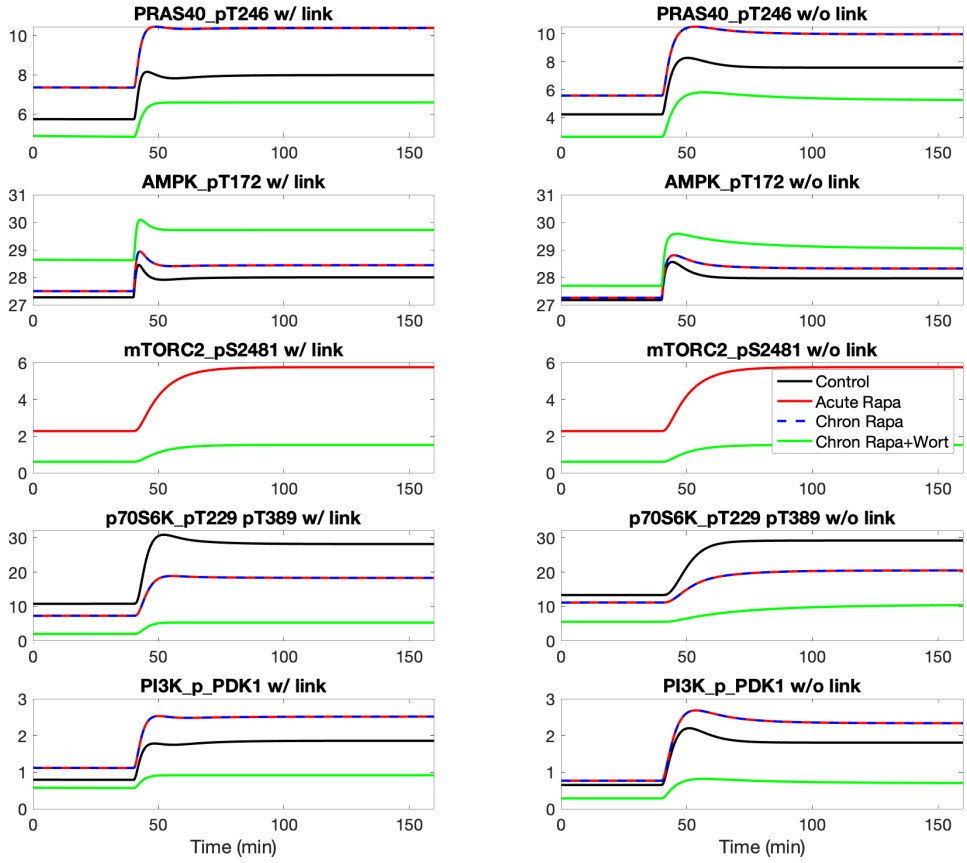

Figure 4. Effects of insulin, rapamycin, and wortmannin on key proteins and their interactions. Insulin was lowered to 10% of its baseline level for the initial 40 min of the simulation, and subsequently returned to baseline level. Simulations are conducted for control, acute and chronic administration of rapamycin, chronic administration of rapamycin with wortmannin. The inhibition of PRAS40 of mTORC1 is represented in the left panels but not the right ones. Model predicts that PRAS40 substantially lowers mTORC1 level under low insulin conditions. That effect is the most prominent under chronic administration of rapamycin and wortmannin.

What are the factors that affect the effectiveness of rapamycin, an mTORC1 inhibitor and anti-cancer agent? We consider both acute and chronic administration of rapamycin. Acute administration of rapamycin is simulated by decreasing total mTORC1 by 75% (162). With chronic rapamycin

administration, mTORC2 is targeted in addition to mTORC1 (102); thus, chronic administration is simulated by decreasing both mTORC1 and mTORC2 by 75%. We seek to answer the question: *Do rapamycin and PRAS40, both of which inhibit mTORC1, interact and produce nonlinear effects?* One might expect that together, rapamycin and PRAS40 may produce more than the sum of individual effects. This is because rapamycin lowers activated mTORC1 level and, as a result, decreases the phosphorylation of PRAS40 to PRAS40_pS183. Taken in isolation, that would increase dephosphorylated PRAS40 and further inactivate mTORC1. To assess the validity of that hypothesis, we simulate the administration of rapamycin with and without PRAS40 regulation. Model simulations predict that, following acute and chronic administration of rapamycin, mTORC1 level decreases by about 75% from its control level (Fig. 2(a,b)), which suggests limited super-additive effect arising from any interactions between rapamycin and PRAS40.

Why doesn't PRAS40 augment the inhibitory effect of rapamycin? As noted above, the lower phosphorylated mTORC1 level, taken in isolation, would increase dephosphorylated PRAS40. However, through a feedback mechanism, the lower phosphorylated mTORC1 level also decreases p70S6K_pT389, increases phosphorylated IRS and phosphorylated PI3K_PDK1, and eventually, increases AKT_pT308 and AKT_pT308_pS473, both of which increase the phosphorylation of PRAS40 to PRAS40_pT246. The competing effects on PRAS40 phosphorylation results in negligible change in unphosphorylated PRAS40 level.

Following chronic rapamycin administration, the lower phosphorylated mTORC2 level slows the phosphorylation of AKT to AKT_pS473, reducing both AKT_pS473 and the downstream AKT_pT308_pS473 (Fig. 3(a,b)). Taken in isolation, these effects, together with the reduced phosphorylated mTORC1, would slow the phosphorylation of PRAS40 and increase dephosphorylated PRAS40 level. But in a competing effect, the lower phosphorylated mTORC1 level increases AKT_pT308, which increases the phosphorylation of PRAS40 to PRAS40_pT246. These competing effects together yield negligible change in unphosphorylated PRAS40 level (Fig. 2c). Therefore, acute or chronic administration of rapamycin alone does not significantly alter PRAS40 levels.

How can we augment the inhibition of mTORC1 by rapamycin, especially at high insulin level? We hypothesize that this be achieved by pharmacological manipulations that elevate PRAS40. To identify an effective compound, we note that in addition to mTORC1, PRAS40 is also phosphorylated by AKT.

This motivates us to consider inhibitors of PI3K_PDK1, which phosphorylate and activates AKT. We simulate such an inhibitor, wortmannin, by lowering total PI3K_PDK1 by 80% (26).

A noticeable effect can be observed in PRAS40 when wortmannin is combined with chronic rapamycin administration. The lower phosphorylated PI3K_PDK1 level decreases AKT_pT308 and AKT_pT308_pS473, slowing the phosphorylation of PRAS40 to PRAS40_pT246. Together with reduced phosphorylated mTORC1, this maneuver substantially increases unphosphorylated PRAS40 at baseline insulin by 55% (Fig. 2c, left). The elevated PRAS40 substantially suppresses mTORC1_pS2448 (Fig. 2a, left). Analogous effects are also obtained for MK-2206, an allosteric inhibitor of AKT.

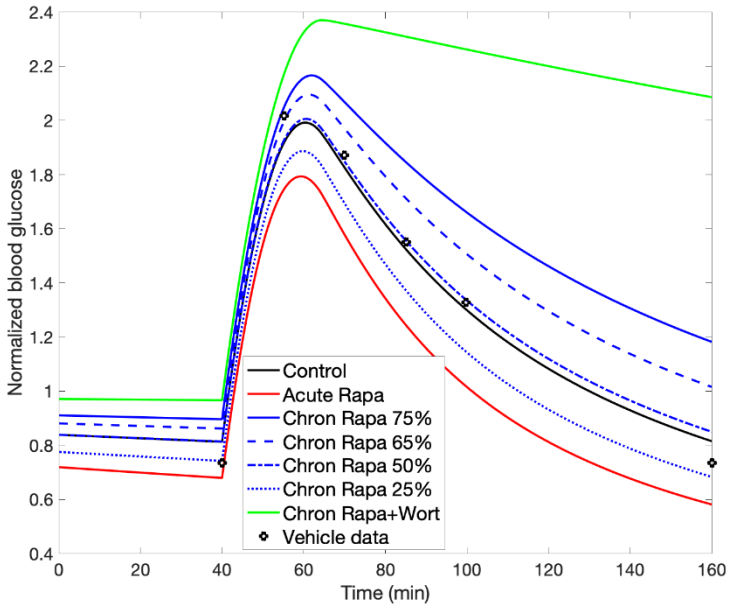

Figure 5. Effect of rapamycin on glucose tolerance. Glucose tolerance test begins at t = 40 min. Normalized plasma glucose profiles are obtained for acute rapamycin administration, and for chronic rapamycin administration at different dosages, with and without wortmannin. Vehicle data from (5).

Optimizing rapamycin dosage to maintain insulin sensitivity while preserving mTORC1 inhibition. Whereas acute treatment with rapamycin prevents nutrient-induced insulin resistance, the chronic administration of rapamycin may lead to glucose intolerance. This adverse side-effect is attributable to the inhibition of mTORC2 by chronic rapamycin treatment, resulting in the attenuation of

AKT_pT308_pS473, which is essential in the translocation of GLUT4 (53, 74). In the next set of simulations, we explore the possibility that an optimal rapamycin dosage may be determined that attenuates its detrimental effect on insulin sensitivity while preserving its inhibition of mTORC1. To accomplish that goal, we simulate the glucose tolerance test and track plasma glucose concentration by

$$\frac{d[G]}{dt} = k_{G,in} - k_{G,meta}\,[G][\text{AKT\_pT308\_pS472}] \quad (2)$$

The cellular uptake rate of plasma glucose is assumed to be proportional to the cellular concentration of AKT_pT308_pS472. As in the previous simulations, the model is initialized at the fasting state with a low insulin level, glucose = 1, and $k_{G,in}$ = 0 which represents the absence of glucose intake; additionally, $k_{G,meta}$ = 7×10^{-4}/min. At t = 40 min, the glucose tolerance test begins, whereby plasma glucose is elevated by setting $k_{G,in}$ to 0.115/min at t = 40 min then linearly decreases to 0 in the next 25 minutes. Additionally, insulin is proportional to plasma glucose.

We simulate the glucose tolerance test under four conditions: control, acute rapamycin administration, chronic rapamycin administration, and chronic rapamycin and wortmannin administration (parameters as described in previous simulations). For chronic rapamycin, we considered mTORC2 inhibition at 75% (baseline), but also at 65%, 50%, and 25%, with mTORC1 inhibition fixed at 75%.

The predicted plasma glucose time-course profiles are shown in Fig. 5, together with experiment data obtained for vehicle (5). Acute rapamycin usage inhibits mTORC1 (but not mTORC2), which suppresses p70S6K_pT389, increases phosphorylated IRS, AKT_pT308 and AKT_pT308_pS473, thereby improving insulin sensitivity. In contrast, chronic rapamycin usage inhibits mTORC2 as well. That lowers AKT_pS473 and AKT_pT308_pS473, and, at sufficiently high dosage (>50% mTORC2 inhibition), leads to impaired glucose tolerance. If wortmannin is added, AKT_pT308_pS473 is further suppressed, resulting in a sustained elevated plasma glucose level.

Findings in PC3 cells (prostate cancer cells) suggest that differing rapamycin dosages may yield near maximal mTORC1 inhibition with a range of mTORC2 inhibition levels (162). Model simulations suggest that lowering rapamycin-induced mTORC2 inhibition from 75% (baseline) to 50% restores insulin sensitivity to control level, consistent with intermittent administration of rapamycin (6, 102). If it is possible to further reduce mTORC2 inhibition to 25% while preserving mTORC1 inhibition at 75%,

one even achieves an improvement in insulin sensitivity, due to the beneficial effect of mTORC1 inhibition overriding the impairment arising from the (attenuated) mTORC2 inhibition.

3.3 Amino acid sensors and mTORC1 regulation.

As noted above, hyperactivation of the mTORC1 is implicated in the pathogenesis of cancer and other ageing-related diseases. mTORC1 promotes growth in response to the availability of nutrients, such as amino acids, which drive mTORC1 to the lysosomal surface, its site of activation. Among the twenty classical L-amino acids, arginine and leucine are two essential amino acids that potently stimulate the activity of mTORC1. However, aspects of the molecular mechanisms by which these specific amino acids stimulate mTORC1 activity remain to be completely understood. Thus, in a set of simulations, we examine the roles of these amino acid sensors in mTORC1 regulation.

We first investigate the regulation of mTORC1 by leucine and its sensor, sestrin2. Sestrin2 and leucine exert opposite effect on mTORC1, with sestrin2 deactivating mTORC1, and leucine increasing mTORC1 activity by binding to sestrin2. To investigate the dependence of mTORC1 activation level on leucine and sestrin2, we consider the steady-state formulation of Eq. 1 (by setting the time-derivative to zero) and solve for [mTORC1_pS2448]. We obtain

$$[\text{mTORC1\_pS2448}] = \frac{k_{\text{AA}}\text{mTORC1}_{\text{tot}}[\text{AA}]\left(\frac{V_{\max}([\text{L}]+c_{\text{LS}})}{[\text{S}]+[\text{L}]+c_{\text{LS}}}\right)}{k_{\text{TSC}}([\text{TSC1\_TSC2}]+[\text{TSC1\_TSC2\_pS1387}])+k_{\text{AA}}[\text{AA}]\frac{V_{\max}([\text{L}]+c_{\text{LS}})}{[\text{S}]+[\text{L}]+c_{\text{LS}}}-f_1([\text{PRAS40}])-f_2([\text{Act ULK1}])} \quad (3)$$

The regulation of mTORC1 activity by leucine and sestrin2 is shown in Fig. 6(a,b), by evaluating Eq. 3 for given AA and TSC1_TSC2 complex levels. Consider the system with a typical lysosomal leucine concentration. At a sufficiently low sestrin2 concentration, GATOR2 is activated, GATOR1 is inhibited, and mTORC1 activation rate is maximized. Conversely, at sufficiently high sestrin2 concentration, mTORC1 is rapidly dephosphorylated. Also, for a fixed sestrin2 concentration, increasing

the concentration of leucine raises the phosphorylation rate of mTORC1. Now for a typical sestrin2 concentration, Fig. 6a exhibits the Michaelis-Menten-like dependence of mTORC1 activity on leucine.

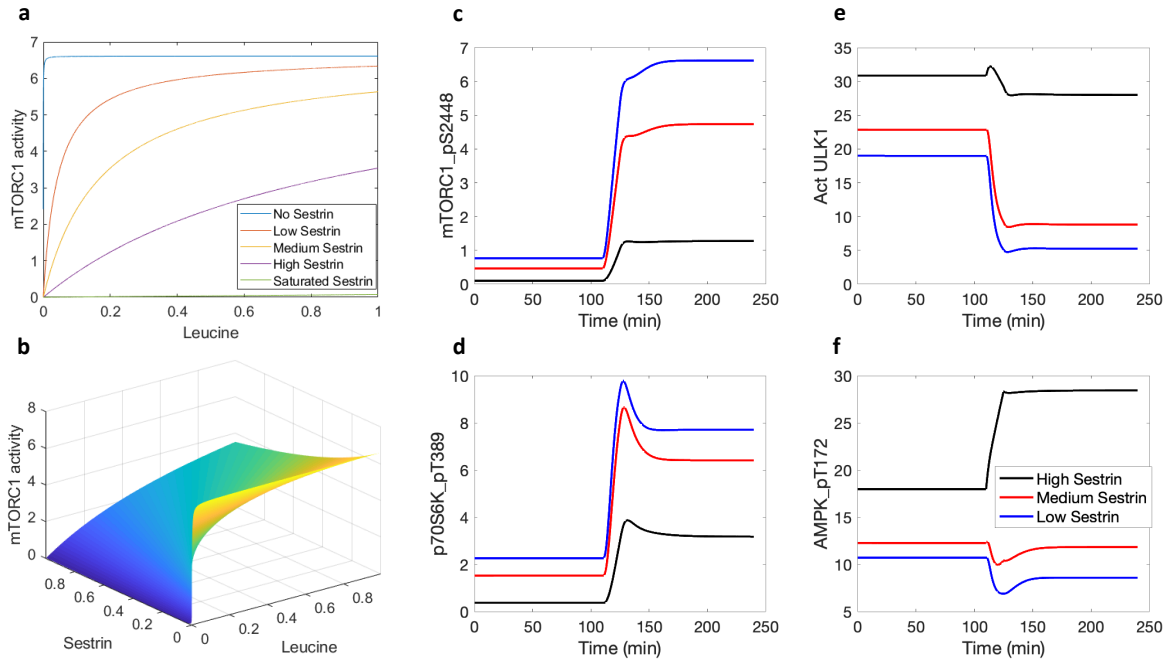

Figure 6. mTORC1 activity as a function of normalized leucine and sestrin concentrations, and model response to protein depletion and restoration. Panel *a*, mTORC1 activity for differing sestrin levels. Panel *b*, mTORC1 activity for the full range of leucine and sestrin concentrations. Predicted levels of mTORC1_pS2448 (*c*), p70S6K_pT389 (*d*), activated ULK1 (*e*), and AMPK_pT172 (*f*) under amino acid depletion (t < 2 h) and restoration (t > 2h), obtained for differing sestrin levels.

Sestrin has been found to induce autophagy during diverse environmental stresses that provoke mitochondrial dysfunction (111), through AMPK activation and mTORC1 inhibition. Specifically, after leucine binds to sestrin2, the resulting complex activates AMPK. Thus, the model assumes that AMPK phosphorylation rate is proportional to the concentration product [Leucine][Sestrin] (27). How does the interaction between sestrin2 and AAs affect the dynamics of AMPK activation, mTORC1 inhibition, and autophagy stimulation? To answer that question, we conduct simulations in which AA levels (including leucine) are initially set to 10% of baseline values, then subsequently increased to baseline levels. Simulations are conducted for high, medium, and low sestrin2 levels.

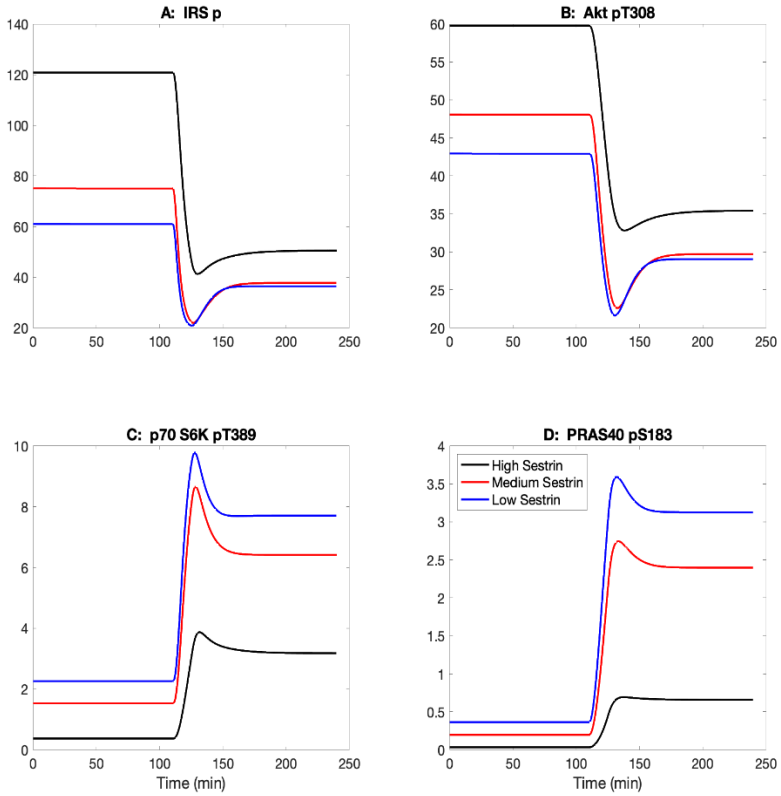

Figure 7. Effect of protein depletion and restoration on key model variables, obtained for differing sestrin2 levels.

Key model variables are exhibited in Figs. 6 and 7. Time profiles of mTORC1_S2448 and p70S6K_pT389 approximate that of AAs, whereas activated ULK1 exhibits the opposite trend. As sestrin2 concentration decreases, the activating effect of AAs on mTORC1 and p70S6K is enhanced (Fig. 6(c,d)), as is their inhibition of ULK1 and autophagy (Fig. 6e). AAs have competing effects on the phosphorylation of AMPK. Leucine and sestrin2 together activate AMPK directly. In addition, through mTORC1 and its inhibition of IRS_p, AAs inhibit AMPK. The model predicts that the latter (inhibition) dominates, resulting in the activation of AMPK when proteins are depleted, consistent with experimental observations (37). The inhibition of AMPK by AAs is modulated by sestrin2 (Fig. 6f). The model predicts that the latter (inhibition) dominates, resulting in the activation of AMPK when proteins are depleted; this result is consistent with experimental observations (37).

The next set of simulations, we focus on the modulation of mTORC1 by two major amino acid regulators, arginine and leucine. During AA starvation, lysosomal AAs (leucine in particular) facilitate mTORC1 activation. The transfer of lysosomal leucine to cytoplasm is mediated by SLC38A9, an arginine-regulated AA transporter (88). We first determine how that transfer process varies as a function of lysosomal amino acid content. Wyant et al. reported that arginine enhances the capacity of SLC38A9 to transport leucine, by increasing its V_{max} without significantly affecting its K_m (192). Taking both leucine and arginine into account, we model leucine transport rate, denoted $V_{max,L}$, as

$$V_{\max,\mathrm{L}} = V^{*}_{\max,\mathrm{L}}([A] + c_A)\left(\frac{[L]}{K_{M,L}+[L]}\right) \quad (4)$$

where c_A denotes the contribution of lysine, which also transports leucine albeit significantly less effectively than arginine. In the absence of either AA groups ([A] + c_A = 0 or [L] = 0), there is no leucine efflux. Under basal conditions, the concentration of lysine is sufficiently low that c_A is taken to 0. The resulting leucine efflux, determined for a range of lysosomal leucine and arginine concentrations (187), is shown in Fig. 8(a,b). The predicted leucine transport rate at basal and +200 μM arginine profiles are consistent with measurements reported by Wyant et al. (192) (Fig. 8a).

To assess the role of arginine in the regulation of mTORC1 and autophagy during AA depletion, we conducted simulations in which cytoplasmic AA progressively decreases during the first 3 hours; afterwards, lysosomal AAs are released (200). We simulate high, medium, low, and zero arginine levels by varying the rate at which cytoplasmic AA increases due to lysosomal leucine efflux. In the presence of insulin, AAs activate mTORC1, which inhibits autophagy by phosphorylating ULK1 (92). Upon AA depletion, mTORC1 activation on the lysosomal surface is no longer maintained (Fig. 8c). Consequently, ULK1 Ser757 is rapidly dephosphorylated (Fig. 8d) (92), resulting in activation of the ULK1 kinase and concomitant autophagy induction. A similar trend is observed for AMPK (Fig. 8e). 5e) (92), resulting in activation of the ULK1 kinase and concomitant autophagy induction. When cytoplasmic AAs are sufficiently depleted, leucine is transported out of the lysosome by arginine-stimulated SLC38A9, activating mTORC1, phosphorylating p70S6K and ULK1, and suppressing autophagy (Fig. 8(c,d)). Additional results can be found in Fig. 9. These results are consistent with reports by Yu et al. (200).

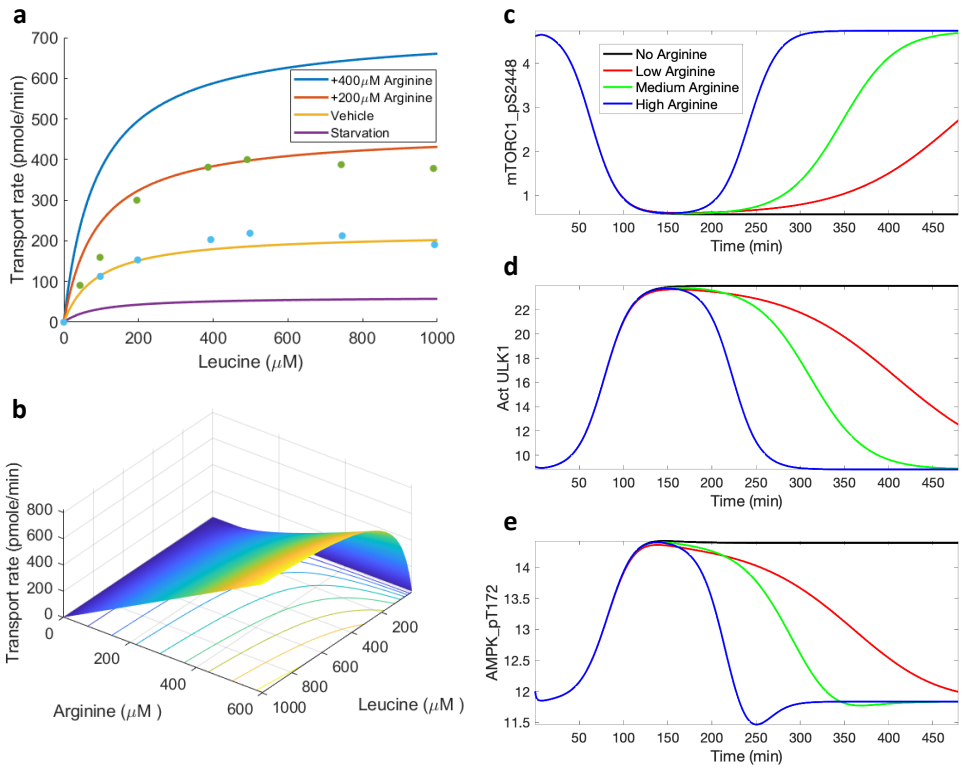

Figure 8. Leucine transport rate as a function of leucine and arginine concentrations, and its effect on mTORC1 reactivation. Panel *a*, leucine transport rate is computed with arginine concentration taken to be 50 μM ("Starvation"), 175 μM ("Vehicle"), 375 μM ("+200 μM Arginine"), 575 μM ("+400 μM Arginine"). Data taken from (192). Panel *b*, leucine transport rate shown for the full range of leucine and arginine concentrations. Predicted levels of mTORC1 pS2448 (*c*), activated ULK1 (*d*), and AMPK_pT172 (*e*) under amino acid depletion, obtained for differing arginine levels.

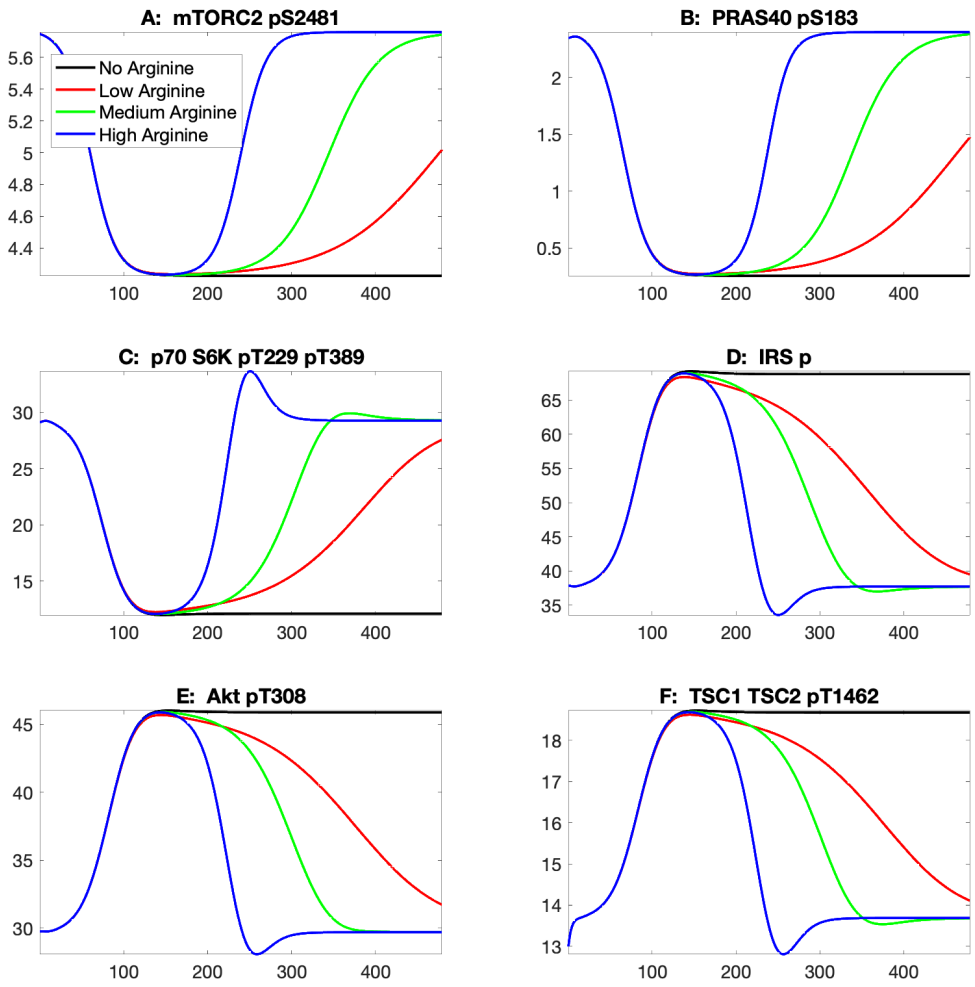

Figure 9. Effect of protein deprivation and subsequent leucine efflux on key model variables, obtained for differing arginine levels.

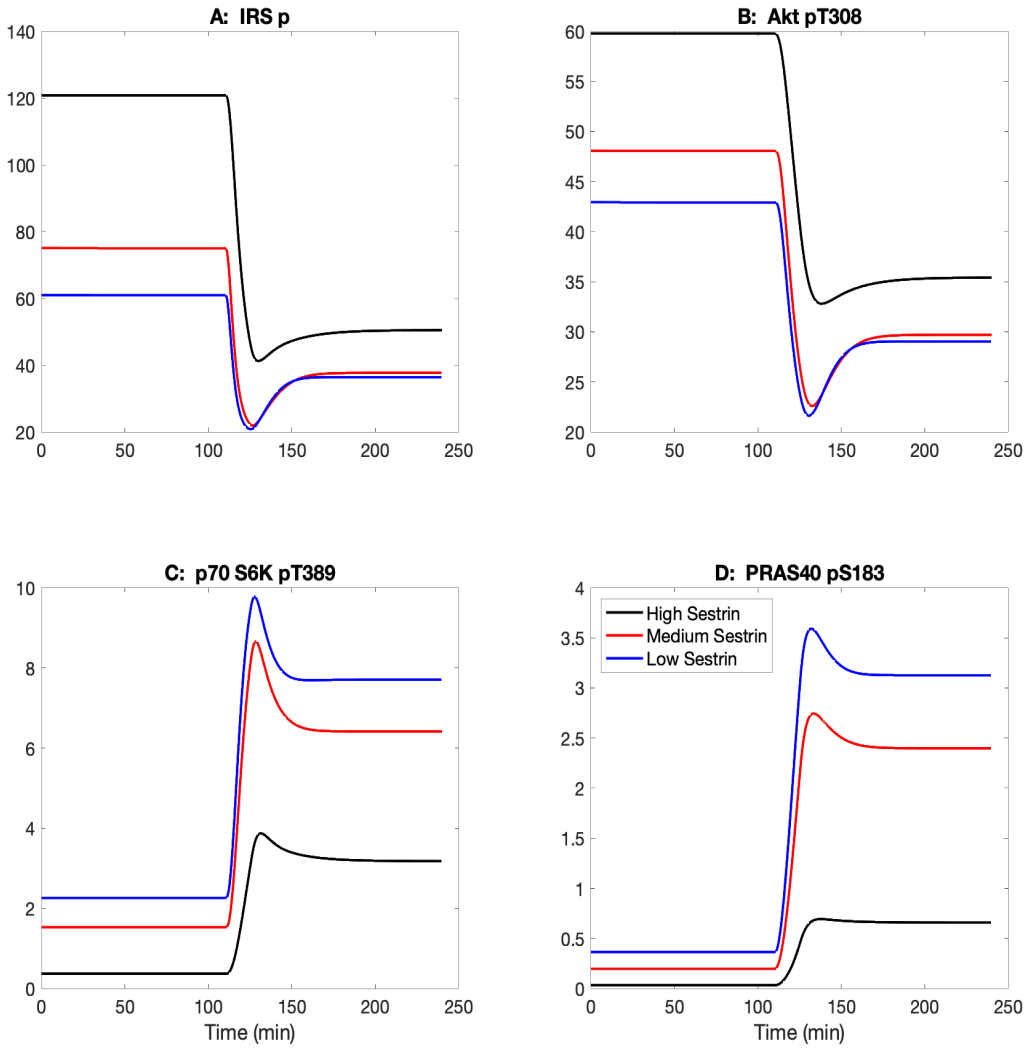

Figure 10. Effect of protein depletion and restoration on key model variables, obtained for differing sestrin2 levels.

3.4 Pharmacological activation of SIRT1.

Resveratrol, a SIRT1 activator, mimics the anti-ageing effects of calorie restriction in lower organisms and mice, and leads to improved exercise performance and insulin sensitivity (75). Other SIRT1-activating compounds (STACs) have been identified that are structurally unrelated to and more potent than resveratrol (75). In the next set of simulations, we seek to unravel the metabolic molecular processes that give rise to both the health benefits and potential side effects of STACs.

STACs and their anti-ageing effects. We compare the effects of resveratrol to three other STACs: SRT2183, SRT1460, and SRT1720. We assume that the STACs alter the Michaelis constant in the dependence of SIRT activity on its substrates (135). Based on in vitro findings by Milne et al. at 10 μM, resveratrol reduces baseline substrate K_m by 20%, SRT2183 by 50%, SRT1460 by 60%, and SRT1720 by 70% (figure 2a in Ref. (120)). As shown in Fig. 11a, at baseline K_m of [NAD+] = 0.029 mM, resveratrol slightly enhances SIRT1 activity by 11%. Other STACs has larger effects; SRT2183 elevates SIRT activity by 29%, SRT1460 by 43%, and SRT1720 by 54%.

As shown in Fig. 11a, the STACs increase SIRT activities to different degrees. SIRT regulates transcription by deacetylating transcription factors FOXO (112). The deacetylation rate of FOXO is described by Michaelis-Menten kinetics (31). Model predicts that all STACs increase FOXO deacetylation but to significantly different degrees (Fig. 11b). At baseline K_m of [FOXO] = 141μm (31), resveratrol increases FOXO deacetylation rate by a moderate degree (11%). Other STACs are more effective, with the largest increase obtained for SRT1720 (54%).

STACS activate AMPK and SIRT1, leading to the deacetylation of peroxisome proliferator-activated receptor-γ coactivator 1-α (PGC-1α). Similar to FOXO, the deacetylation rate of PGC-1α is also described by Michaelis-Menten kinetics (31). PGC-1α activation improves mitochondrial biogenesis. At baseline PGC-1α K_m level, resveratrol increases PGC-1α deacetylation rate by 12%. Larger improvements are obtained for other STACs (Fig. 11c).

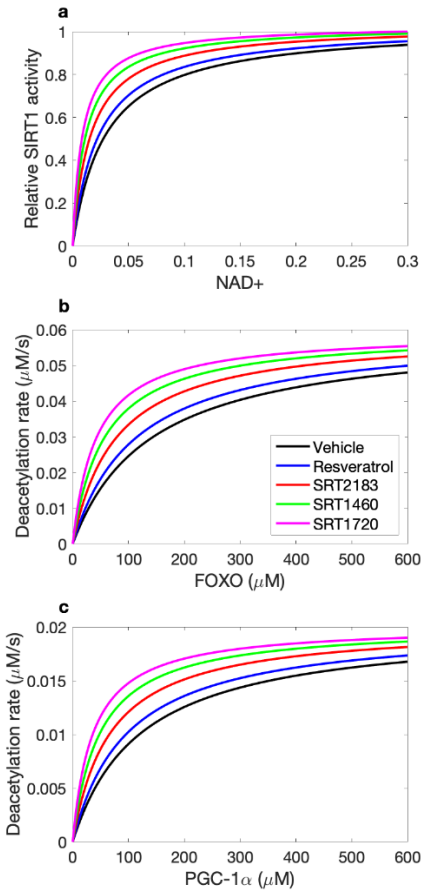

Figure 11. STACs activate SIRT1 (normalized values shown) by lowering the Michaelis-Menten constant for NAD+ (panel *a*). The deacetylation rates of FOXO and PGC-1α are subsequently affected (panels *b* and *c*).

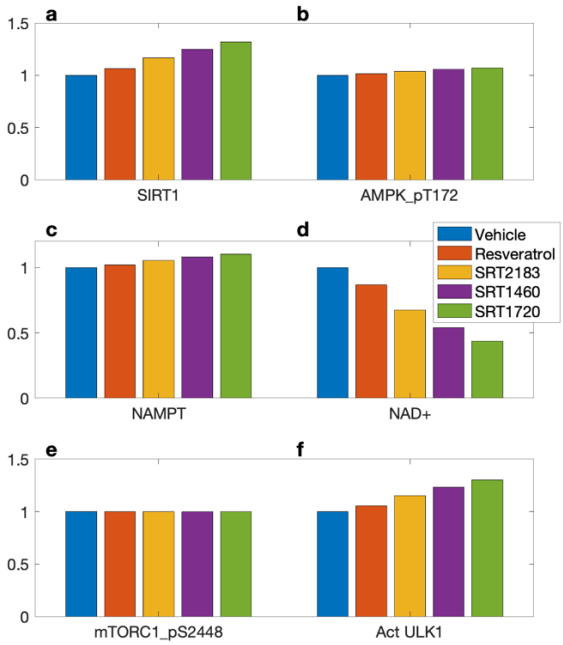

Figure 12. Predicted effects of STACs on SIRT1 activity (panel *a*), AMPK_pT172 (*b*), NAMPT (*c*), NAD+ (*d*), mTORC1_pS2448 (*e*), and activated ULK1 (*f*). Values are shown relative to control.

The effects of these compounds on key protein activities are shown in Fig. 12. Consistent with results in Fig. 11a, STACs raise SIRT1 levels, by as much as 32% (SRT1720; Fig. 12a). SIRT1 in turn activates AMPK, although the SIRT1-induced increase in AMPK_pT172 is relatively small compared to SIRT1 (Fig. 12b).

AMPK regulates nicotinamide phosphoribosyl transferase (NAMPT) (23), which acts as a limiting enzyme in the conversion of NAM to nicotinamide mononucleotide (NMN). Taken in isolation, the STAC-induced elevation in NAMPT (Fig. 12c) would accelerate the conversion of nicotinamide (NAM) to NMN, resulting in an increase in the downstream NAD+. However, the STACs also accelerate the consumption of NAD+ by binding on the allosteric site of SIRT1. Indeed, the enhanced SIRT1 consumption is the stronger effect, resulting in lower NAD+ following the administration of STACs (Fig. 12d), by as much as 56% with SRT1720.

The present model is based on C2C12 cells, in which AMPK does not regulate mTORC1 directly but instead facilitates the phosphorylation of TSC1_TSC2 at ser S1387 (39). Because both TSC1_TSC2

and its phosphorylated form TSC1_TSC2_pS1387 deactivate mTORC1, AMPK has a negligible effect on mTORC1 inhibition. AMPK regulates autophagy through direct phosphorylation of ULK1 (92). Thus, despite mTORC1's insensitivity to STACs, the level of activated ULK1 is predicted to be increased by STACs (Fig. 12f).

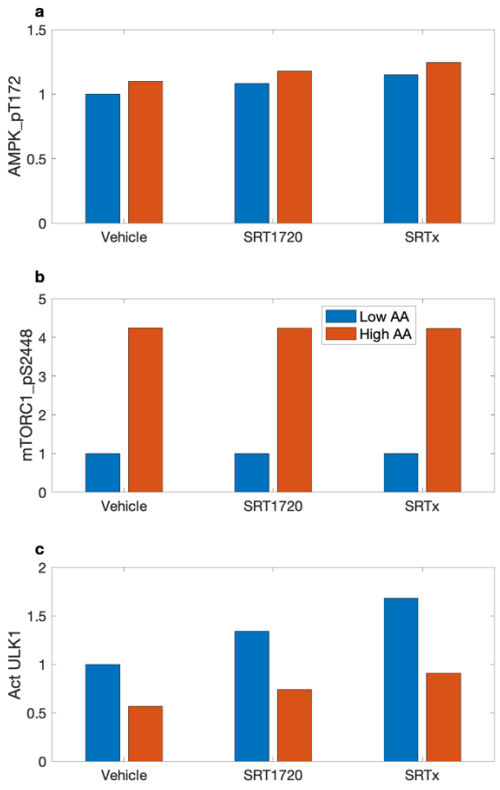

Figure 13. Potential overactivation of autophagy by STACs at high nutrient level. *a*, normalized levels of AMPK_pT172 obtained for control ("Vehicle"), for SRT1720, where SIRT1 substrate K_m is reduced by 70%, and for a hypothetical STAC where K_m is reduced by 90% ("SRTx"). For each case, AMPK_pT172 levels are determined at an AA level is 25% of control ("Low AA") and for reference AA conditions ("High AA"). *b*, normalized levels of mTORC1_pS2448. *c*, activated ULK1. With a sufficiently strong STAC ("SRTx" and "High AA"), autophagy may be activated at a level close to that at AA deprivation (compare with "Vehicle" and "Low AA").

Given that STACs enhance AMPK and ULK1, we investigate the following possibility: *Can STAC intake lead to premature autophagy, i.e., protein catabolism under an abundance of nutrients?* The inhibitory phosphorylation of ULK1 by mTORC1 serves as a negative feedback to prevent overactive autophagy and to avoid a futile cycle in which newly synthesized cellular building blocks are prematurely broken down again. But is this safeguard sufficient under the actions of STACs? To answer these questions, we consider three groups: control, SRT1720, and a (hypothetical) higher-performing STAC (called "SRTx") which we assume reduces substrate K_m by 90%. Simulations are conducted for baseline AA level, and a low AA level that is 25% of baseline. Predicted AMPK_pT172, mTORC1_pS2448, and ULK1 activation levels are shown in Fig. 13. STAC and AA both increase AMPK_pT172, whereas mTORC1_pS288 is substantially elevated by AA, but is relatively insensitive to STAC. ULK1 is activated by AMPK (Fig. 1), and thus simulations predict that STAC increases activated ULK1 level. In contrast, ULK1 is inhibited by mTORC1, and thus AA abundance is predicted to suppress ULK1. Simulation results indicate that, with abundance of nutrients, SRTx yields ULK1 activation level that is 91% of the analogous level obtained for the control group under AA deprivation. The similar autophagy activation under these two sets of conditions, despite the widely differing AA abundance levels, suggests that a sufficiently potent STAC may induce premature autophagy (110).

3.5 Parameter sensitivity analysis.

We perform local sensitivity analysis to assess the response of model outputs to small variations in selected parameter values (Fig. 14). Sensitivity of model output x to a parameter p is given by the relative change in x with respect to a 1% relative change in p, i.e.,

$$\text{Sensitivity} = \frac{\left({}^{x(p+\Delta p)}/_{x(p)}\right)-1}{{}^{\Delta p}/_{p}} \qquad (5)$$

where in our computations, $\Delta p = 0.01\ p$. Other parameters are fixed and all model outputs are updated simultaneously when p is varied.

Two distinguishable heat-map regions are identified with mostly non-zero entries. These regions are associated with the original model components: the insulin/IGF-1 signaling pathway (top-left region) and the Preiss-Handler and salvage signaling pathways (bottom-right region). These two components are coupled via the effects of AMPK on NAMPT, and of SIRT on AMPK. Variations in parameters in one region have typically minor (but nonzero) effects on outputs in the other region.

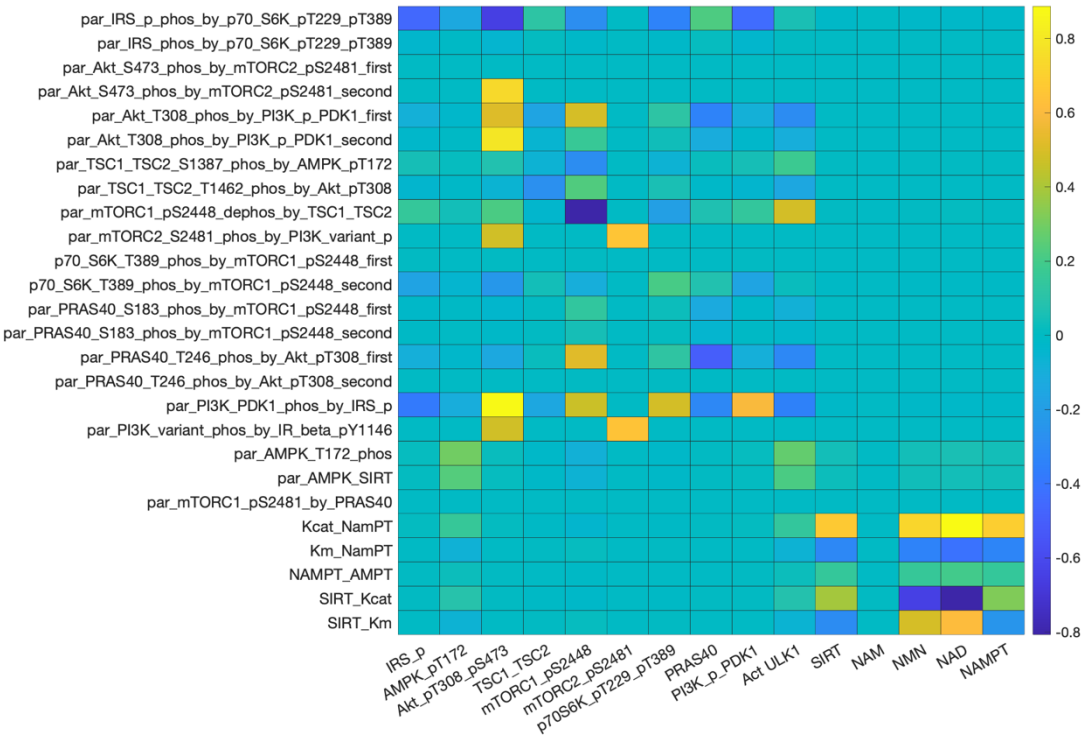

Figure 14. Heat map that illustrates the sensitivity of key model outputs (horizontal axis) to local variations in selected model parameters (vertical axis). Definition of the parameters can be found in the Supplemental Materials.

Within the insulin/IGF-1 signaling pathway, model outputs are particularly sensitive to variations in links that activate or inhibit proteins that have a large number of downstream effects. E.g., the activation of IRS_p by p70S6K_pT229_pT389 ("par_IRS_phos_by_p70_S6K_pT229_pT389"). Except for mTORC2_pS2481, other outputs in the insulin/IGF-1 signaling pathway exhibit significant sensitivity to variations in that activation strength, because IRS_p directly modulates major model variables such as PI3K_PDK1 and AMPK. In contrast, model solution is insensitive to changes in the activation of IRS_pS636 by p70S6K_pT229_pT389, in large part because the IRS_pS636 has no direct downstream effect.

Within the Preiss-Handler and salvage signaling pathways, most model outputs exhibit significant sensitivity to variations in the selected parameters associated with the pathways. NAM exhibits remarkable stability, because of the robust negative feedback cycle involves itself, NMN, NAD+, and

SIRT1. Proteins in this pathway are particularly sensitive to changes in the abundance of active NAMPT ("Kcat_NAMPT"). This result suggests that an NAMPT activator may be a promising pharmacological approach for raising intracellular NAD+ and SIRT1, to realize diverse and potentially impactful therapeutic benefits.

Chapter 4

Mathematical Model of Circadian Clock

4.1 Introduction

In this chapter we present a state-of-the-art computational model that couples the metabolism and circadian pathways, to investigate the roles of these pathways in ageing and metabolism in mammals. We aim to apply the model to answer important questions: *What are the key factors that advice the liver circadian clock about the cellular nutritional state, and facilitate its entrainment to a feeding schedule? How might variations in daily food intake or nutritional stress disrupt the clock? How do those processes change as one ages? What time of day should one take an anti-ageing medication to maximize its efficacy?* To address these questions, we present a comprehensive model that includes (i) the insulin/IGF-1 pathway, which couples energy and nutrient abundance to the execution of cell growth and division, (ii) the mechanistic target of rapamycin complex 1 (mTORC1) and amino acid sensors, (iii) the salvage pathway, which regulates the metabolism of NAD+ and the NAD+-consuming factor SIRT1, (iv) the energy sensor adenosine monophosphate-activated protein kinase (AMPK), and (v) the circadian pathway in the mouse liver. We formulate the model for a young mouse and an aged mouse, and we apply the model to investigate the synergy among regulators of nutrients, energy, metabolism, and circadian rhythms. Last but not the least, we conduct simulations to assess the effect of dosing schedule on the pharmacodynamics of anti-ageing drugs, of which the key molecular target of these drugs is SIRT1. Because SIRT1 is under major influence by the circadian clock(180), the optimal dosing times for these medications remain an essential but unanswered question. The model also can be used to aid in the interpretation of time dynamic genomic and proteomic data.

4.2 Model description

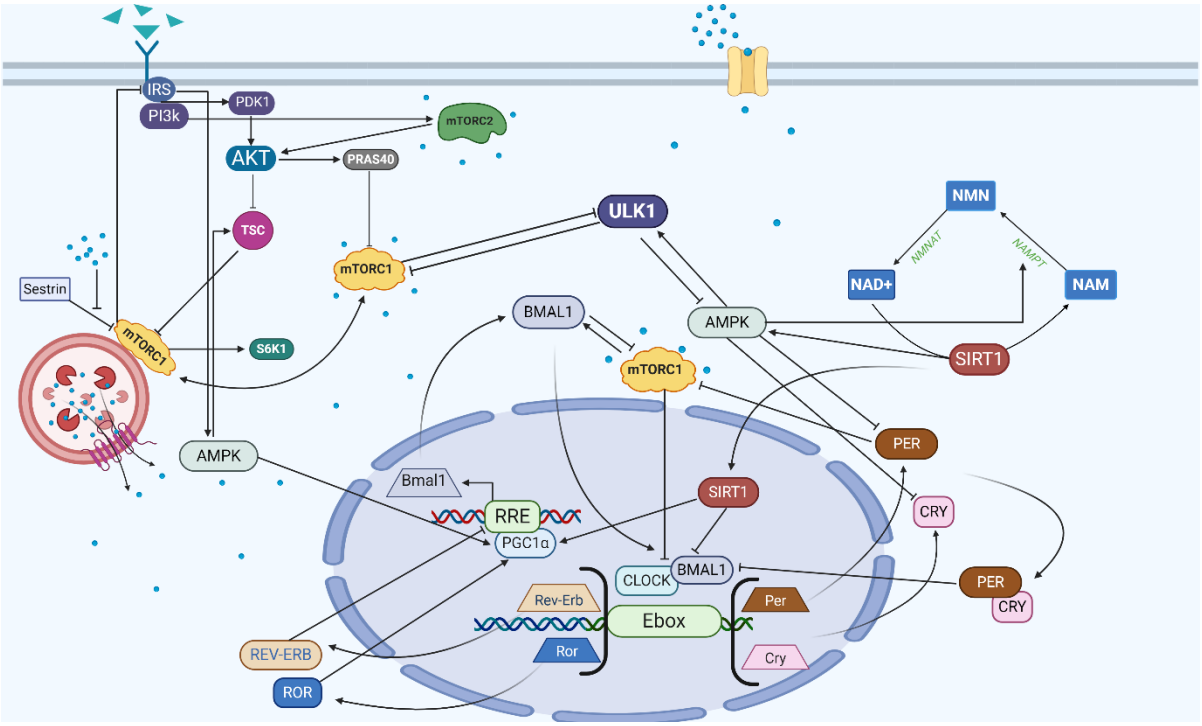

Figure 15. Schematic representation of the circadian clock, energy and metabolism pathways, and their coupling. Some components in the metabolism pathway may be activated by amino acids, such as leucine (blue circles) and insulin (green triangles). The model represents three distinct areas in the cell: the cytoplasm, lysosome, and the nucleus.

Main model components include the insulin/IGF-1 and mTOR signaling pathway(154), the core circadian clock pathway(188), and key metabolism regulators AMPK, NAD+, and SIRT1. The dynamics of the signaling pathways are modelled as a system of ODEs. Figure 15 depicts the pathways and protein interactions. The reactions and associated parameters are presented in Table S1 in the Supplemental Materials. Model parameters are taken from published studies (39, 154, 188). New parameters that characterize the coupling between the energy/metabolic pathways and the circadian system are shown in Table S2. Additional parameters that are adjusted to fit experimental data(188) are also included in Table S2. Parameter fitting was performed using the interior point optimization method in MATLAB.

Within the insulin/IGF-1 signaling and mTOR pathways, insulin activates the insulin receptor (IR), which triggers the IRS and PI3K, resulting in the phosphorylation of PDK1 and mTORC2,

respectively. mTORC2 phosphorylates AKT on the S473 and T308 residues, whereas PDK1 activates AKT. Active AKT phosphorylates a variety of proteins, including TSC1_TSC2 and PRAS40. Phosphorylation of TSC1_TSC2 by AKT inactivates the TSC complex, thereby activating mTORC1 and resulting in a number of downstream effects, including the repression of the autophagy pathway and elevation of core clock protein BMAL1. A detailed description of the insulin/IGF-1 signaling and mTOR pathway model can be found in the previous chapters. A detailed description of the insulin/IGF-1 signaling and mTOR pathway model can be found in Ref (154).

The clock model comprises several transcription factors that regulate gene expression: period (Per), cryptochromes (Cry), Rev-Erb and ROR-related orphan receptor retinoic acid receptor-related orphan receptor (Ror), brain and muscle ARNT-Like 1 (Bmal1), and circadian locomotor output cycles kaput (CLOCK). These core clock components exhibit circadian oscillations, driven by a network of interlocked transcriptional-translational feedback loops. In the primary negative feedback loop, CLOCK and BMAL1 heterodimerize to initiate the transcription of target clock genes, including Per (with isoforms Per1, Per2, Per3) and Cry (with isoforms Cry1 and Cry2), by binding the E-box elements in the promoter region (46, 204). PERs and CRYs then heterodimerize to inhibit their own transcription by acting on CLOCK:BMAL1 protein complex. In the secondary feedback loop, activators of CLOCK and BMAL1 dimerize to initiate the transcription of Rev-Erbα and Ror (141, 175). REV-ERBs and RORs are shown to repress and activate Bmal1 transcription, respectively (35, 64, 108). In addition, REV-ERB also inhibits Cry transcription to ensure robust oscillations (28, 146). Following the approach in Ref. (188), we represent the two period homologs (Per1 and Per2) as a single Per gene and ignore Per3, and we represent the two cryptochromes (Cry1, Cry2) as a single Cry gene.

Circadian rhythms play a critical role in the physiological processes involved in energy metabolism and energy balance. In turn, mTORC1 regulates the proteostasis of the core clock protein BMAL1, affecting its translation, degradation, and subcellular localization (107). Specifically, activation of mTORC1 results in elevated levels of BMAL1, but also translocates BMAL1 to the cytoplasm and reduces its nuclear accumulation (107, 143). In a negative feedback loop, BMAL1 inhibits the phosphorylation of mTORC1, as does another core clock protein PER2 (190). SIRT1 triggers the deacetylation of PGC1-α, the deacetylation of CLOCK-BMAL1 complex, and the degradation of PER2. AMPK accelerates the phosphorylation of PGC1-α, as well as the degradation of PER2 and CRY1. Deacetylated and phosphorylated PGC1-α increases the generation rate of Bmal1 genes.

Chapter 5

Modeling the Effect of Ageing on the Circadian Clock and Metabolism: Implications on Timing of Medication

5.1 Introduction

In the previous chapter we described a computational model that consists of both metabolism and clock key players. In this chapter, we conduct model simulations to (1) demonstrate the agreement between model predictions and experimental data; (2) investigate how our feeding and fasting cycle can affect liver circadian clock, and how these feeding behaviors affect key metabolism regulators such as mTORC1; (3) study the effect of ageing on key clock components; (4) analyze the pharmacological effects of ageing drugs such as STACs and NAD supplements on clock, and how these effects differ between old and aged groups.

5.2 Model predicts expression time-profiles of core clock genes in the mouse liver

The intricate coupling of the energy and metabolism pathways and the circadian system is represented in the model; see Fig 15. The phosphorylation of mTORC1 elevates BMAL1, whereas BMAL1 and PER2 inhibit mTORC1. As such, the circadian rhythms drive oscillations in phosphorylated mTORC1 level (Fig. 16B). The model predicts a phase difference between mTORC1 and Bmal1 mRNA of ~9 hours. Similar oscillations are seen in other variables in the insulin pathway model. These results were obtained for the "young" model with a constant baseline insulin level.

To assess the validity of the model, we compare the predicted time-profiles of core clock genes with mRNA levels measured in mouse livers (78). In that study, the mice were entrained to a 12:12 light/dark cycle, then put in constant darkness and fed ad libitum. The predicted core clock mRNA time-profiles for Bmal1 (Fig. 16A), Per2 (Fig. 16C), Cry1 (Fig. 16D), Rev-Erb (Fig. 16E), and Ror (Fig. 16F) all exhibit reasonable agreement with the mouse liver data (closed circles).

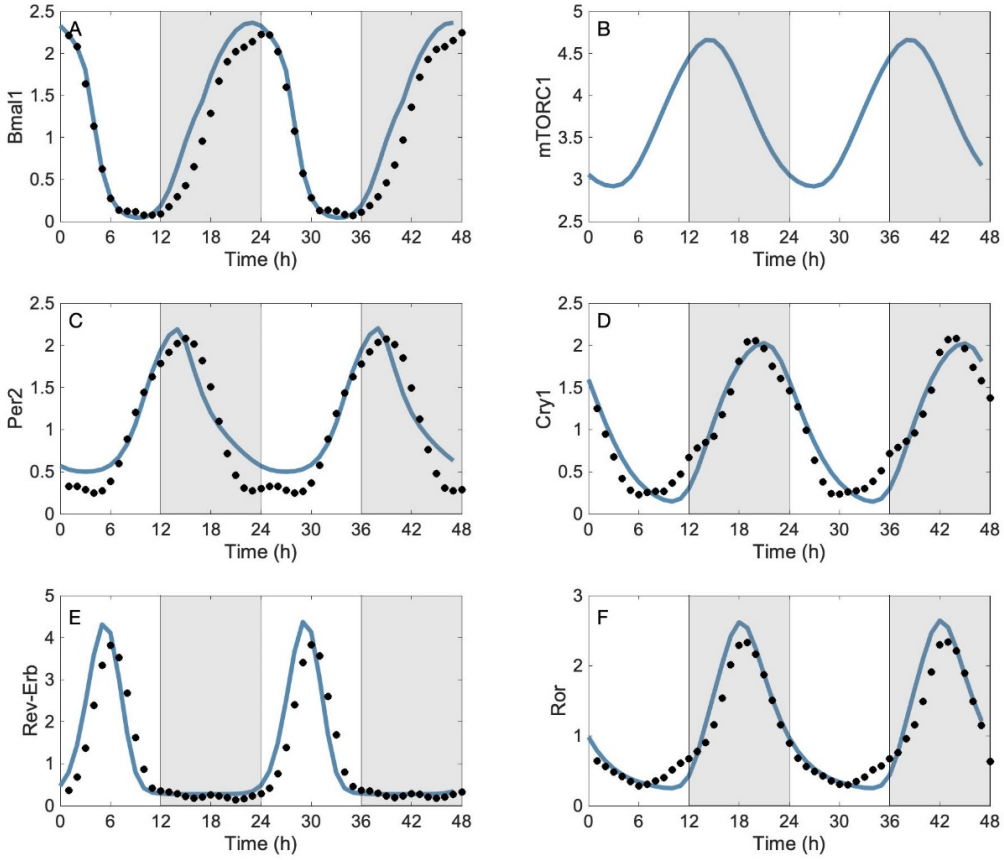

Figure 16. Predicted oscillations in core clock gene and mTORC1 levels. *A*, predicted Bmal1 mRNA time profile. *B*, mTORC1 level, driven to oscillate by the clock. *C*-*F*, predicted Per2, Cry1, Rev-Erb, and Ror time-profiles. Experimental data are shown in closed circles.

5.3 Effect of feeding on mTORC1 and liver clock genes

The circadian system, metabolism, and feeding are intertwined. To better understand the effect of food on liver circadian rhythms, we simulate a fed-like state and a fasted-like state. Nutrition levels (i.e., insulin and amino acid) are assumed to stay high at the baseline levels in a fed-like state, to stay low in a fasted-like state. When insulin and amino acid levels are low, they are taken to be 10% and 50% of baseline, respectively.

The time-profiles predicted for mTORC1 and key clock proteins are shown in Fig. 17 (blue and red curves). mTORC1 is activated by a high-energy diet through the uptake of glucose and amino acids (Fig. 17B). At high nutrition levels, the elevated insulin and growth factor levels promote the phosphorylation of Akt, which inhibits TSC1-TSC2 and activates mTORC1. Conversely, in the fast-like state, phosphorylated mTORC1 drops to ¼ of its value in the fed-like state, and its circadian oscillations essentially vanish. Recall that activation of mTORC1 results in elevated levels of BMAL1. Thus, fasting lowers BMAL1 level (Fig. 17C). CLOCK-BMAL and CRY1 are similarly affected, whereas the effect on PER2 is the opposite (Figs. 17D-17F).

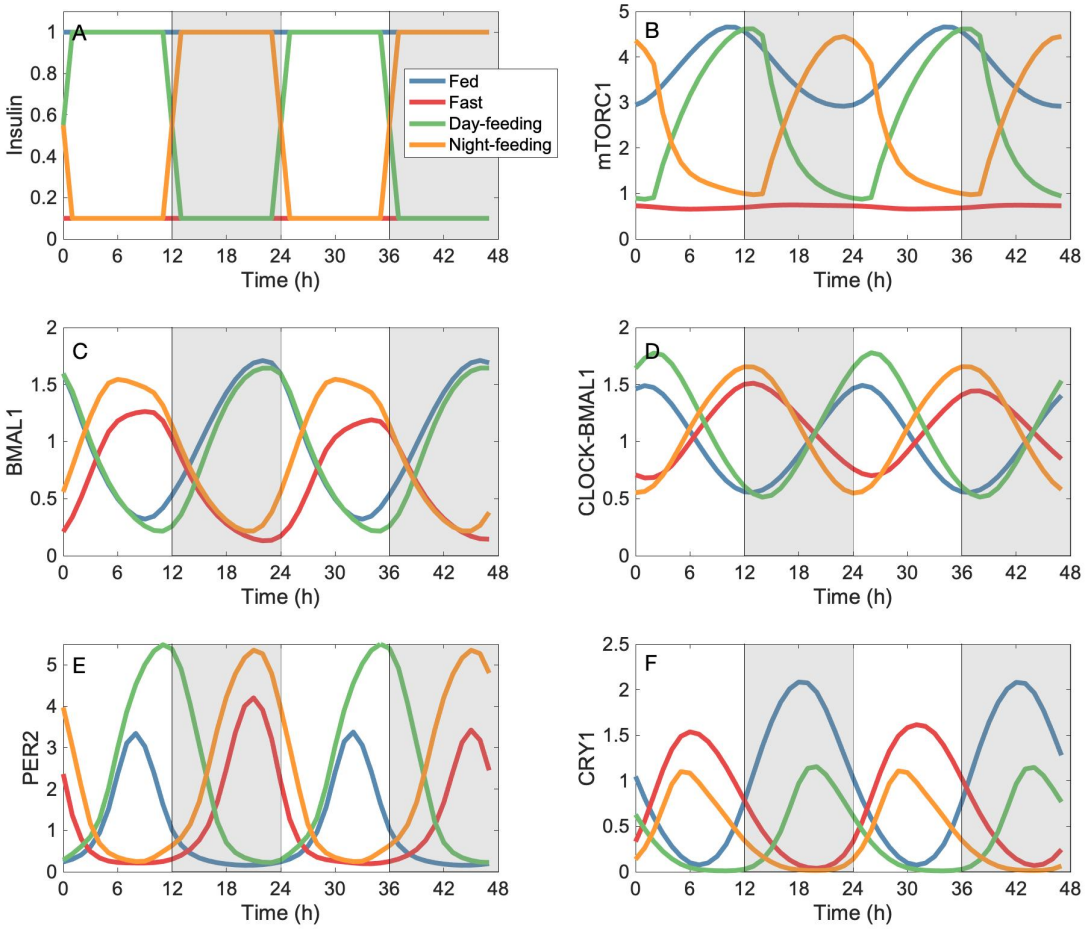

Figure 17. Effects of feeding schedule on mTORC1 and core clock gene levels. *A*, insulin levels for a fed-like state (constant at 1), a fasted-like state (constant at 0.1), day-time feeding, and night-time feeding.

B, mTORC1 levels, driven to oscillate by the clock and feeding schedule, and elevated at high insulin levels. *C*-*F*, core clock protein time-profiles.

5.4 The liver circadian clock entrains to an altered feeding schedule

Food is known to be a potent zeitgeber for the liver circadian cycle. To assess the effect of an altered feeding schedule on the circadian rhythm, we simulate day-time and night-time feeding by varying the insulin and amino acid levels during the day. The simulated insulin levels for the different feeding patterns are shown in Fig. 17A, green and orange curves. The simulated amino acid levels follow the same trend and vary between 0.5 and 1. The model predicts that variations in nutrition levels yield oscillations in mTORC1 (see explanation above). Night-time feeding induces a half-day phase shift in the mTORC1 (Fig. 17B) relative to the constant fed-like case, and the coupling between mTORC1 and BMAL1 induces a corresponding phase shift in the clock as well (see orange curves in Figs. 17C-17F). This result suggests that the liver circadian clock may entrain to an altered feeding schedule via its coupling with mTORC1.

5.5 Effect of ageing on the circadian clock

As we age, our circadian system undergoes significant changes, such that rhythmic activities such as sleep/wake patterns change markedly, and in many cases become increasingly fragmented. Ageing is also associated with the reduction in the cellular concentration of NAD+ and SIRT1. To study the effect of key age-related changes in metabolism on the circadian system, we formulate an aged model by lowering the mean NAD+ and SIRT1 levels to 25% and 40%, respectively, of the baseline (young) model (113). We acknowledge that ageing is associated with a multitude of other physiological changes. But here we focus on the effect of NAD+ and SIRT1, which are known to play an essential role in the mechanism that translates the regulation of energy metabolism into ageing and longevity.

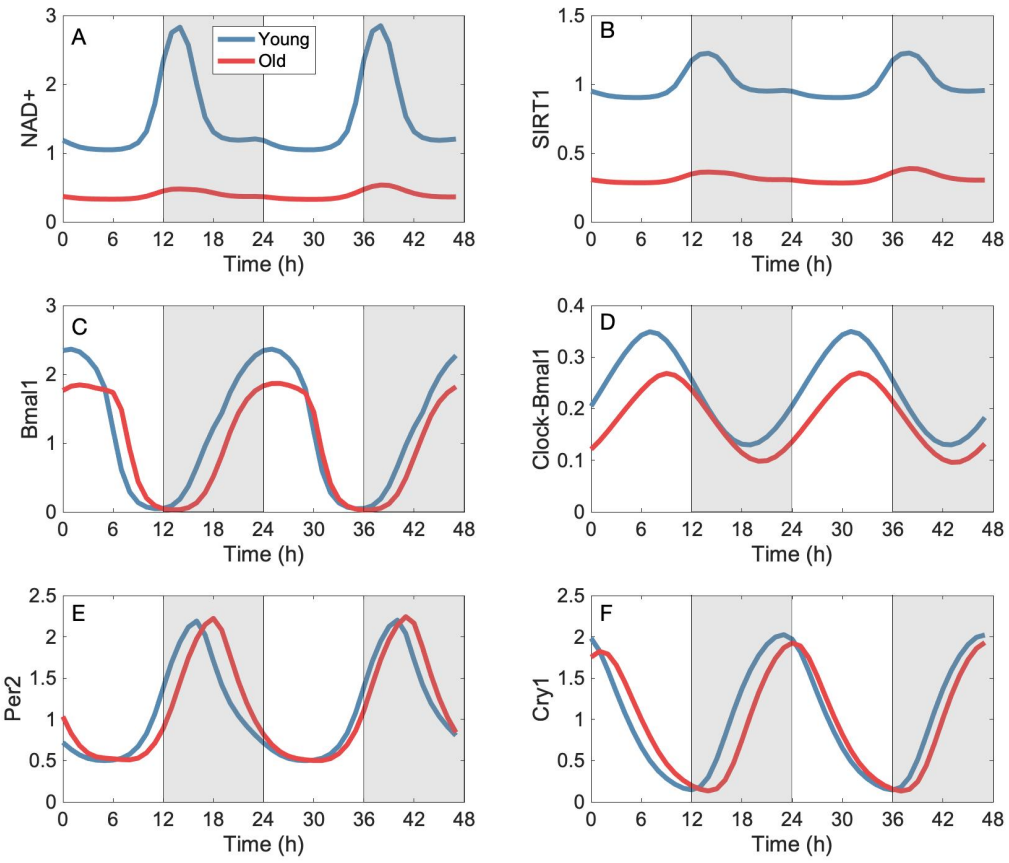

Figure 18. Effect of ageing on metabolism and the circadian clock. Ageing reduces the bioavailability of NAD+ (*A*) and SIRT1 (*B*), which lowers Bmal1 (*C*) and Clock-Bmal1 levels (*D*) but has a negligible effect on the abundance of Per2 (*E*) and Cry1 (*F*). Ageing shortens the circadian period.

The resulting time-profiles of core clock genes are shown in Fig. 18. SIRT1 deacetylates the liver kinase B1 (LKB1), which stimulates AMPK. Through their actions on PGC1-α, SIRT1 and AMPK raise the level of Bmal1. Thus, the lower SIRT1 and AMPK levels in the aged model yield correspondingly reduce Bmal1 and Clock-Bmal1 (Figs. 18C and 18D). Taken in isolation, the lower Clock-Bmal1 level would decrease the generation rates of Per2 and Cry. However, in a competing effect, the lower SIRT1 level in the aged model also inhibits the deacetylation of Clock-Bmal1, thereby accelerating the formation of Per2 and Cry1. These two competing effects result in negligible effects on the abundance of Per2 and Cry1 (Figs. 18E and 18F). What is noteworthy is that the lower SIRT1 level shortens the circadian period in the aged model, from the baseline 24 hours to 22 hours, consistent with experimental findings (195).

5.6 Effect of dosing schedule on pharmacodynamics

Resveratrol and other SIRT1-activating compounds (STACs) increase SIRT1 activity and mimic the anti-ageing effects of calorie restriction in lower organisms and mice (75). Given the modulation of SIRT1 by the circadian clock and vice versa, we investigate how the dosing schedule may differentially affect the pharmacodynamics of STAC on the young and aged models. The models compute SIRT1 activity as a Michaelis-Menten function of [NAD+]. To simulate the effect of STAC, we reduce the Michaelis-Menten constant K_m (120) and vary SIRT1 generation during the day. We compare the cases where the STAC is taken at ZT6, ZT12, and ZT24. The predicted NAD+ time-profiles are shown in Figs. 19D and 19G for the young and aged models, respectively. All NAD+ profiles are normalized with respect to the mean NAD+ value in the young model. The corresponding predicted SIRT1 time-profiles are in Figs. 19E and 19H, normalized by the mean SIRT1 value in the young model. Recall that NAD+ and SIRT1 levels are attenuated in ageing. As a result, the pharmacodynamics of STAC and its dosing schedule differ significantly between the two populations.

The young and aged models exhibit different responses to the dosing schedule. Given that mammalian SIRT1 deacetylates a host of target proteins that are important for apoptosis, the cell cycle, circadian rhythms, mitochondrial function, and metabolism, we will assess drug response using two measures of SIRT1 levels, its mean and peak, computed over a representative circadian period. The peak value is important in threshold-based processes. Relative changes in mean and peak SIRT1 for the young and aged models are given by percentage changes relative to the respective control group (no drug).

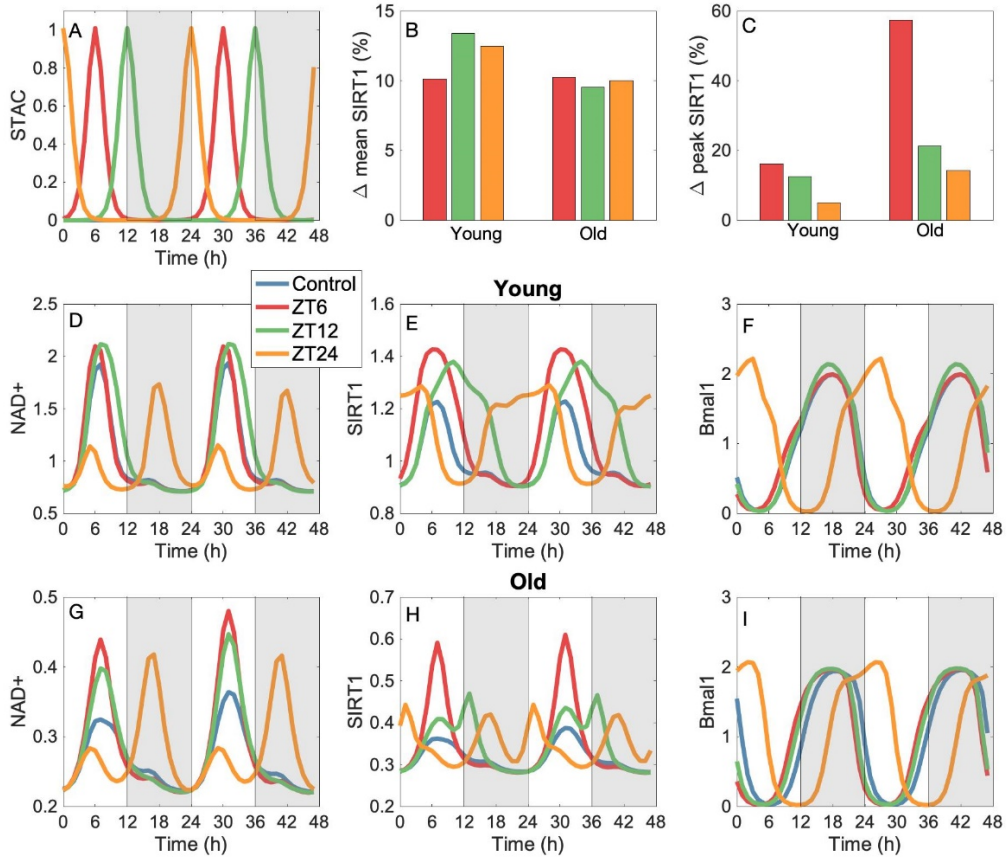

Figure 19. Effect of dosing schedule on STAC efficacy. Simulations are conducted for STAC administered at ZT6, ZT12, and ZT24 (*A*), and in the young model (results in the second row) and aged model (third row). STAC has a major impact on the dynamics of NAD+ (*D* and *G*) and SIRT1 (*E* and *H*). Dosing schedule has a significant effect on mean SIRT1 in the young model but not the aged model (*B*), whereas the effect on peak SIRT is significant in the young model and even stronger in the old model (*C*). Δ mean and peak SIRT1 for the young and aged models are computed as percentage changes with respect to the respective control group (no drug).

In terms of mean SIRT1, the young and aged models exhibit similar relative increases (approximately +10%) when STAC is administered at ZT6, which is the middle of the light cycle and coincides approximately with the circadian peaks of the NAD+ and SIRT1 in the control group (no drug).

See Fig. 19. Because baseline SIRT1 is much higher in the young model, the same relative increase implies a much larger net increase in the young model. When administered at ZT12, the beginning of the dark cycle, STAC induces the largest increase in mean SIRT1 in the young model (+13.4%), whereas the analogous response of the aged model is essentially insensitive to the dosing schedule (+9.5%, Fig. 19B). When administered at the end of the dark cycle (ZT24), STAC induces +12.7% and +9.8% increases in mean SIRT1 the young and aged models, respectively. In terms of peak SIRT1, drug timing has a significant effect on both the young and aged models (see Fig. 19C). The most marked increase in relative peak SIRT1 is obtained when STAC is administered to the aged model at ZT6. Alternative dosing schedules and the young model yield significant but weaker response in peak SIRT1.

Further discussion is warranted for the ZT24 case (dosing at the beginning of the light period). Double peaks emerge in the NAD+ and SIRT1 time-profiles (orange curves in Figs. 19D, 19E, 19G, 19H), with one peak corresponding to the circadian peak, the other to the STAC-induced peak. Also, Bmal1 time-profiles indicate a 7-hour shift in the circadian clock, in both the young and aged models (Figs. 19F and 19I). Such a shift may be undesirable.

NAD+ is a central regulator of metabolism, and its decline is linked to DNA damage (20), metabolic stress, chronic inflammation (80), and ageing (22, 114). The consumption of nicotinamide riboside (NR), a precursor of NAD+ and is similar to B3, has been proposed as a means to elevate NAD+ levels and to improve health span (199). To represent the effect of NAD+ supplements, we increase the total NAD+ and NAM concentration during specific hours of the day, depending on the dosing schedule (Figs. 20A and 20B). We compare the cases where the NAD+ supplements are taken at ZT6, ZT12, and ZT24. The predicted NAD+ and SIRT1 time-profiles are shown in Fig. 20 for the young model (panels D and E) and the aged model (panels G and H).

The model predicts that NAD+ supplements exert the strongest effect, as measured by either mean or peak SIRT1, if taken during the middle of the light cycle, at ZT6, which coincides with the peak of the circadian peak (Figs. 20B and 20C). The model predicts that mean SIRT1 increases by 7.5% in the young case and 5.6% in the aged case. If peak SIRT1 is the measure, then a larger increase of 14.2% is predicted in the aged model, compared to 36.0% in the young model. Administering NAD+ supplements at a different hour may generate significantly smaller effect. Taken at ZT12, mean SIRT1 increases by 6.6% in the young model and 3.0% in the aged model (Fig. 20B). Unlike the ZT6 case, the ZT12 case results in a smaller increase in peak SIRT1 in the aged model (5.7%), compared to 10.8% in the young model (Fig. 20C). Taken at ZT24, mean SIRT1 increases by only 3.9% in the baseline model, but

essentially has no response (+0.5%) in the aged model (Fig. 20B). Even more remarkably, peak SIRT1 decreases by 7.9% in the aged model (Fig. 20C). Furthermore, unlike STAC, taking NAD+ supplements at ZT24 does not result in a phase shift of the circadian rhythms; see Bmal1 time-profiles in Figs. 20F and 20I.

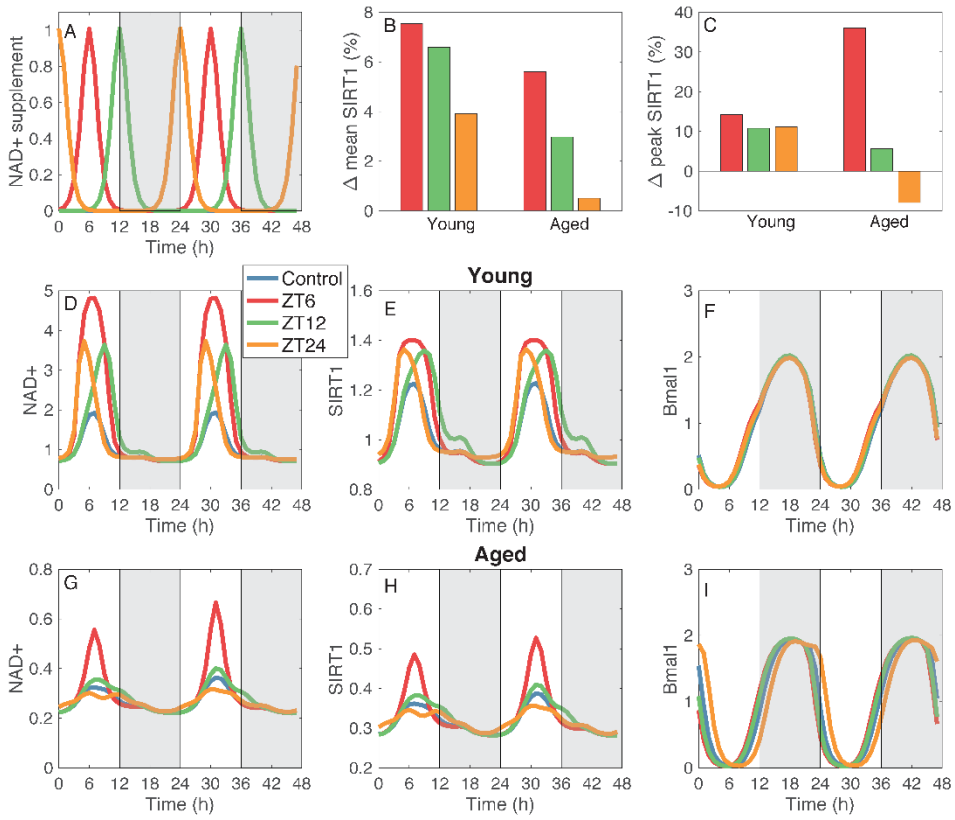

Figure 20. Effect of dosing schedule on NAD+ supplement efficacy. Simulations are conducted for NAD+ supplement administered at ZT6, ZT12, and ZT24 (*A*), and in the young model (second row) and aged model (third row). NAD+ supplement has a major impact on the dynamics of NAD+ (*D* and *G*) and SIRT1 (*E* and *H*). Dosing schedule has a significant effect on drug efficacy in both the young and old models, as measured by mean SIRT1 (*B*) and peak SIRT1 (*C*).

Chapter 6

Conclusions

6.1 Cell energy balance and metabolism

6.1.1 Interactions among mTORC, AMPK, and SIRT

Traditionally, the investigation of human ageing and disease has relied on cell cultures and animal models, including non-vertebrates (e.g., yeast, worm, and fly) and vertebrates (e.g., zebrafish, mice, dogs, and primates), as well as clinical trials. With the advent of bioinformatics and computational biology, computational modeling and analysis techniques can provide accurate simulations of biological processes. Chapters 2 and 3 describe a state-of-the-art computational model for investigating signaling pathways in growth, ageing, metabolism, and disease in mammals. Major model components include the insulin/IGF-1 or mTOR signaling pathway (103), the Preiss-Handler and salvage pathways (43), energy sensor AMPK, and transcription factors FOXO and PGC-1α. The mTOR signaling pathway couples energy and nutrient abundance to the execution of cell growth and division. That function can be attributed to the ability of mTORC1 to sense energy, nutrients, and growth factors, by regulating other important kinases, such as S6K and AKT. The Preiss-Handler and salvage pathways regulate the metabolism of NAD+ as well as NAD+-consuming proteins such as sirtuins. Key findings include:

- Model simulations indicate that simultaneously inhibiting AKT or PI3K_PDK1, and inhibiting mTORC1 effectively suppresses PRAS40 phosphorylation on both Ser183 and Thr246 sites, further enhancing the inhibition of mTORC1 by PRAS40 (Fig. 2). This result suggests a clinically important role of PRAS40 in controlling tumor growth.
- We provide the first computational model that capitulates the interplay between sestrin2 and leucine, and the effect on mTORC1 activity. With a crucial role in metabolic regulation through the activation of AMPK and inhibition of mTORC1, sestrin2 might serve as a therapeutic target for cancers, metabolic diseases, and neurodegenerative diseases.
- Given that sestrin2's inhibitory effect on mTORC1 activity can be significantly impacted by AAs such as leucine (Fig. 6), dietary modifications may enhance the efficacy of therapies that target mTORC1 and sestrin2.
- The model captures the interactions between arginine and leucine during protein deprivation, and predicts a signal that reactivates mTORC1 and downregulates autophagy (Fig. 8).

- The model capitulates the regulation of autophagy by SIRT1. Simulations indicate that, by activating SIRT1, STACs in high dosages may lead to premature autophagy (Fig. 12).

mTORC1 signaling is switched on by a number of oncogenic signaling pathways and is hyperactive in up to 70% of all human tumors (50). Thus, there is much interest in targeting mTORC1 signaling as a potential therapeutic avenue for anti-cancer therapy. Rapamycin, originally developed as an immunosuppressant that targets T-cells, is arguably the best known mTORC1 inhibitor and has been shown to extend lifespan in mice.(69) However, despite its specificity, rapamycin in typical dosages does not completely inhibit all mTORC1 activities (173), limiting its efficacy as an anti-cancer agent. In fact, cancer patients whose tumors exhibit a mutational activation of PI3K/AKT signaling have a low response rate for rapamycin and its rapalogs (e.g. breast, colon and prostate cancer, and glioblastoma (13, 62)). This inadequate therapeutic response is believed to result from rapamycin and its rapalogs' incomplete inhibition of mTORC1-mediated phosphorylation of 4E-BP1 and a concomitant activation of AKT via loss of a negative feedback mechanism (103).

Mi et al. suggested that the acquired resistance to rapamycin in cancer cells may be attributable to the redundant phosphorylation of PRAS40 by both AKT and mTORC1 signaling (118). Their findings indicate that the concurrent inhibition of AKT and mTORC1 yields effective inhibition of PRAS40 phosphorylation on both Ser183 and Thr246 sites, enhancing PRAS40's inhibition of mTORC1-mediated 4E-BP1 phosphorylation and translation, associated with suppression of tumor growth and cell motility (118). Similarly, while PI3K inhibitors such as wortmannin are potential anti-cancer agents on their own (172), a more nearly complete inhibition of mTORC1 may be achieved when inhibitors of the PI3K/AKT pathway are administered in conjunction with rapamycin (Fig. 2). These results suggest a potentially important role of PRAS40 in the translational control of tumor progression. Indeed, dual inhibition of PI3K and mTORC1 signaling by rapalogs in combination with PI3K or AKT inhibitors has demonstrated profound efficacy in preclinical cancer models (21, 49, 106, 138).

Chronic administration of rapamycin leads to insulin resistance due to its suppression of mTORC2, resulting in glucose intolerance and hepatic insulin resistance (102). The loss of insulin sensitivity is due to the reduction of AKT_T308_S473, which plays a pivotal role in the translocation of GLUT4 (53, 74). Sebastian and co-workers demonstrated intermittent administration of rapamycin (e.g., once every 5 days) mitigates its detrimental effect on glucose homeostasis (5, 6). Our model simulations indicate that an optimal rapamycin dosage can be identified which, in chronic and continuous usage, attenuates the detrimental effect on insulin sensitivity while preserving rapamycin's anti-cancer and anti-ageing effects via mTORC1 inhibition (Fig. 5).

6.1.2 Amino acid sensors and mTORC1 regulation

Sestrin2 is a highly conserved stress-inducible metabolic protein known to provide protection to cells against oxidative stress, endoplasmic reticulum (ER) stress, and hypoxia. Sestrin2 also plays a key role in metabolic regulation through the activation of AMPK and inhibition of mTORC1, with downstream effects including autophagy activation, antiapoptotic effects in normal cells, and proapoptotic effects in cancer cells (72). As such, sestrin2 might serve as a potential therapeutic target for cancers (77), (189), metabolic diseases, and neurodegenerative diseases (136).

The present model provides the first computational platform that capitulates the regulation of mTORC1 by sestrin2, and its modulation of leucine. The action of sestrin2 on mTORC1 begins with its inhibition of GATOR2. During acute starvation, sestrin2 binds to GATOR2 and impedes the latter's inhibition of GATOR1, resulting in the suppression of mTORC1. Sestrin2 binds with leucine; the addition of leucine would reduce free sestrin2, promote the downstream inhibition of GATOR1 and ultimately enhance the activation of mTORC1. The interplay between sestrin2 and leucine, and the effect on mTORC1 activity is captured in Fig. 6. As noted above, sestrin2 is a potential target for anti-cancer and other disease treatments. Given that sestrin2's inhibitory effect on mTORC1 activity can be significantly impacted by AAs such as leucine, dietary modifications may enhance the efficacy of therapies that target mTORC1 and sestrin2.

GATOR1 negatively regulates mTORC1 and appears to function as a tumor suppressor. In cancer cells with loss-of-function mutations in GATOR1, which include some lung, breast, ovarian cancers, and glioblastomas (11), mTORC1 is hyperactive and these cancer cells have been shown to be hypersensitive to rapamycin. Thus, the associated cancers may be particularly amenable to therapeutic strategies that limit mTORC1 activity. For rapamycin-resistant cancers, and for diabetes and neurodegenerative diseases, GATOR may be a potential therapeutic target. In fact, as an upstream regulator of mTORC1, GATOR1 has been identified as a potential therapeutic target for epilepsy, in which mTORC1 hyperactivation has been implicated (126).

Also contributing to cellular AA sensing for the mTORC1 pathway is the CASTOR family (33). CASTOR1/2 binds to GATOR1 and obstructs the binding process between GATOR1 and GATOR2, freeing up GATOR1 to inhibit mTORC1. Unlike sestrin2 which is inhibited by leucine, CASTOR1 binds to arginine. Thus, the addition of arginine elevates mTORC1 activity by reducing free CASTOR1.

Another arginine sensor is the lysosomal AA transporter SLC38A9. Arginine stimulates SLC38A9 and promotes its interaction with the Rag GTPase-Regulator complex, which results in the activation of mTORC1. Wyant et al. reported that a mutant of SLC38A9 that does not interact with arginine lacks the ability to signal AA sufficiency to mTORC1 (192). Another important role of SLC38A9 in AA homeostasis is to transport AAs produced by lysosomal proteolysis, such as leucine, from lysosomes to the cytosol, thereby reactivating mTORC1. The critical role of SLC38A9 in this process is evinced by the SLC38A9-null HEK293T cells, which exhibit whole-cell AA levels similar to wild-type, but significantly higher lysosomal AA concentrations including leucine (192). The efflux of lysosomal leucine and the subsequent activation of mTORC1 may regulate autophagy. During starvation, mTORC1 is inhibited, which attenuates its inhibitory phosphorylation of ULK1 and promotes autophagy. Thus, intracellular nutrients produced by autophagy can stimulate mTORC1 signaling and provide a negative feedback signal to downregulate autophagy (more below) (200). The present model is unique in that it explicitly and separately represents arginine and leucine, rather than lumping them into a single AA category. Consequently, the model captures the exquisite interactions of these AAs, and the resulting signal to the mTORC1 pathway and its reactivation during protein deprivation. Indeed, the model is the first to recapitulate the reactivation of mTORC1 by proteolysis following autophagy (Fig. 8) (200).

6.1.3 Pharmacological activation of SIRT1

STACs enhance autophagy via its activation of SIRT1, followed by the activation of AMPK and inhibition of the mTORC1. The elevated SIRT1 activity also facilitates the deacetylation of FOXOs, which are transcription factors that have major impacts on longevity and cancer. In the absence of growth factors or AAs, the reduction in activated AKT leads to the dephosphorylation of FOXOs and drives their relocalization from the cytoplasm to the nucleus. The subsequent deacetylation of FOXOs by SIRT1 mediates stress resistance response. AMPK phosphorylation also increases the transcription activity of FOXOs. Emerging evidence suggests that FOXO factors act as a tumor suppressor in a variety of cancers (183).

Additionally, SIRT1 regulates autophagy through the direct deacetylation of autophagy-related genes such as ATG. Studies have demonstrated an essential role for SIRT1 in the induction of autophagy (68, 104), as well as the protective effects of the SIRT1-induced autophagy in preventing or attenuating neurotoxicity (85, 191). However, by activating SIRT1, STACs may lead to the decoupling of the autophagic response from the organisms' nutrient and energy status. Model simulations suggest that a

sufficiently potent STAC may yield premature autophagy (Fig. 12), in which newly synthesized cellular building blocks are prematurely and unnecessarily catabolized despite an abundance of nutrients.

The insulin/IGF-1 signaling pathway of the present model is fitted primarily for C2C12 cells,(40) whereas the Preiss-Holder and salvage pathway is formulated primarily using non-specific mammalian cell data (16). Because different cells have diverse energetic and metabolic needs, their metabolic pathways often exhibit significantly different functions and regulations. For instance, SIRT1 is activated by starvation in most cells (131) but in the mouse pancreas, SIRT1 is inactivated by the reduction in the NAD+/NADH ratio (18). In C2C12 cells, AMPK does not directly regulate mTORC1 but promotes TSC1_TSC2 phosphorylation at ser S1387. Because mTORC1 is inhibited by both TSC1_TSC2 and its phosphorylated form TSC1_TSC2_pS1387, in C2C12 cells AMPK appears to have only a limited regulatory effect on mTORC1. In contrast, AMPK is known to directly inhibit mTORC1 in HEK293T cells (66). Furthermore, sex and age differences have been reported. In the mouse, mTORC1 and mTORC2 activity levels are known to vary between males and females (9). In human skeletal muscle, mTORC1 is activated under different conditions depending on the age of the individuals (54, 55). Similarly, marked changes have been reported in SIRT1 activity and NAD+ levels as individuals age (30, 196). Last but not the least, molecular mechanisms have been identified that are differentially regulated in long- and short-lived species; e.g., perturbed insulin/ IGF-1 signaling in long-lived species due to reduced plasma IGF-1 and brain IGF-1 receptor expression (174). Thus, an interesting question is: Multiple regulatory mechanisms are known to modulate lifespan in model organisms, such as the insulin/IGF-1 signaling, the mTOR pathway, and the AMPK pathway. To what extent do these mechanisms account for the huge variation of mammalian lifespans in natural species? Taken together, these observations highlight the importance of taking into account cell or tissue specificity, together with sex and age, when developing therapeutic strategies that target these pathways. Investigating how the key ageing regulatory pathways interact during normal ageing is a worthwhile future extension.

In sum, we have developed a state-of-the-art computational model for investigating the interactions among signaling pathways and environmental stimuli in growth, ageing, metabolism, and diseases. The model can be used as an essential component to simulate (1) gene manipulation, (2) therapies for cancer, metabolic diseases, and neurodegenerative diseases, (3) calorie restrictions, and (4) chronic stress. Simulation results can be interpreted to assess the implications on longevity and ageing-related diseases.

6.2 Circadian rhythms, metabolism, and ageing

6.2.1 Metabolism and the circadian rhythms

Early work in mammalian rhythms identified the hypothalamic SCN as the master circadian pacemaker that drives behavioral rhythms (185). Soon after, it was realized that circadian genes expression is by no means limited to the SCN but can be found in cells throughout the body (46). Indeed, the cell-autonomous clock is ubiquitous (10, 127, 198), with most peripheral organs and tissues simultaneously exhibiting autonomous circadian oscillations and receiving signals from the SCN. In different cell types, the circadian oscillators respond differently to entraining signals. SCN gene expression responds rapidly to light, a tight coupling that is mediated by the neural connections from the SCN and the retina to the SCN. As a result, SCN gene expression entrains to a shifted light/dark schedule within a day (194). Interestingly, while other nonphotic stimuli, like a shifted feeding schedule, can dominate light in entraining behavioral and peripheral rhythms, the SCN is hard-wired to the light/dark rhythm.

Unlike the SCN, light exerts only a weak entraining effect on the liver. Experiments in the rat demonstrate the even after 16 days of an altered light/dark regimen, the liver clock does not completely adapt to the new schedule (194). In contrast, feeding is a potent zeitgeber for the liver circadian cycle. A restricted feeding protocol, in which mice are given food access for a limited period during the light (inactive) phase, almost immediately resets the phase of circadian gene expression in the liver (42, 169). Indeed, the liver circadian clock is one of the fastest tissue clocks to entrain to an altered feeding schedule, indicating that its coupling to food intake is significantly stronger than to peripheral or central oscillators. To understand the mechanism that underlies this entrainment, we conduct a simulation of day-time and night-time feeding. Simulation results indicate that the coupling of the liver circadian clock to mTORC1 plays a key role in its entrainment to an altered feeding schedule (Fig. 17).

The interactions between metabolism and circadian rhythms in humans can be gleaned from clinical observations in shift workers. Shift work involves alternations in feeding schedule and other zeitgebers. A higher incidence of diabetes, obesity, and cardiovascular events has been reported among shift workers (12, 168), although the underlying mechanisms have yet to be elucidated. Participants subjected to forced circadian misalignment (a simulation of shift work) have been found to exhibit insulin resistance and elevated blood pressure (161). Our simulation of nighttime feeding (one aspect of shift work) predicts lowered phosphorylated Akt levels, compared to daytime feedback. Phosphorylated Akt is essential to the translocation of GLUT4; thus, our result suggests that nighttime feedback may lead to

impaired glucose tolerance. It is noteworthy that patients with diabetes exhibit a dampened amplitude of circadian rhythms of insulin secretion (17) and glucose tolerance. Given this bidirectional nature of the relationship between circadian disruption and metabolic pathologies, circadian disruption may lead to a vicious cycle and contribute to the progression and worsening of metabolic diseases.

6.2.2 Ageing and the circadian rhythms

In ageing, a gradual decline is seen in a number of physiological functions, including the robustness of the circadian clock. Documented age-related changes in circadian rhythms include shortening of the circadian period (124, 139, 184, 186), alteration in the phase angle of entrainment to the light/dark cycle (124, 160, 202), fragmentation of the activity rhythm (160), decreased precision in the onset of daily activity (160, 202), and alterations in the response to the phase-shifting effects of light (153, 203) and nonphotic stimuli (176). These age-related changes in the circadian system may disrupt the proper phase relationships among numerous physiological and behavioral 24-h rhythms, as well as between these rhythms and daily environmental cycles. The disruption of those relations may negatively impact the organism's health and its adaptation to the environment (24).

The interactions between ageing and the circadian clock are complex and likely involve a bidirectional relationship (97, 100, 129). Possible mechanisms that contribute to the ageing of the circadian clock include changes in the SCN, including its structure (171, 206), neuronal coupling (115, 130, 159), and clock gene expression (115, 130, 159). The model presented in Chapter 4 focuses on the role of SIRT1 and NAD+. *In vitro*, SIRT1 regulates the acetylation of Bmal1 and Per2 in the mouse liver (7, 128) and human hepatocytes (181). SIRT1 expression in the mouse brain and liver decreases with age, and Sirt1 knockouts display a premature ageing phenotype, including disrupted activity rhythms comparable to those in aged (19–22 months) wild-type mice (32), as well as shortened lifespan and increased levels of proinflammatory markers in blood (181). The aged model in Chapter 4 predicts attenuated Bmal1, consistent with observations in a knockout of Sirt1 in the brain (32), and a shortened circadian period (Fig. 18). Taken together, model simulations and experimental findings concur on a role for an age-dependent decrease in SIRT1 activity in mediating changes in the molecular circadian clockwork (32, 195). Taken together, model simulations and experimental findings concur on a role for an age-dependent decrease in SIRT1 in mediating changes in the molecular circadian clockwork.

Circadian rhythm disturbances in the elderly are associated with a wide range of health conditions, including hypertension and cardiac insufficiency (1, 84, 105), impaired immune functions and increased susceptibility to disease (83), depression and poor cognitive and psychological functioning (123). Common treatments for circadian rhythm disorders in ageing include the use of melatonin(57, 67) and light therapy (121). Given the likely involvement of SIRT1 in the dysfunction of the circadian clock in ageing, therapies that elevate SIRT1 activity may restore the circadian rhythms and reverse other age-related effects. In recent studies, supplementation of NAD+ intermediates such as nicotinamide mononucleotide (NMN) and NR was reported to dramatically reverse the effects of ageing at the cellular and organismal levels (58). Importantly, NAD^+ intermediate supplementation appears to restore NAD^+ levels in both nuclear and mitochondrial compartments of cells, and the benefits of NAD^+ intermediate supplementation appear to be due to the reactivation of sirtuins. Given the role of the circadian clock in optimizing and maintaining health, some of the benefits of NAD+ intermediate supplementation may be attributed to the restoration of the circadian rhythms.

6.2.3 Dosing schedule and the circadian rhythms

In recent years, interest in resveratrol and NAD+ supplements has increased enormously after reports emerged on their benefits on metabolism and increased lifespan of various organisms(70, 75). Key molecular targets common to these drugs are SIRT1 and NAD+, both of which exhibit significant circadian variations (180). Thus, a salient question is: *To what extent do dosing times impact the anti-ageing effects of resveratrol and NAD+ supplements?* Indeed, the circadian rhythms have been known to modulate drug pharmacokinetics and pharmacodynamics (41). Experimental data involving targeted anticancer agents have indicated that both circadian timing and drug dosage are critical factors in determining systemic exposure and thus pharmacological effects. For example, Everolimus, an immunosuppressant that inhibits mTOR, exerts a higher antitumor efficacy if taken at ZT12 compared to ZT0 (134). A link between dosing schedule and drug efficacy was also revealed for a number of other anticancer drugs (96, 106, 201), analgesic (44, 86), antidiabetic drugs (122), and antibiotics (167).

The exact effect of dosing time on pharmacodynamics and pharmacokinetics depends on the drug and likely on patient characteristics. The present model focuses on one patient characteristic, age. We seek to answer the important clinical question: *Given the age of a patient, what is the best time to administer STACs or NAD+ supplements, to maximize the drugs' potential anti-ageing effects?* The answer depends, first of all, on the measure of drug efficacy. If the goal is to elevate peak SIRT1 (to

maximize physiological processes that activate above a SIRT1 threshold), then the best time to administer either STACs or NAD+ supplements is to coincide with the circadian peaks of NAD+ and SIRT1 in the control group (no drug), i.e., in the middle of the light periods (ZT6). If the goal is to maximize mean SIRT1, then the answer depends on the drug (STACs or NAD+ supplements) and on patient's age. For STACs, administering the drug in the young model at the beginning or end of the light periods (ZT12 or ZT24) yields a significant, albeit not drastic, improvement in terms of mean SIRT1, over administering it in the middle of the light periods (ZT6). The aged model is largely insensitive to dosing timing. For NAD+ supplements, administering the drug in the middle of the light periods (ZT6) yields the largest increase in mean SIRT1 in both models. These results are summarized in Figs. 19 and 20, panels B and C.

A noteworthy finding of this work is that caution should be taken when STACs or NAD+ supplements are to be taken early in the morning (ZT24). For STACs, not only does this timing yield the smallest increase in peak SIRT1, it may also have an undesirable side-effect of shifting the circadian clock (Figs. 19F and 19I). The model predicts a 7-hour shift, although in practice other zeitgebers and inputs will likely render the circadian clock more robust. For NAD+ supplements, this timing generates the smallest increases in both mean and peak SIRT1, and in the aged population, it may even lower the SIRT1 peak.

6.2.4 Comparison with previous models and future extension

In a recent study (63), Guerrero-Morín and Santillán studied the regulation of the circadian clock by coupling the minimal genetic oscillator model by Goodwin(59) with a simple mTORC1 activation model. That Goodwin model represents the feedback loop involving BMAL1, PER, and CRY, and can reproduce features of circadian oscillators such as light entrainment. However, it neglects the feedback loop involving BMAL1, REV-ERB, and ROR. That model (63) only considers the unidirectional control of BMAL1 by mTROC1, but not the circadian regulation of metabolism, or the influence of other metabolic sensors (e.g., AMPK) on the circadian rhythms.

The goal of this work is to better understand the bidirectional interactions among metabolism and the circadian clock, and how those interactions changes in ageing and pharmacological manipulation. To achieve that goal, we have developed a more comprehensive mathematical model of circadian rhythms and metabolism. We adopt the mammalian liver circadian clock model by Woller et al. (188). In addition to the dynamics of the core clock regulatory network, that model also incorporates metabolic sensors

SIRT1 and AMPK, and represents additional mechanisms through which metabolism drives the clock. Specifically, the model (188) simulates the action of SIRT1 in modulating the transcriptional activity of CLOCK:BMAL1 and destabilizing PER2. SIRT1 also activates PGC1a, which co-activates ROR and increases Bmal1 expression. But before PGC1a can be deacetylated by SIRT1, phosphorylation by AMPK is required. Additionally, activated AMPK destabilizes PER and CRY.

While the model by Woller et al. can predict how the activation of AMPK alters the circadian clock, (i) the AMPK level is assumed known *a priori*, and (ii) their model does not consider the role of mTORC1, which plays a central role in regulating fundamental cell processes, from protein synthesis to autophagy, and the signaling of which when dysregulated is implicated in the progression of cancer and diabetes, as well as the ageing process. Thus, we couple the circadian clock model (188) to our published model of insulin pathway (154), which includes the insulin/IGF-1 pathway, mTORC1, and AMPK, and predicts how mTORC1, AMPK, and SIRT1 respond to variations in energy and nutrient abundance. The insulin pathway and mTORC1 model (154) and the circadian clock model (188) are coupled by representing the increase of BMAL1 protein expression by mTORC1 (107, 143), and the inhibition of mTORC1 phosphorylation by BMAL1 and PER2 (190).

The present model provides a state-of-the-art computational platform for investigating the interplay among ageing, metabolism, and circadian rhythms. Model simulations have identified altered mTORC1 signaling as a mechanism leading to clock disruption and its associated metabolic effects, and suggested a pharmacological approach to resetting the clock in obesity and metabolic diseases. Further, mTORC1 signaling is switched on by a number of oncogenic signaling pathways and may be hyperactive in up to 70% of all human tumors (50). Thus, there is much interest in targeting mTORC1 signaling as a potential therapeutic avenue for anti-cancer therapy. The potential effect of these treatments on the circadian clock may be studied using the present model.

A limitation of the present model is that it considers only the influence of variations in mTORC1, AMPK, and SIRT1, and neglects the influence of systemic signals from the SCN. This simplification is justified for the liver circadian clock, the entrainment phase of which is determined primarily by the feeding schedule. If the present model is to be adapted to other peripheral circadian clocks, the SCN inputs should be incorporated.

Bibliography

1. **Ahmed S and Layton AT.** Sex-specific computational models for blood pressure regulation in the rat. *Am J Physiol Renal Physiol*, 2019.
2. **Akhtar RA, Reddy AB, Maywood ES, Clayton JD, King VM, Smith AG, Gant TW, Hastings MH, and Kyriacou CP.** Circadian cycling of the mouse liver transcriptome, as revealed by cDNA microarray, is driven by the suprachiasmatic nucleus. *Current biology* 12: 540-550, 2002.
3. **Aksamitiene E, Kholodenko BN, Kolch W, Hoek JB, and Kiyatkin A.** PI3K/Akt-sensitive MEK-independent compensatory circuit of ERK activation in ER-positive PI3K-mutant T47D breast cancer cells. *Cellular signalling* 22: 1369-1378, 2010.
4. **Araujo RP, Liotta LA, and Petricoin EF.** Proteins, drug targets and the mechanisms they control: the simple truth about complex networks. *Nature reviews Drug discovery* 6: 871-880, 2007.
5. **Arriola Apelo SI, Neuman JC, Baar EL, Syed FA, Cummings NE, Brar HK, Pumper CP, Kimple ME, and Lamming DW.** Alternative rapamycin treatment regimens mitigate the impact of rapamycin on glucose homeostasis and the immune system. *Aging cell* 15: 28-38, 2016.
6. **Arriola Apelo SI, Pumper CP, Baar EL, Cummings NE, and Lamming DW.** Intermittent administration of rapamycin extends the life span of female C57BL/6J mice. *Journals of Gerontology Series A: Biomedical Sciences and Medical Sciences* 71: 876-881, 2016.
7. **Asher G, Gatfield D, Stratmann M, Reinke H, Dibner C, Kreppel F, Mostoslavsky R, Alt FW, and Schibler U.** SIRT1 regulates circadian clock gene expression through PER2 deacetylation. *Cell* 134: 317-328, 2008.
8. **Ayyadevara S, Alla R, Thaden JJ, and Shmookler Reis RJ.** Remarkable longevity and stress resistance of nematode PI3K-null mutants. *Aging cell* 7: 13-22, 2008.
9. **Baar EL, Carbajal KA, Ong IM, and Lamming DW.** Sex-and tissue-specific changes in mTOR signaling with age in C57 BL/6J mice. *Aging cell* 15: 155-166, 2016.
10. **Balsalobre A, Damiola F, and Schibler U.** A serum shock induces circadian gene expression in mammalian tissue culture cells. *Cell* 93: 929-937, 1998.
11. **Bar-Peled L, Chantranupong L, Cherniack AD, Chen WW, Ottina KA, Grabiner BC, Spear ED, Carter SL, Meyerson M, and Sabatini DM.** A Tumor suppressor complex with GAP activity for the Rag GTPases that signal amino acid sufficiency to mTORC1. *Science* 340: 1100-1106, 2013.
12. **Bass J and Takahashi JS.** Circadian integration of metabolism and energetics. *Science* 330: 1349-1354, 2010.
13. **Benjamin D, Colombi M, Moroni C, and Hall MN.** Rapamycin passes the torch: a new generation of mTOR inhibitors. *Nature reviews Drug discovery* 10: 868-880, 2011.
14. **Berchtold NC, Cribbs DH, Coleman PD, Rogers J, Head E, Kim R, Beach T, Miller C, Troncoso J, and Trojanowski JQ.** Gene expression changes in the course of normal brain aging are sexually dimorphic. *Proceedings of the National Academy of Sciences* 105: 15605-15610, 2008.
15. **Bibi Z, Ahmad J, Siddiqa A, Paracha RZ, Saeed T, Ali A, Janjua HA, Ullah S, Ben Abdallah E, and Roux O.** Formal modeling of mTOR associated biological regulatory network reveals novel therapeutic strategy for the treatment of cancer. *Frontiers in physiology* 8: 416, 2017.
16. **Bockwoldt M, Houry D, Niere M, Gossmann TI, Reinartz I, Schug A, Ziegler M, and Heiland I.** Identification of evolutionary and kinetic drivers of NAD-dependent signaling. *Proceedings of the National Academy of Sciences* 116: 15957-15966, 2019.
17. **Boden G, Chen X, and Polansky M.** Disruption of circadian insulin secretion is associated with reduced glucose uptake in first-degree relatives of patients with type 2 diabetes. *Diabetes* 48: 2182-2188, 1999.

18. **Bordone L, Motta MC, Picard F, Robinson A, Jhala US, Apfeld J, McDonagh T, Lemieux M, McBurney M, and Szilvasi A.** Sirt1 regulates insulin secretion by repressing UCP2 in pancreatic β cells. *PLoS Biol* 4: e31, 2005.
19. **Borisov N, Aksamitiene E, Kiyatkin A, Legewie S, Berkhout J, Maiwald T, Kaimachnikov NP, Timmer J, Hoek JB, and Kholodenko BN.** Systems-level interactions between insulin–EGF networks amplify mitogenic signaling. *Molecular systems biology* 5: 256, 2009.
20. **Bouchard VJ, Rouleau M, and Poirier GG.** PARP-1, a determinant of cell survival in response to DNA damage. *Experimental hematology* 31: 446-454, 2003.
21. **Brachmann SM, Hofmann I, Schnell C, Fritsch C, Wee S, Lane H, Wang S, Garcia-Echeverria C, and Maira S-M.** Specific apoptosis induction by the dual PI3K/mTor inhibitor NVP-BEZ235 in HER2 amplified and PIK3CA mutant breast cancer cells. *Proceedings of the National Academy of Sciences* 106: 22299-22304, 2009.
22. **Braidy N, Poljak A, Grant R, Jayasena T, Mansour H, Chan-Ling T, Guillemin GJ, Smythe G, and Sachdev P.** Mapping NAD+ metabolism in the brain of ageing Wistar rats: potential targets for influencing brain senescence. *Biogerontology* 15: 177-198, 2014.
23. **Brandauer J, Vienberg SG, Andersen MA, Ringholm S, Risis S, Larsen PS, Kristensen JM, Frøsig C, Leick L, and Fentz J.** AMP-activated protein kinase regulates nicotinamide phosphoribosyl transferase expression in skeletal muscle. *The Journal of physiology* 591: 5207-5220, 2013.
24. **Brock MA.** Chronobiology and aging. *Journal of the American Geriatrics Society* 39: 74-91, 1991.
25. **Brunet A, Datta SR, and Greenberg ME.** Transcription-dependent and-independent control of neuronal survival by the PI3K–Akt signaling pathway. *Current opinion in neurobiology* 11: 297-305, 2001.
26. **Brunn GJ, Williams J, Sabers C, Wiederrecht G, Lawrence Jr J, and Abraham RT.** Direct inhibition of the signaling functions of the mammalian target of rapamycin by the phosphoinositide 3-kinase inhibitors, wortmannin and LY294002. *The EMBO journal* 15: 5256-5267, 1996.
27. **Budanov AV and Karin M.** p53 target genes sestrin1 and sestrin2 connect genotoxic stress and mTOR signaling. *Cell* 134: 451-460, 2008.
28. **Bugge A, Feng D, Everett LJ, Briggs ER, Mullican SE, Wang F, Jager J, and Lazar MA.** Rev-erbα and Rev-erbβ coordinately protect the circadian clock and normal metabolic function. *Genes & development* 26: 657-667, 2012.
29. **Bulterijs S, Hull RS, Björk VC, and Roy AG.** It is time to classify biological aging as a disease. *Frontiers in genetics* 6: 205, 2015.
30. **Camacho-Pereira J, Tarragó MG, Chini CC, Nin V, Escande C, Warner GM, Puranik AS, Schoon RA, Reid JM, and Galina A.** CD38 dictates age-related NAD decline and mitochondrial dysfunction through an SIRT3-dependent mechanism. *Cell metabolism* 23: 1127-1139, 2016.
31. **Cao D, Wang M, Qiu X, Liu D, Jiang H, Yang N, and Xu R-M.** Structural basis for allosteric, substrate-dependent stimulation of SIRT1 activity by resveratrol. *Genes & development* 29: 1316-1325, 2015.
32. **Chang H-C and Guarente L.** SIRT1 mediates central circadian control in the SCN by a mechanism that decays with aging. *Cell* 153: 1448-1460, 2013.
33. **Chantranupong L, Scaria SM, Saxton RA, Gygi MP, Shen K, Wyant GA, Wang T, Harper JW, Gygi SP, and Sabatini DM.** The CASTOR proteins are arginine sensors for the mTORC1 pathway. *Cell* 165: 153-164, 2016.
34. **Chen WY, Wang DH, Yen RC, Luo J, Gu W, and Baylin SB.** Tumor suppressor HIC1 directly regulates SIRT1 to modulate p53-dependent DNA-damage responses. *Cell* 123: 437-448, 2005.

35. **Cho H, Zhao X, Hatori M, Ruth TY, Barish GD, Lam MT, Chong L-W, DiTacchio L, Atkins AR, and Glass CK.** Regulation of circadian behaviour and metabolism by REV-ERB-α and REV-ERB-β. *Nature* 485: 123-127, 2012.
36. **Comet J-P, Bernot G, Das A, Diener F, Massot C, and Cessieux A.** Simplified models for the mammalian circadian clock. *Procedia Computer Science* 11: 127-138, 2012.
37. **Coughlan KA, Valentine RJ, Ruderman NB, and Saha AK.** Nutrient excess in AMPK downregulation and insulin resistance. *Journal of endocrinology, diabetes & obesity* 1: 1008, 2013.
38. **D'Alessandro M, Beesley S, Kim JK, Chen R, Abich E, Cheng W, Yi P, Takahashi JS, and Lee C.** A tunable artificial circadian clock in clock-defective mice. *Nature communications* 6: 1-11, 2015.
39. **Dalle Pezze P, Nelson G, Otten EG, Korolchuk VI, Kirkwood TB, von Zglinicki T, and Shanley DP.** Dynamic modelling of pathways to cellular senescence reveals strategies for targeted interventions. *PLoS Comput Biol* 10: e1003728, 2014.
40. **Dalle Pezze P, Ruf S, Sonntag AG, Langelaar-Makkinje M, Hall P, Heberle AM, Navas PR, Van Eunen K, Tölle RC, and Schwarz JJ.** A systems study reveals concurrent activation of AMPK and mTOR by amino acids. *Nature communications* 7: 1-19, 2016.
41. **Dallmann R, Brown SA, and Gachon F.** Chronopharmacology: new insights and therapeutic implications. *Annual review of pharmacology and toxicology* 54: 339-361, 2014.
42. **Damiola F, Le Minh N, Preitner N, Kornmann B, Fleury-Olela F, and Schibler U.** Restricted feeding uncouples circadian oscillators in peripheral tissues from the central pacemaker in the suprachiasmatic nucleus. *Genes & development* 14: 2950-2961, 2000.
43. **de Figueiredo LF, Gossmann TI, Ziegler M, and Schuster S.** Pathway analysis of NAD+ metabolism. *Biochemical Journal* 439: 341-348, 2011.
44. **DeBruyne JP, Weaver DR, and Dallmann R.** The hepatic circadian clock modulates xenobiotic metabolism in mice. *Journal of biological rhythms* 29: 277-287, 2014.
45. **Desa U.** United nations department of economic and social affairs, population division. world population prospects: The 2015 revision, key findings and advance tables. In: *Technical Report: Working Paper No. ESA/P/WP. 241*, 2015.
46. **Dibner C, Schibler U, and Albrecht U.** The mammalian circadian timing system: organization and coordination of central and peripheral clocks. *Annual review of physiology* 72: 517-549, 2010.
47. **Eckel-Mahan K and Sassone-Corsi P.** Metabolism and the circadian clock converge. *Physiological reviews* 93: 107-135, 2013.
48. **Fisher DA.** Physiological variations in thyroid hormones: physiological and pathophysiological considerations. *Clinical Chemistry* 42: 135-139, 1996.
49. **Floc'h N, Kinkade CW, Kobayashi T, Aytes A, Lefebvre C, Mitrofanova A, Cardiff RD, Califano A, Shen MM, and Abate-Shen C.** Dual targeting of the Akt/mTOR signaling pathway inhibits castration-resistant prostate cancer in a genetically engineered mouse model. *Cancer research* 72: 4483-4493, 2012.
50. **Forbes SA, Bindal N, Bamford S, Cole C, Kok CY, Beare D, Jia M, Shepherd R, Leung K, and Menzies A.** COSMIC: mining complete cancer genomes in the Catalogue of Somatic Mutations in Cancer. *Nucleic acids research* 39: D945-D950, 2010.
51. **Forger DB and Peskin CS.** A detailed predictive model of the mammalian circadian clock. *Proceedings of the National Academy of Sciences* 100: 14806-14811, 2003.
52. **Forger DB and Peskin CS.** Stochastic simulation of the mammalian circadian clock. *Proceedings of the National Academy of Sciences* 102: 321-324, 2005.
53. **Fraenkel M, Ketzinel-Gilad M, Ariav Y, Pappo O, Karaca M, Castel J, Berthault M-F, Magnan C, Cerasi E, and Kaiser N.** mTOR inhibition by rapamycin prevents β-cell adaptation to hyperglycemia and exacerbates the metabolic state in type 2 diabetes. *Diabetes* 57: 945-957, 2008.

54. **Francaux M, Demeulder B, Naslain D, Fortin R, Lutz O, Caty G, and Deldicque L.** Aging reduces the activation of the mTORC1 pathway after resistance exercise and protein intake in human skeletal muscle: potential role of REDD1 and impaired anabolic sensitivity. *Nutrients* 8: 47, 2016.
55. **Fry CS, Drummond MJ, Glynn EL, Dickinson JM, Gundermann DM, Timmerman KL, Walker DK, Dhanani S, Volpi E, and Rasmussen BB.** Aging impairs contraction-induced human skeletal muscle mTORC1 signaling and protein synthesis. *Skeletal muscle* 1: 1-11, 2011.
56. **Funakoshi M, Tsuda M, Muramatsu K, Hatsuda H, Morishita S, and Aigaki T.** A gain-of-function screen identifies wdb and lkb1 as lifespan-extending genes in Drosophila. *Biochemical and biophysical research communications* 405: 667-672, 2011.
57. **Garfinkel D, Laudon M, Nof D, and Zisapel N.** Improvement of sleep quality in elderly people by controlled-release melatonin. *The Lancet* 346: 541-544, 1995.
58. **Gomes AP, Price NL, Ling AJ, Moslehi JJ, Montgomery MK, Rajman L, White JP, Teodoro JS, Wrann CD, and Hubbard BP.** Declining NAD+ induces a pseudohypoxic state disrupting nuclear-mitochondrial communication during aging. *Cell* 155: 1624-1638, 2013.
59. **Goodwin BC.** Oscillatory behavior in enzymatic control processes. *Advances in enzyme regulation* 3: 425-437, 1965.
60. **Granados-Fuentes D, Prolo LM, Abraham U, and Herzog ED.** The suprachiasmatic nucleus entrains, but does not sustain, circadian rhythmicity in the olfactory bulb. *Journal of Neuroscience* 24: 615-619, 2004.
61. **Griffith J.** Mathematics of cellular control processes I. Negative feedback to one gene. *Journal of theoretical biology* 20: 202-208, 1968.
62. **Grzmil M and Hemmings BA.** Overcoming resistance to rapalogs in gliomas by combinatory therapies. *Biochimica et Biophysica Acta (BBA)-Proteins and Proteomics* 1834: 1371-1380, 2013.
63. **Guerrero-Morín JG and Santillán M.** Crosstalk dynamics between the circadian clock and the mTORC1 pathway. *Journal of Theoretical Biology*: 110360, 2020.
64. **Guillaumond F, Dardente H, Giguère V, and Cermakian N.** Differential control of Bmal1 circadian transcription by REV-ERB and ROR nuclear receptors. *Journal of biological rhythms* 20: 391-403, 2005.
65. **Guo S and Sonenshein GE.** Forkhead box transcription factor FOXO3a regulates estrogen receptor alpha expression and is repressed by the Her-2/neu/phosphatidylinositol 3-kinase/Akt signaling pathway. *Molecular and cellular biology* 24: 8681-8690, 2004.
66. **Gwinn DM, Shackelford DB, Egan DF, Mihaylova MM, Mery A, Vasquez DS, Turk BE, and Shaw RJ.** AMPK phosphorylation of raptor mediates a metabolic checkpoint. *Molecular cell* 30: 214-226, 2008.
67. **Haimov I, Lavie P, Laudon M, Herer P, Vigder C, and Zisapel N.** Melatonin replacement therapy of elderly insomniacs. *Sleep* 18: 598-603, 1995.
68. **Hariharan N, Maejima Y, Nakae J, Paik J, DePinho RA, and Sadoshima J.** Deacetylation of FoxO by Sirt1 plays an essential role in mediating starvation-induced autophagy in cardiac myocytes. *Circulation research* 107: 1470-1482, 2010.
69. **Harrison DE, Strong R, Sharp ZD, Nelson JF, Astle CM, Flurkey K, Nadon NL, Wilkinson JE, Frenkel K, and Carter CS.** Rapamycin fed late in life extends lifespan in genetically heterogeneous mice. *nature* 460: 392-395, 2009.
70. **Hashimoto T, Horikawa M, Nomura T, and Sakamoto K.** Nicotinamide adenine dinucleotide extends the lifespan of Caenorhabditis elegans mediated by sir-2.1 and daf-16. *Biogerontology* 11: 31, 2010.
71. **Hinnells JR.** Persian Mythology; 1997: Chancellor Press, imprint of.
72. **Ho A, Cho C-S, Namkoong S, Cho U-S, and Lee JH.** Biochemical basis of sestrin physiological activities. *Trends in biochemical sciences* 41: 621-632, 2016.

73. **Hosokawa N, Hara T, Kaizuka T, Kishi C, Takamura A, Miura Y, Iemura S-i, Natsume T, Takehana K, and Yamada N.** Nutrient-dependent mTORC1 association with the ULK1–Atg13–FIP200 complex required for autophagy. *Molecular biology of the cell* 20: 1981-1991, 2009.
74. **Houde VP, Brûlé S, Festuccia WT, Blanchard P-G, Bellmann K, Deshaies Y, and Marette A.** Chronic rapamycin treatment causes glucose intolerance and hyperlipidemia by upregulating hepatic gluconeogenesis and impairing lipid deposition in adipose tissue. *Diabetes* 59: 1338-1348, 2010.
75. **Howitz KT, Bitterman KJ, Cohen HY, Lamming DW, Lavu S, Wood JG, Zipkin RE, Chung P, Kisielewski A, and Zhang L-L.** Small molecule activators of sirtuins extend Saccharomyces cerevisiae lifespan. *Nature* 425: 191-196, 2003.
76. **Hsieh AC, Liu Y, Edlind MP, Ingolia NT, Janes MR, Sher A, Shi EY, Stumpf CR, Christensen C, and Bonham MJ.** The translational landscape of mTOR signalling steers cancer initiation and metastasis. *Nature* 485: 55-61, 2012.
77. **Hua X, Xu J, Deng X, Xu J, Li J, Zhu DQ, Zhu J, Jin H, Tian Z, and Huang H.** New compound ChlA-F induces autophagy-dependent anti-cancer effect via upregulating Sestrin-2 in human bladder cancer. *Cancer letters* 436: 38-51, 2018.
78. **Hughes ME, DiTacchio L, Hayes KR, Vollmers C, Pulivarthy S, Baggs JE, Panda S, and Hogenesch JB.** Harmonics of circadian gene transcription in mammals. *PLoS Genet* 5: e1000442, 2009.
79. **Ikenoue T, Inoki K, Yang Q, Zhou X, and Guan KL.** Essential function of TORC2 in PKC and Akt turn motif phosphorylation, maturation and signalling. *The EMBO journal* 27: 1919-1931, 2008.
80. **Imai S-i and Guarente L.** NAD+ and sirtuins in aging and disease. *Trends in cell biology* 24: 464-471, 2014.
81. **Imai S-i and Yoshino J.** The importance of NAMPT/NAD/SIRT1 in the systemic regulation of metabolism and ageing. *Diabetes, Obesity and Metabolism* 15: 26-33, 2013.
82. **Ingram DK, Zhu M, Mamczarz J, Zou S, Lane MA, Roth GS, and DeCabo R.** Calorie restriction mimetics: an emerging research field. *Aging cell* 5: 97-108, 2006.
83. **Irwin M, McClintick J, Costlow C, Fortner M, White J, and Gillin JC.** Partial night sleep deprivation reduces natural killer and celhdar immune responses in humans. *The FASEB journal* 10: 643-653, 1996.
84. **Jensen E, Dehlin O, Hagberg B, Samuelsson G, and Svensson T.** Insomnia in an 80-year-old population: Relationship to medical, psychological and social factors. *Journal of Sleep Research* 7: 183-189, 1998.
85. **Jeong J-K, Moon M-H, Bae B-C, Lee Y-J, Seol J-W, Kang H-S, Kim J-S, Kang S-J, and Park S-Y.** Autophagy induced by resveratrol prevents human prion protein-mediated neurotoxicity. *Neuroscience research* 73: 99-105, 2012.
86. **Johnson BP, Walisser JA, Liu Y, Shen AL, McDearmon EL, Moran SM, McIntosh BE, Vollrath AL, Schook AC, and Takahashi JS.** Hepatocyte circadian clock controls acetaminophen bioactivation through NADPH-cytochrome P450 oxidoreductase. *Proceedings of the National Academy of Sciences* 111: 18757-18762, 2014.
87. **Johnson SC, Rabinovitch PS, and Kaeberlein M.** mTOR is a key modulator of ageing and age-related disease. *Nature* 493: 338-345, 2013.
88. **Jung J, Genau HM, and Behrends C.** Amino acid-dependent mTORC1 regulation by the lysosomal membrane protein SLC38A9. *Molecular and cellular biology* 35: 2479-2494, 2015.
89. **Kaminsky YG, Kosenko EA, and Kondrashova MN.** Analysis of the circadian rhythm in energy metabolism of rat liver. *International journal of Biochemistry* 16: 629-639, 1984.
90. **Kanis JA.** Assessment of fracture risk and its application to screening for postmenopausal osteoporosis: synopsis of a WHO report. *Osteoporosis international* 4: 368-381, 1994.

91. **Karlsson BH, Knutsson AK, Lindahl BO, and Alfredsson LS.** Metabolic disturbances in male workers with rotating three-shift work. Results of the WOLF study. *International archives of occupational and environmental health* 76: 424-430, 2003.
92. **Kim J, Kundu M, Viollet B, and Guan K-L.** AMPK and mTOR regulate autophagy through direct phosphorylation of Ulk1. *Nature cell biology* 13: 132-141, 2011.
93. **Kim JK and Forger DB.** A mechanism for robust circadian timekeeping via stoichiometric balance. *Molecular systems biology* 8: 630, 2012.
94. **Kim Y-M, Jung CH, Seo M, Kim EK, Park J-M, Bae SS, and Kim D-H.** mTORC1 phosphorylates UVRAG to negatively regulate autophagosome and endosome maturation. *Molecular cell* 57: 207-218, 2015.
95. **Klein DC and Weller JL.** Indole metabolism in the pineal gland: a circadian rhythm in N-acetyltransferase. *Science* 169: 1093-1095, 1970.
96. **Kloth JS, Binkhorst L, de Wit AS, de Bruijn P, Hamberg P, Lam MH, Burger H, Chaves I, Wiemer EA, and van der Horst GT.** Relationship between sunitinib pharmacokinetics and administration time: preclinical and clinical evidence. *Clinical pharmacokinetics* 54: 851-858, 2015.
97. **Kondratov RV, Kondratova AA, Gorbacheva VY, Vykhovanets OV, and Antoch MP.** Early aging and age-related pathologies in mice deficient in BMAL1, the core componentof the circadian clock. *Genes & development* 20: 1868-1873, 2006.
98. **Kondratova AA and Kondratov RV.** The circadian clock and pathology of the ageing brain. *Nature Reviews Neuroscience* 13: 325-335, 2012.
99. **Kriete A, Bosl WJ, and Booker G.** Rule-based cell systems model of aging using feedback loop motifs mediated by stress responses. *PLoS Comput Biol* 6: e1000820, 2010.
100. **Krishnan N, Kretzschmar D, Rakshit K, Chow E, and Giebultowicz JM.** The circadian clock gene period extends healthspan in aging Drosophila melanogaster. *Aging (Albany NY)* 1: 937, 2009.
101. **Kuepfer L, Peter M, Sauer U, and Stelling J.** Ensemble modeling for analysis of cell signaling dynamics. *Nature biotechnology* 25: 1001-1006, 2007.
102. **Lamming DW, Ye L, Katajisto P, Goncalves MD, Saitoh M, Stevens DM, Davis JG, Salmon AB, Richardson A, and Ahima RS.** Rapamycin-induced insulin resistance is mediated by mTORC2 loss and uncoupled from longevity. *science* 335: 1638-1643, 2012.
103. **Laplante M and Sabatini DM.** mTOR signaling in growth control and disease. *Cell* 149: 274-293, 2012.
104. **Lee IH, Cao L, Mostoslavsky R, Lombard DB, Liu J, Bruns NE, Tsokos M, Alt FW, and Finkel T.** A role for the NAD-dependent deacetylase Sirt1 in the regulation of autophagy. *Proceedings of the National Academy of Sciences* 105: 3374-3379, 2008.
105. **Leete J and Layton AT.** Sex-specific long-term blood pressure regulation: Modeling and analysis. *Comput Biol Med* 104: 139-148, 2019.
106. **Li Z, Yan S, Attayan N, Ramalingam S, and Thiele CJ.** Combination of an allosteric Akt Inhibitor MK-2206 with etoposide or rapamycin enhances the antitumor growth effect in neuroblastoma. *Clinical Cancer Research* 18: 3603-3615, 2012.
107. **Lipton JO, Boyle LM, Yuan ED, Hochstrasser KJ, Chifamba FF, Nathan A, Tsai PT, Davis F, and Sahin M.** Aberrant proteostasis of BMAL1 underlies circadian abnormalities in a paradigmatic mTOR-opathy. *Cell reports* 20: 868-880, 2017.
108. **Liu AC, Tran HG, Zhang EE, Priest AA, Welsh DK, and Kay SA.** Redundant function of REV-ERBα and β and non-essential role for Bmal1 cycling in transcriptional regulation of intracellular circadian rhythms. *PLoS Genet* 4: e1000023, 2008.
109. **Liu B, Oltvai ZN, Bayır H, Silverman GA, Pak SC, Perlmutter DH, and Bahar I.** Quantitative assessment of cell fate decision between autophagy and apoptosis. *Scientific reports* 7: 1-14, 2017.

110. **Liu GY and Sabatini DM.** mTOR at the nexus of nutrition, growth, ageing and disease. *Nature Reviews Molecular Cell Biology*: 1-21, 2020.
111. **Maiuri MC, Malik SA, Morselli E, Kepp O, Criollo A, Mouchel P-L, Carnuccio R, and Kroemer G.** Stimulation of autophagy by the p53 target gene Sestrin2. *Cell cycle* 8: 1571-1576, 2009.
112. **Martins R, Lithgow GJ, and Link W.** Long live FOXO: unraveling the role of FOXO proteins in aging and longevity. *Aging cell* 15: 196-207, 2016.
113. **Massudi H, Grant R, Braidy N, Guest J, Farnsworth B, and Guillemin GJ.** Age-associated changes in oxidative stress and NAD+ metabolism in human tissue. *PloS one* 7: e42357, 2012.
114. **Massudi H, Grant R, Guillemin GJ, and Braidy N.** NAD+ metabolism and oxidative stress: the golden nucleotide on a crown of thorns. *Redox Report* 17: 28-46, 2012.
115. **Masuda T, Watanabe Y, Fukuda K, Watanabe M, Onishi A, Ohara K, Imai T, Koepsell H, Muto S, Vallon V, and Nagata D.** Unmasking a sustained negative effect of SGLT2 inhibition on body fluid volume in the rat. *Am J Physiol Renal Physiol* 315: F653-F664, 2018.
116. **Menon S and Manning BD.** Common corruption of the mTOR signaling network in human tumors. *Oncogene* 27: S43-S51, 2008.
117. **Mettinger TN.** *The Eden Narrative: A Literary and Religio-historical Study of Genesis 2-3*: Eisenbrauns, 2007.
118. **Mi W, Ye Q, Liu S, and She Q-B.** AKT inhibition overcomes rapamycin resistance by enhancing the repressive function of PRAS40 on mTORC1/4E-BP1 axis. *Oncotarget* 6: 13962, 2015.
119. **Millar-Craig M, Bishop C, and Raftery E.** Circadian variation of blood-pressure. *The Lancet* 311: 795-797, 1978.
120. **Milne JC, Lambert PD, Schenk S, Carney DP, Smith JJ, Gagne DJ, Jin L, Boss O, Perni RB, and Vu CB.** Small molecule activators of SIRT1 as therapeutics for the treatment of type 2 diabetes. *Nature* 450: 712-716, 2007.
121. **Mishima E, Fukuda S, Kanemitsu Y, Saigusa D, Mukawa C, Asaji K, Matsumoto Y, Tsukamoto H, Tachikawa T, Tsukimi T, Fukuda NN, Ho HJ, Kikuchi K, Suzuki C, Nanto F, Suzuki T, Ito S, Soga T, Tomioka Y, and Abe T.** Canagliflozin reduces plasma uremic toxins and alters the intestinal microbiota composition in a chronic kidney disease mouse model. *Am J Physiol Renal Physiol* 315: F824-F833, 2018.
122. **Miyazaki M, Fujii T, Takeda N, Magotani H, Iwanaga K, and Kakemi M.** Chronopharmacological assessment identified GLUT4 as a responsible factor for the circadian variation of the hypoglycemic effect of tolbutamide in rats. *Drug metabolism and pharmacokinetics*: 1106210195-1106210195, 2011.
123. **Moe KE, Vitiello MV, Larsen LH, and Prinz PN.** Sleep/wake patterns in Alzheimer's disease: relationships with cognition and function. *Journal of sleep research* 4: 15-20, 1995.
124. **Morin LP.** Age-related changes in hamster circadian period, entrainment, and rhythm splitting. *Journal of Biological Rhythms* 3: 237-248, 1988.
125. **Muller JE, Stone PH, Turi ZG, Rutherford JD, Czeisler CA, Parker C, Poole WK, Passamani E, Roberts R, and Robertson T.** Circadian variation in the frequency of onset of acute myocardial infarction. *New England Journal of Medicine* 313: 1315-1322, 1985.
126. **Myers KA and Scheffer IE.** DEPDC5 as a potential therapeutic target for epilepsy. *Expert Opinion on Therapeutic Targets* 21: 591-600, 2017.
127. **Nagoshi E, Saini C, Bauer C, Laroche T, Naef F, and Schibler U.** Circadian gene expression in individual fibroblasts: cell-autonomous and self-sustained oscillators pass time to daughter cells. *Cell* 119: 693-705, 2004.
128. **Nakahata Y, Kaluzova M, Grimaldi B, Sahar S, Hirayama J, Chen D, Guarente LP, and Sassone-Corsi P.** The NAD+-dependent deacetylase SIRT1 modulates CLOCK-mediated chromatin remodeling and circadian control. *Cell* 134: 329-340, 2008.

129. **Nakahata Y, Sahar S, Astarita G, Kaluzova M, and Sassone-Corsi P.** Circadian control of the NAD+ salvage pathway by CLOCK-SIRT1. *Science* 324: 654-657, 2009.
130. **Nakamura TJ, Nakamura W, Yamazaki S, Kudo T, Cutler T, Colwell CS, and Block GD.** Age-related decline in circadian output. *Journal of Neuroscience* 31: 10201-10205, 2011.
131. **Nemoto S, Fergusson MM, and Finkel T.** Nutrient availability regulates SIRT1 through a forkhead-dependent pathway. *Science* 306: 2105-2108, 2004.
132. **Nguyen LK and Kholodenko BN.** Feedback regulation in cell signalling: Lessons for cancer therapeutics. *Seminars in cell & developmental biology*. Elsevier, 2016, p. 85-94.
133. **Nogiec C, Burkart A, Dreyfuss JM, Lerin C, Kasif S, and Patti M-E.** Metabolic modeling of muscle metabolism identifies key reactions linked to insulin resistance phenotypes. *Molecular metabolism* 4: 151-163, 2015.
134. **Okazaki H, Matsunaga N, Fujioka T, Okazaki F, Akagawa Y, Tsurudome Y, Ono M, Kuwano M, Koyanagi S, and Ohdo S.** Circadian regulation of mTOR by the ubiquitin pathway in renal cell carcinoma. *Cancer research* 74: 543-551, 2014.
135. **Ondracek CR, Frappier V, Ringel AE, Wolberger C, and Guarente L.** Mutations that Allow SIR2 Orthologs to Function in a NAD+-Depleted Environment. *Cell reports* 18: 2310-2319, 2017.
136. **Pasha M, Eid AH, Eid AA, Gorin Y, and Munusamy S.** Sestrin2 as a novel biomarker and therapeutic target for various diseases. *Oxidative medicine and cellular longevity* 2017, 2017.
137. **PERIOD YS.** LUCIFERASE real-time reporting of circadian dynamics reveals persistent circadian oscillations in mouse peripheral tissues. *Proc Natl Acad Sci USA* 101: 5339-5346, 2004.
138. **Petrich AM, Leshchenko V, Kuo P-Y, Xia B, Thirukonda VK, Ulahannan N, Gordon S, Fazzari MJ, Ye BH, and Sparano JA.** Akt inhibitors MK-2206 and nelfinavir overcome mTOR inhibitor resistance in diffuse large B-cell lymphoma. *Clinical Cancer Research* 18: 2534-2544, 2012.
139. **Pittendrigh CS and Daan S.** Circadian oscillations in rodents: a systematic increase of their frequency with age. *Science* 186: 548-550, 1974.
140. **Podkolodnaya OA, Tverdokhleb NN, and Podkolodnyy NL.** Computational modeling of the cell-autonomous mammalian circadian oscillator. *BMC systems biology* 11: 27-42, 2017.
141. **Preitner N, Damiola F, Zakany J, Duboule D, Albrecht U, and Schibler U.** The orphan nuclear receptor REV-ERBα controls circadian transcription within the positive limb of the mammalian circadian oscillator. *Cell* 110: 251-260, 2002.
142. **Qin X, Jiang B, and Zhang Y.** 4E-BP1, a multifactor regulated multifunctional protein. *Cell cycle* 15: 781-786, 2016.
143. **Ramanathan C, Kathale ND, Liu D, Lee C, Freeman DA, Hogenesch JB, Cao R, and Liu AC.** mTOR signaling regulates central and peripheral circadian clock function. *PLoS genetics* 14: e1007369, 2018.
144. **Reddy AB, Maywood ES, Karp NA, King VM, Inoue Y, Gonzalez FJ, Lilley KS, Kyriacou CP, and Hastings MH.** Glucocorticoid signaling synchronizes the liver circadian transcriptome. *Hepatology* 45: 1478-1488, 2007.
145. **Refinetti R and Menaker M.** The circadian rhythm of body temperature. *Physiology & behavior* 51: 613-637, 1992.
146. **Relógio A, Westermark PO, Wallach T, Schellenberg K, Kramer A, and Herzel H.** Tuning the mammalian circadian clock: robust synergy of two loops. *PLoS Comput Biol* 7: e1002309, 2011.
147. **Reznick RM, Zong H, Li J, Morino K, Moore IK, Hannah JY, Liu Z-X, Dong J, Mustard KJ, and Hawley SA.** Aging-associated reductions in AMP-activated protein kinase activity and mitochondrial biogenesis. *Cell metabolism* 5: 151-156, 2007.
148. **Richter JD and Sonenberg N.** Regulation of cap-dependent translation by eIF4E inhibitory proteins. *Nature* 433: 477-480, 2005.

149. **Riera CE, Merkwirth C, De Magalhaes Filho CD, and Dillin A.** Signaling networks determining life span. *Annual review of biochemistry* 85: 35-64, 2016.
150. **Robinson JL, Foustock S, Chanez M, Bois-Joyeux B, and Peret J.** Circadian variation of liver metabolites and amino acids in rats adapted to a high protein, carbohydrate-free diet. *The Journal of Nutrition* 111: 1711-1720, 1981.
151. **Rockne RC, Hawkins-Daarud A, Swanson KR, Sluka JP, Glazier JA, Macklin P, Hormuth II DA, Jarrett AM, Lima EA, and Oden JT.** The 2019 mathematical oncology roadmap. *Physical biology* 16: 041005, 2019.
152. **Roenneberg T and Merrow M.** Circadian systems and metabolism. *Journal of Biological Rhythms* 14: 449-459, 1999.
153. **Rosenberg RS, Zee PC, and Turek FW.** Phase response curves to light in young and old hamsters. *American Journal of Physiology-Regulatory, Integrative and Comparative Physiology* 261: R491-R495, 1991.
154. **Sadria M and Layton AT.** Interactions among mTORC, AMPK, and SIRT: A Computational Model for Cell Energy Balance and Metabolism. 2020.
155. **Salgado-Delgado R, Angeles-Castellanos M, Buijs M, and Escobar C.** Internal desynchronization in a model of night-work by forced activity in rats. *Neuroscience* 154: 922-931, 2008.
156. **Salminen A and Kaarniranta K.** AMP-activated protein kinase (AMPK) controls the aging process via an integrated signaling network. *Ageing research reviews* 11: 230-241, 2012.
157. **Sancak Y, Thoreen CC, Peterson TR, Lindquist RA, Kang SA, Spooner E, Carr SA, and Sabatini DM.** PRAS40 is an insulin-regulated inhibitor of the mTORC1 protein kinase. *Molecular cell* 25: 903-915, 2007.
158. **Sarbassov DD, Guertin DA, Ali SM, and Sabatini DM.** Phosphorylation and regulation of Akt/PKB by the rictor-mTOR complex. *Science* 307: 1098-1101, 2005.
159. **Satinoff E, Li H, Tcheng TK, Liu C, McArthur A, Medanic M, and Gillette M.** Do the suprachiasmatic nuclei oscillate in old rats as they do in young ones? *American Journal of Physiology-Regulatory, Integrative and Comparative Physiology* 265: R1216-R1222, 1993.
160. **Scarbrough K, Losee-Olson S, Wallen EP, and Turek FW.** Aging and photoperiod affect entrainment and quantitative aspects of locomotor behavior in Syrian hamsters. *American Journal of Physiology-Regulatory, Integrative and Comparative Physiology* 272: R1219-R1225, 1997.
161. **Scheer FA, Hilton MF, Mantzoros CS, and Shea SA.** Adverse metabolic and cardiovascular consequences of circadian misalignment. *Proceedings of the National Academy of Sciences* 106: 4453-4458, 2009.
162. **Schreiber KH, Apelo SIA, Yu D, Brinkman JA, Velarde MC, Syed FA, Liao C-Y, Baar EL, Carbajal KA, and Sherman DS.** A novel rapamycin analog is highly selective for mTORC1 in vivo. *Nature communications* 10: 1-12, 2019.
163. **Schürmann A, Brauers A, Maßmann S, Becker W, and Joost H-G.** Cloning of a novel family of mammalian GTP-binding proteins (RagA, RagBs, RagB1) with remote similarity to the Ras-related GTPases. *Journal of Biological Chemistry* 270: 28982-28988, 1995.
164. **Shimobayashi M and Hall MN.** Making new contacts: the mTOR network in metabolism and signalling crosstalk. *Nature reviews Molecular cell biology* 15: 155-162, 2014.
165. **Smith GR and Shanley DP.** Modelling the response of FOXO transcription factors to multiple post-translational modifications made by ageing-related signalling pathways. *PloS one* 5: e11092, 2010.
166. **Sonntag AG, Dalle Pezze P, Shanley DP, and Thedieck K.** A modelling–experimental approach reveals insulin receptor substrate (IRS)-dependent regulation of adenosine monosphosphate-dependent kinase (AMPK) by insulin. *The FEBS journal* 279: 3314-3328, 2012.

167. **Souayed N, Chennoufi M, Boughattas F, Hassine M, Attia MB, Aouam K, Reinberg A, and Boughattas NA.** Circadian-time dependent tolerance and haematological toxicity to isoniazid in murine. *Biomedicine & Pharmacotherapy* 71: 233-239, 2015.
168. **Spiegel K, Tasali E, Leproult R, and Van Cauter E.** Effects of poor and short sleep on glucose metabolism and obesity risk. *Nature Reviews Endocrinology* 5: 253, 2009.
169. **Stokkan K-A, Yamazaki S, Tei H, Sakaki Y, and Menaker M.** Entrainment of the circadian clock in the liver by feeding. *Science* 291: 490-493, 2001.
170. **Sulaimanov N, Klose M, Busch H, and Boerries M.** Understanding the mTOR signaling pathway via mathematical modeling. *Wiley Interdisciplinary Reviews: Systems Biology and Medicine* 9: e1379, 2017.
171. **Swaab DF, Fliers E, and Partiman T.** The suprachiasmatic nucleus of the human brain in relation to sex, age and senile dementia. *Brain Res* 342: 37-44, 1985.
172. **Thobe K, Sers C, and Siebert H.** Unraveling the regulation of mTORC2 using logical modeling. *Cell Communication and Signaling* 15: 6, 2017.
173. **Thoreen CC and Sabatini DM.** Rapamycin inhibits mTORC1, but not completely. *Autophagy* 5: 725-726, 2009.
174. **Tian X, Seluanov A, and Gorbunova V.** Molecular mechanisms determining lifespan in short- and long-lived species. *Trends in Endocrinology & Metabolism* 28: 722-734, 2017.
175. **Triqueneaux G, Thenot S, Kakizawa T, Antoch MP, Safi R, Takahashi JS, Delaunay F, and Laudet V.** The orphan receptor Rev-erbα gene is a target of the circadian clock pacemaker. *Journal of molecular endocrinology* 33: 585-608, 2004.
176. **Turek FW, Penev P, Zhang Y, Van Reeth O, Takahashi JS, and Zee P.** Alterations in the circadian system in advanced age. *Ciba Foundation Symposium 183-Circadian Clocks and their Adjustment: Circadian Clocks and their Adjustment: Ciba Foundation Symposium 183*. Wiley Online Library, 2007, p. 212-234.
177. **Valenzano DR, Terzibasi E, Genade T, Cattaneo A, Domenici L, and Cellerino A.** Resveratrol prolongs lifespan and retards the onset of age-related markers in a short-lived vertebrate. *Current biology* 16: 296-300, 2006.
178. **Van Amelsvoort L, Schouten E, and Kok F.** Duration of shiftwork related to body mass index and waist to hip ratio. *International journal of obesity* 23: 973-978, 1999.
179. **Vollmers C, Gill S, DiTacchio L, Pulivarthy SR, Le HD, and Panda S.** Time of feeding and the intrinsic circadian clock drive rhythms in hepatic gene expression. *Proceedings of the National Academy of Sciences* 106: 21453-21458, 2009.
180. **Wallace E, Wright S, Schoenike B, Roopra A, Rho JM, and Maganti RK.** Altered circadian rhythms and oscillation of clock genes and sirtuin 1 in a model of sudden unexpected death in epilepsy. *Epilepsia* 59: 1527-1539, 2018.
181. **Wang R-H, Zhao T, Cui K, Hu G, Chen Q, Chen W, Wang X-W, Soto-Gutierrez A, Zhao K, and Deng C-X.** Negative reciprocal regulation between Sirt1 and Per2 modulates the circadian clock and aging. *Scientific reports* 6: 1-15, 2016.
182. **Wang R-S, Saadatpour A, and Albert R.** Boolean modeling in systems biology: an overview of methodology and applications. *Physical biology* 9: 055001, 2012.
183. **Wang X, Hu S, and Liu L.** Phosphorylation and acetylation modifications of FOXO3a: Independently or synergistically? *Oncology letters* 13: 2867-2872, 2017.
184. **Weitzman ED, Moline ML, Czeisler CA, and Zimmerman JC.** Chronobiology of aging: temperature, sleep-wake rhythms and entrainment. *Neurobiology of aging* 3: 299-309, 1982.
185. **Welsh DK, Takahashi JS, and Kay SA.** Suprachiasmatic nucleus: cell autonomy and network properties. *Annual review of physiology* 72: 551-577, 2010.

186. **Witting W, Mirmiran M, Bos NP, and Swaab DF.** The effect of old age on the free-running period of circadian rhythms in rat. *Chronobiology international* 11: 103-112, 1994.
187. **Wolfson RL and Sabatini DM.** The dawn of the age of amino acid sensors for the mTORC1 pathway. *Cell metabolism* 26: 301-309, 2017.
188. **Woller A, Duez H, Staels B, and Lefranc M.** A mathematical model of the liver circadian clock linking feeding and fasting cycles to clock function. *Cell reports* 17: 1087-1097, 2016.
189. **Won D-H, Chung SH, Shin J-A, Hong K-O, Yang I-H, Yun J-W, and Cho S-D.** Induction of sestrin 2 is associated with fisetin-mediated apoptosis in human head and neck cancer cell lines. *Journal of clinical biochemistry and nutrition* 64: 97-105, 2019.
190. **Wu R, Dang F, Li P, Wang P, Xu Q, Liu Z, Li Y, Wu Y, Chen Y, and Liu Y.** The circadian protein Period2 suppresses mTORC1 activity via recruiting Tsc1 to mTORC1 complex. *Cell metabolism* 29: 653-667. e656, 2019.
191. **Wu Y, Li X, Zhu JX, Xie W, Le W, Fan Z, Jankovic J, and Pan T.** Resveratrol-activated AMPK/SIRT1/autophagy in cellular models of Parkinson's disease. *Neurosignals* 19: 163-174, 2011.
192. **Wyant GA, Abu-Remaileh M, Wolfson RL, Chen WW, Freinkman E, Danai LV, Vander Heiden MG, and Sabatini DM.** mTORC1 activator SLC38A9 is required to efflux essential amino acids from lysosomes and use protein as a nutrient. *Cell* 171: 642-654. e612, 2017.
193. **Xu M, Pirtskhalava T, Farr JN, Weigand BM, Palmer AK, Weivoda MM, Inman CL, Ogrodnik MB, Hachfeld CM, and Fraser DG.** Senolytics improve physical function and increase lifespan in old age. *Nature medicine* 24: 1246-1256, 2018.
194. **Yamazaki S, Numano R, Abe M, Hida A, Takahashi R-i, Ueda M, Block GD, Sakaki Y, Menaker M, and Tei H.** Resetting central and peripheral circadian oscillators in transgenic rats. *Science* 288: 682-685, 2000.
195. **Yamazaki S, Straume M, Tei H, Sakaki Y, Menaker M, and Block GD.** Effects of aging on central and peripheral mammalian clocks. *Proceedings of the National Academy of Sciences* 99: 10801-10806, 2002.
196. **Yang H, Yang T, Baur JA, Perez E, Matsui T, Carmona JJ, Lamming DW, Souza-Pinto NC, Bohr VA, and Rosenzweig A.** Nutrient-sensitive mitochondrial NAD+ levels dictate cell survival. *Cell* 130: 1095-1107, 2007.
197. **Yang Q, Inoki K, Ikenoue T, and Guan K-L.** Identification of Sin1 as an essential TORC2 component required for complex formation and kinase activity. *Genes & development* 20: 2820-2832, 2006.
198. **Yoo S-H, Yamazaki S, Lowrey PL, Shimomura K, Ko CH, Buhr ED, Siepka SM, Hong H-K, Oh WJ, and Yoo OJ.** PERIOD2:: LUCIFERASE real-time reporting of circadian dynamics reveals persistent circadian oscillations in mouse peripheral tissues. *Proceedings of the National Academy of Sciences* 101: 5339-5346, 2004.
199. **Yoshino J, Baur JA, and Imai S-i.** NAD+ intermediates: the biology and therapeutic potential of NMN and NR. *Cell metabolism* 27: 513-528, 2018.
200. **Yu L, McPhee CK, Zheng L, Mardones GA, Rong Y, Peng J, Mi N, Zhao Y, Liu Z, and Wan F.** Termination of autophagy and reformation of lysosomes regulated by mTOR. *Nature* 465: 942-946, 2010.
201. **Zappe DH, Crikelair N, Kandra A, and Palatini P.** Time of administration important? Morning versus evening dosing of valsartan. *Journal of hypertension* 33: 385, 2015.
202. **Zee PC, Rosenberg RS, and Turek FW.** Effects of aging on entrainment and rate of resynchronization of circadian locomotor activity. *American Journal of Physiology-Regulatory, Integrative and Comparative Physiology* 263: R1099-R1103, 1992.

203. **Zhang Y, Kornhauser J, Zee PC, Mayo KE, Takahashi J, and Turek FW.** Effects of aging on light-induced phase-shifting of circadian behavioral rhythms, fos expression and CREB phosphorylation in the hamster suprachiasmatic nucleus. *Neuroscience* 70: 951-961, 1996.
204. **Zheng B, Albrecht U, Kaasik K, Sage M, Lu W, Vaishnav S, Li Q, Sun ZS, Eichele G, and Bradley A.** Nonredundant roles of the mPer1 and mPer2 genes in the mammalian circadian clock. *Cell* 105: 683-694, 2001.
205. **Zhou G, Myers R, Li Y, Chen Y, Shen X, Fenyk-Melody J, Wu M, Ventre J, Doebber T, and Fujii N.** Role of AMP-activated protein kinase in mechanism of metformin action. *The Journal of clinical investigation* 108: 1167-1174, 2001.
206. **Zhou JN and Swaab DF.** Activation and degeneration during aging: a morphometric study of the human hypothalamus. *Microscopy research and technique* 44: 36-48, 1999.
207. **Zhou M, Kim JK, Eng GWL, Forger DB, and Virshup DM.** A Period2 phosphoswitch regulates and temperature compensates circadian period. *Molecular cell* 60: 77-88, 2015.

Appendix A

A.1 Model equations and parameters for metabolic signaling pathway model.

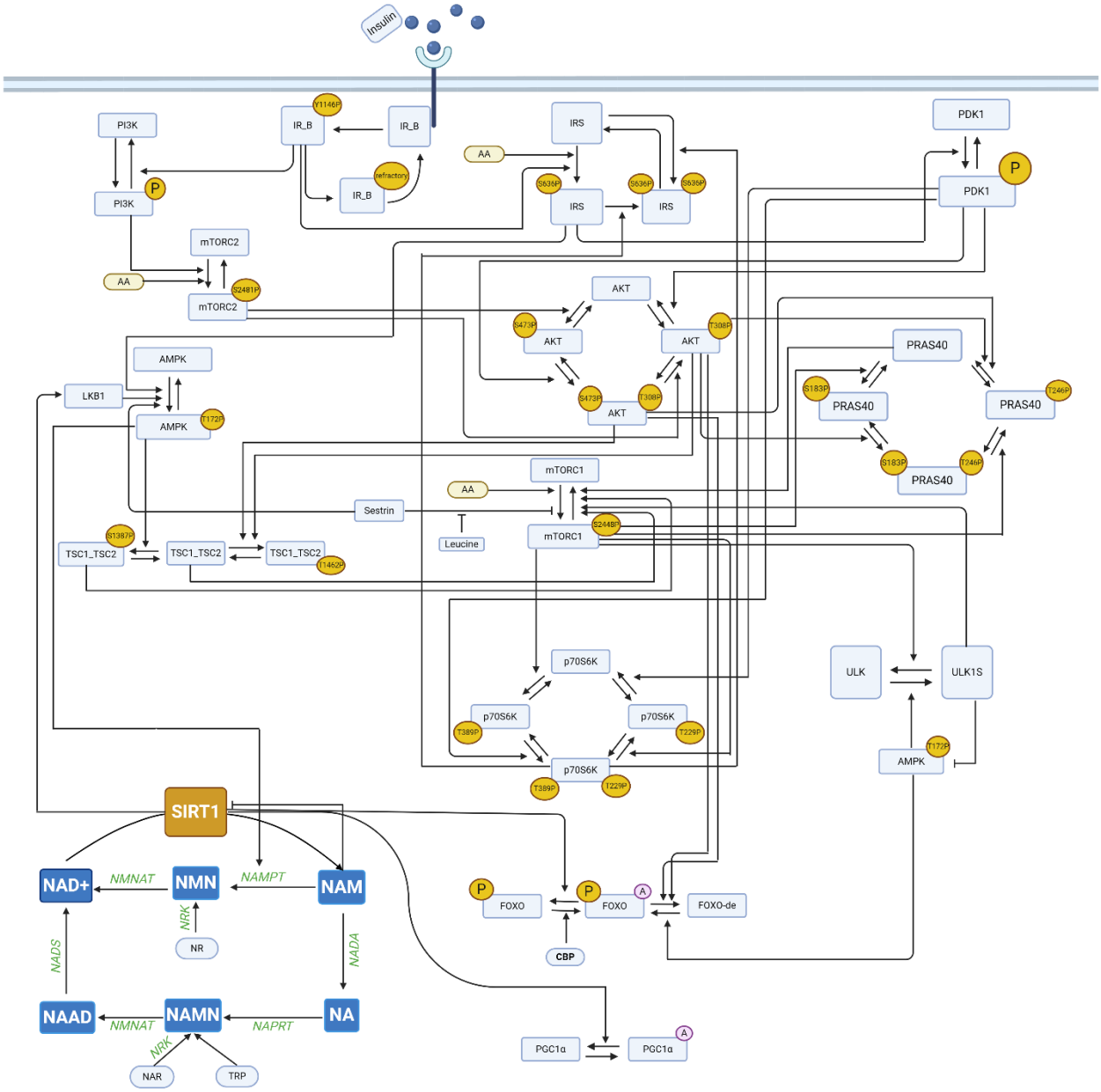

Figure A1. Schematic diagram depicting connections among model components that form the signaling pathways. AA represents amino acids; "A" in purple circles denote the acetylated form of the complex; "P" in yellow circles denote the phosphorylated form.

Below is a complete list of equations used in the metabolic signaling pathway model described in Chapter 2 and illustrated in Fig. A1. Model parameters are given in Table A1.

$$\frac{d[IR\beta]}{dt} = +(par\_IR\_beta\_ready * [IR\beta\_refractory]) - ([IR\beta] * par\_IR\_beta\_phos\_by\_Insulin * [Insulin])$$

$$\frac{d[IR\beta\_pY1146]}{dt} = +([IR\beta] * par\_IR\_beta\_phos\_by\_Insulin * [Insulin]) - (par\_IR\_beta\_pY1146\_dephos * [IR\beta\_pY1146])$$

$$\frac{d[IR\beta\_refractory]}{dt} = +(par\_IR\_beta\_pY1146\_dephos * [IR\beta\_pY1146]) - (par\_IR\_beta\_ready * [IR\beta\_refractory])$$

$$\frac{d[mTORC1\_pS2448]}{dt} = -([TSC1\_TSC2] + [TSC1\_TSC2\_pS1387]) * [mTORC1\_pS2448] * par\_mTORC1\_pS2448\_dephos\_by\_TSC1\_TSC2) - (b\_pras\_mtorc1 * 0.00068 * [mTORC1\_pS2448] * 10\^(0.25 * [PRAS40])) - ([mTORC1\_pS2448] * [Act\_ULK1] * 0.00016) + [Amino\_Acid] * [mTORC1] * par\_mTORC1\_S2448\_activation\_by\_Amino\_Acids * \left(\frac{mTORC1_{vmax} * ([leucine_a] + [leucine_{conc}])}{[leucine_a] + [leucine_{conc}] + [sestrin2]}\right)$$

$$\frac{d[mTORC1]}{dt} = +([TSC1\_TSC2] + [TSC1\_TSC2\_pS1387]) * [mTORC1\_pS2448] * par\_mTORC1\_pS2448\_dephos\_by\_TSC1\_TSC2) + (b\_pras\_mtorc1 * 0.00068 * [mTORC1\_pS2448] * 10\^(0.25 * [PRAS40])) + ([mTORC1\_pS2448] * [Act\_ULK1] * 0.00016) - [Amino\_Acid] * [mTORC1] * par\_mTORC1\_S2448\_activation\_by\_Amino\_Acids * \left(\frac{mTORC1_{vmax} * ([leucine_a] + [leucine_{conc}])}{[leucine_a] + [leucine_{conc}] + [sestrin2]}\right)$$

$$\frac{d[mTORC2]}{dt} = -([Amino\_Acid] * [mTORC2] * par\_mTORC2\_S2481\_phos\_by\_Amino\_Acids) - ([PI3K\_p] * [mTORC2] * par\_mTORC2\_S2481\_phos\_by\_PI3K\_variant\_p) + (par\_mTORC2\_pS2481\_dephos * [mTORC2\_pS2481])$$

$$\frac{d[mTORC2\_pS2481]}{dt} = +([Amino\_Acid] * [mTORC2] * par\_mTORC2\_S2481\_phos\_by\_Amino\_Acids) + ([PI3K\_p] * [mTORC2] * par\_mTORC2\_S2481\_phos\_by\_PI3K\_variant\_p) - (par\_mTORC2\_pS2481\_dephos * [mTORC2\_pS2481])$$

$$\frac{d[IRS]}{dt} = -([Amino\_acid] * [IRS] * par\_IRS\_phos\_by\_Amino\_Acids) - ([IRS] * par\_IRS\_phos\_by\_IR\_beta\_pY1146 * [IR\beta - pY1146]) - ([IRS] * par\_IRS\_phos\_by\_p70\_S6K\_pT229\_pT389 * [p70\_S6K\_pT229\_pT389]) + (par\_IRS\_pS636\_turnover * [IRS\_pS636])$$

$$\frac{d[IRS\_p]}{dt} = +([Amino\_Acid] * [IRS] * par\_IRS\_phos\_by\_Amino\_Acids) + ([IRS] * par\_IRS\_phos\_by\_IR\_beta\_pY1146 * [IR\beta - pY1146]) - ([IRS\_p] * par\_IRS\_p\_phos\_by\_p70\_S6K\_pT229\_pT389 * [p70S6K\_pT229\_pT389])$$

$$\frac{d[IRS\_pS636]}{dt} = +([IRS\_p] * par\_IRS\_p\_phos\_by\_p70\_S6K\_pT229\_pT389 * [p70S6K\_pT229\_pT389]) + ([IRS] * par\_IRS\_phos\_by\_p70\_S6K\_pT229\_pT389 * [p70S6K\_pT229\_pT389]) - (par\_IRS\_pS636\_turnover * [IR\_pS636])$$

$$\frac{d[TSC1\_TSC2]}{dt} = -([AMPK\_pT172] * [TSC1\_TSC2] * par\_TSC1\_TSC2\_S1387\_phos\_by\_AMPK\_pT172) - (([AKT\_pT308] + [AKT\_pT3089\_pS473]) * [TSC1\_TSC2] * par\_TSC1\_TSC2\_T1462\_phos\_by\_Akt\_pT308) + (par\_TSC1\_TSC2\_pS1387\_dephos * [TSC1\_TSC2\_pS1387]) + (par\_TSC1\_TSC2\_pT1462\_dephos * [TSC1\_TSC2\_pT1462])$$

$$\frac{d[TSC1\_TSC2\_pT1462]}{dt} = +(([Akt - pT308] + [Akt\_pT308\_pS473]) * [TSC1\_TSC2] * par\_TSC1\_TSC2\_T1462\_phos\_by\_Akt\_pT308) - (par\_TSC1\_TSC2\_pT1462\_dephos * [TSC1\_TSC2\_pT1462])$$

$$\frac{d[TSC1\_TSC2\_pS1387]}{dt} = +([AMPK - pT172] * [TSC1\_TSC2] * par\_TSC1\_TSC2\_S1387\_phos\_by\_AMPK\_pT172) - (par\_TSC1\_TSC2\_pS1387\_dephos * [TSC1\_TSC2\_pS1387])$$

$$\frac{d[PRAS40]}{dt} = -([PRAS40] * par\_PRAS40\_S183\_phos\_by\_mTORC1\_pS2448\_first * [mTORC1\_pS2448]) - (([Akt\_pT308] + [Akt\_pT308\_pS473]) * [PRAS40] * par\_PRAS40\_T246\_phos\_by\_Akt\_pT308\_first) + (par\_PRAS40\_pS183\_dephos\_first * [PRAS40\_pS183]) + (par\_PRAS40\_pT246\_dephos\_first * [PRAS40\_pT246])$$

$$\frac{d[PRAS40\_pS183]}{dt} = +([PRAS40] * par\_PRAS40\_S183\_phos\_by\_mTORC1\_pS2448\_first * [mTORC1\_pS2448]) - (([Akt\_pT308] + [Akt\_pT308\_pS473]) * [PRAS40\_pS183] * par\_PRAS40\_T246\_phos\_by\_Akt\_pT308\_second) - (par\_PRAS40\_pS183\_dephos\_first * [PRAS40\_pS183]) + (par\_PRAS40\_pT246\_dephos\_second * [PRAS40\_pT246\_pS183])$$

$$\frac{d[PRAS40\_pT246]}{dt} = -(par\_PRAS40\_S183\_phos\_by\_mTORC1\_pS2448\_second * [PRAS40\_pT246] * [mTORC1\_pS2448]) - (par\_PRAS40\_pT246\_dephos\_first * [PRAS40\_pT246]) + ([Akt\_pT308] * [Akt\_pT308\_pS473] * [PRAS40] * par\_PRAS40\_T246\_phos\_by\_Akt\_pT308\_first) + (par\_PRAS40\_pS183\_dephos\_second * [PRAS40\_pT246\_pS183])$$

$$\frac{d[PRAS40\_pT246\_pS183]}{dt} = +(([Akt\_pT308] + [Akt\_pT308\_pS473]) * [PRAS40\_pS183] * par\_PRAS40\_T246\_phos\_by\_Akt\_pT308\_second) + (par\_PRAS40\_S183\_phos\_by\_mTORC1\_pS2448\_second * [PRAS40\_pT246] * [mTORC1\_pS2448]) - (par\_PRAS40\_pS183\_dephos\_second * [PRAS40\_pT246\_pS183]) - (par\_PRAS40\_pT246\_dephos\_second * [PRAS40\_pT246\_pS183])$$

$$\frac{\mathbf{d[AKT]}}{\mathbf{dt}} = -([AKT] * par\_Akt\_T308\_phos\_by\_PI3K\_p\_PDK1\_first * [PDK1\_p])$$
$$-([AKT] * par\_Akt\_S473\_phos\_by\_mTORC2\_pS2481\_first * [mTORC2\_pS2481])$$
$$+(par\_Akt\_pT308\_dephos\_first * [Akt\_pT308])$$
$$+(par\_Akt\_pS473\_dephos\_first * [Akt\_pS473])$$

$$\frac{\mathbf{d[Akt\_pT308\_pS473]}}{\mathbf{dt}} = +(par\_Akt\_T308\_phos\_by\_PI3K\_p\_PDK1\_second * [Akt\_pS473] * [PDK1\_p])$$
$$+(par\_Akt\_S473\_phos\_by\_mTORC2\_pS2481\_second * [Akt\_pT308] * [mTORC2\_pS2481])$$
$$-(par\_Akt\_pT308\_dephos\_first * [Akt\_pT308])$$
$$-(par\_Akt\_pS473\_dephos\_second * [Akt\_pT308\_pS473])$$

$$\frac{\mathbf{d[Akt\_pT308]}}{\mathbf{dt}} = +([AKT] * par\_Akt\_T308\_phos\_by\_PI3K\_p\_PDK1\_first * [PDK1\_p])$$
$$-(par\_Akt\_S473\_phos\_by\_mTORC2\_pS2481\_second * [Akt\_pT308] * [mTORC2\_pS2481])$$
$$-(par\_Akt\_pT308\_dephos\_first * [Akt\_pT308])$$
$$+(par\_Akt\_pS473\_dephos\_second * [Akt\_pT308\_pS473])$$

$$\frac{\mathbf{d[Akt\_pS473]}}{\mathbf{dt}} = +(par\_Akt\_pS473\_dephos\_second * [AKT\_pT308\_pS473])$$
$$-(par\_Akt\_pT308\_dephos\_first * [AKT\_pT308])$$
$$+(par\_PI3K\_PDK1\_phos\_by\_IRS\_p * [AKT] * [PI3K\_p\_PDK1])$$
$$-(par\_Akt\_S473\_phos\_by\_mTORC2\_pS2481\_first) * [AKT\_pT308] * [mTORC2\_pS2481])$$

$$\frac{\mathbf{d[p70S6K]}}{\mathbf{dt}} = -([PDK1\_p] * [p70S6K] * par\_p70\_S6K\_T229\_phos\_by\_PI3K\_p\_PDK1\_first)$$
$$-([mTORC1\_pS2448] * [p70S6K] * par\_p70\_S6K\_T389\_phos\_by\_mTORC1\_pS2448\_first)$$
$$+(par\_p70\_S6K\_pT229\_dephos\_first * [p70S6K\_pT229])$$
$$+(par\_p70\_S6K\_pT389\_dephos\_first * [p70S6K\_pT389])$$

$$\frac{\boldsymbol{d[p70S6K\_pT229]}}{\boldsymbol{dt}} = +([PDK1\_p] * [p70S6K] * par\_p70\_S6K\_T229\_phos\_by\_PI3K\_p\_PDK1\_first)$$

$$-([mTORC1\_pS2448] * par\_p70\_S6K\_T389\_phos\_by\_mTORC1\_pS2448\_second * [p70S6K\_pT229])$$

$$+(par\_p70\_S6K\_pT389\_dephos\_second * [p70S6K\_pT229\_pT389])$$

$$-(par\_p70\_S6K\_pT229\_dephos\_first * [p70S6K\_pT229])$$

$$\frac{d[\mathbf{p70S6K\_pT389}]}{dt} = +([mTORC1\_pS2448] * [p70S6K] * par\_p70\_S6K\_T389\_phos\_by\_mTORC1\_pS2448\_first)$$

$$-([PDK1\_p] * par\_p70\_S6K\_T229\_phos\_by\_PI3K\_p\_PDK1\_second * [p70S6K\_pT389])$$

$$-(par\_p70\_S6K\_pT389\_dephos\_first * [p70S6K\_pT389])$$

$$+(par\_p70\_S6K\_pT229\_dephos\_second * [p70S6K\_pT229\_pT389])$$

$$\frac{d[\mathbf{p70S6K\_pT389\_pT229}]}{dt} = +([PDK1_p] * par\_p70\_S6K\_T229\_phos\_by\_PI3K\_p\_PDK1\_second * [p70S6K\_pT389])$$

$$+([mTORC1_{pS2448}] * par\_p70\_S6K\_T389\_phos\_by\_mTORC1\_pS2448\_second * [p70S6K\_pT229])$$

$$-(par\_p70\_S6K\_pT229\_dephos\_second * [p70S6K\_pT229\_pT389])$$

$$-(par\_p70\_S6K\_pT389\_dephos\_second * [p70S6K\_pT229\_pT389])$$

$$\frac{d[\mathbf{PI3K}]}{dt} = +(par\_PI3K\_variant\_p\_dephos * [PI3K\_p])$$

$$-([IR\beta\_pY1146] * [PI3K] * par\_PI3K\_variant\_phos\_by\_IR\_beta\_pY1146)$$

$$\frac{d[\mathbf{PI3K\_p}]}{dt} = -(par\_PI3K\_variant\_p\_dephos * [PI3K\_p])$$

$$+([IR\beta\_pY1146] * [PI3K] * par\_PI3K\_variant\_phos\_by\_IR\_beta\_pY1146)$$

$$\frac{d[\mathbf{PDK1}]}{dt} = +(par\_PI3K\_p\_PDK1\_dephos * [PDK1\_p])$$

$$-([IRS\_p] * [PDK1] * par\_PI3K\_PDK1\_phos\_by\_IRS\_p)$$

$$\frac{d[\mathbf{PDK1\_p}]}{dt} = -(par\_PI3K\_p\_PDK1\_dephos * [PDK1\_p])$$

$$+([IRS\_p] * [PDK1] * par\_PI3K\_PDK1\_phos\_by\_IRS\_p)$$

$$\frac{d[AMPK]}{dt} = -(100 * [AMPK] * par\_AMPK\_T172\_phos\_by\_AminoAcids * [leucine\_conc] * [sestrine\_conc])$$
$$-([AMPK] * par\_AMPK\_T172\_phos * [IRS\_p])$$
$$+(par\_AMPK\_pT172\_dephos * [AMPK\_pT172])$$
$$-(ksirt * [SIRT] * [AMPK])$$
$$+([Act\_ULK1] * [AMPK\_pT172] * kUKAP)$$

$$\frac{d[AMPK\_pT172]}{dt} = +(100 * [AMPK] * par\_AMPK\_T172\_phos\_by\_AminoAcids * [leucine\_conc] * [sestrine\_conc])$$
$$+([AMPK] * par\_AMPK\_T172\_phos * [IRS\_p])$$
$$-(par\_AMPK\_pT172\_dephos * [AMPK\_pT172])$$
$$+(ksirt * [SIRT] * [AMPK])$$
$$-([Act\_ULK1] * [AMPK\_pT172] * kUKAP)$$

$$\frac{d[FOXO\_de]}{dt} = +kAKT * ([Akt\_pT308] + [Akt\_pT308\_pS473]) * [FOXO\_AC\_P] - kAMPK * [AMPK\_pT172] * [FOXO\_de]$$

$$\frac{d[FOXO\_AC\_P]}{dt} = + kAMPK * [FOXO\_de] * [AMPK\_pT172] - kAKT * ([Akt\_pT308\_pS473] + [Akt\_pT308]) * [FOXO\_AC\_P]$$
$$- kSIRTFOXO * [FOXO\_AC\_P] * [SIRT] + kCBp * [FOXO\_P] * [CBP]$$

$$\frac{d[FOXO\_P]}{dt} = +kSIRTFOXO * [FOXO\_AC\_P] * [SIRT] - kCBp * [FOXO\_P] * [CBP]$$

$$\frac{d[PGC1\alpha]}{dt} = + kdn * [AC\_PGC1\alpha]$$
$$-\left(\frac{Vspgc * PGC1\alpha * SIRT}{kAPGC + SIRT}\right)$$

$$\frac{d[AC\_PGC1\alpha]}{dt} = +Vopgc$$
$$-\left(\frac{Vspgc * PGC1\alpha * SIRT}{kAPGC + SIRT}\right)$$
$$-\left(Vdpgc * \frac{[AC\_PGC1\alpha]}{kdpgc + [AC\_PGC1\alpha]}\right)$$

$$- kdn * [AC\_PGC1\alpha]$$

$$\frac{\mathbf{d[ULK1]}}{\mathbf{dt}} = -k10 * [ULK1] * [AMPK\_pT172] + kULKd * [Act\_ULK1] + KULKM * [Act\_ULK1] * [mTORC1\_pS2448]$$

$$\frac{\mathbf{d[AC\_ULK1]}}{\mathbf{dt}} = k10 * [ULK1] * [AMPK\_pT172] - kULKd * [Act\_ULK1] - KULKM * [Act\_ULK1] * [mTORC1\_pS2448]$$

$$\frac{\mathbf{d[Nam\_ex]}}{\mathbf{dt}} = (-(NAMimport) + 0.9625 * (NAMimport) + (Nam\_uptake))$$

$$\frac{\mathbf{d[NADbound]}}{\mathbf{dt}} = (1/NamPT\_compartment * (NAD\_binding))$$

$$\frac{\mathbf{d[NR]}}{\mathbf{dt}} = (1/NamPT\_compartment * ((NT5\_NMN) - (PNP\_NR) - (NR\_efflux) - (NRK1\_NMN)))$$

$$\frac{\mathbf{d[NaAD]}}{\mathbf{dt}} = (1/NamPT\_compartment * ((NMNAT1\_NaMN) - (NADS)))$$

$$\frac{\mathbf{d[NMN]}}{\mathbf{dt}} = (1/NamPT\_compartment * (-(NMN\_efflux) - (NMNAT1\_NMN) - (NT5\_NMN) + (NAMPT) + (NRK1\_NMN)))$$

$$\frac{\mathbf{d[NA]}}{\mathbf{dt}} = (1/NamPT\_compartment * (-(NAPRT) + (NADA) - (NA\_efflux) + (PNP\_NAR)))$$

$$\frac{\mathbf{d[NaMN]}}{\mathbf{dt}} = (1/NamPT\_compartment * ((NAPRT) - (NMNAT1\_NaMN) - (NT5\_NaMN) + (NRK1\_NaMN)))$$

$$\frac{\mathbf{d[NAM]}}{\mathbf{dt}} = (1/NamPT\_compartment * ((PNP\_NR) - (NNMT) - (Nam\_efflux) + (SIRT) + (NAD\_consumption\_without\_Nam\_inhibition) - (NADA) + (NAMimport) - (NAMPT)))$$

$$\frac{\mathbf{d[NAD]}}{\mathbf{dt}} = (1/NamPT\_compartment * ((NMNAT1\_NMN) + (NADS) - (SIRT) - (NAD\_consumption\_without\_Nam\_inhibition) - (NAD\_binding) - (NAD\_efflux)))$$

$$\frac{\mathbf{d[NAR]}}{\mathbf{dt}} = (1/NamPT\_compartment * ((NT5\_NaMN) - (NAR\_efflux) - (NRK1\_NaMN) - (PNP\_NAR)))$$

$$\mathbf{NMN\_efflux} = (NamPT\_compartment * celldivision\_rate\_NamPT\_compartment * NMN)$$

$$\mathbf{NAPRT} = \left(\frac{NamPT\_compartment * NAPRT\_E\_T * NAPRT\_turnovver * NA * ATP * NAPRT\_scaling}{NAPRT\_Km + NA}\right)$$

$$\mathbf{NMNAT1\_NMN} = \frac{NamPT\_compartment * (ETNMNAT * NMNAT1\_NMN\_scaling * \left(\left(NMNAT\_NMN\_kcat\_A * \frac{NMN}{NMNAT\_NMN\_km\_A}\right) - \left(NMNAT1\_NMN\_kcat\_PA * \frac{NAD}{NMNAT1\_NMN\_km\_PA}\right)\right)}{1 + \frac{NMN}{NMNAT1\_NMN\_Km\_A} + \frac{NaMN}{NMNAT1\_NMN\_Km\_B} + \frac{NAD}{NMNAT1\_NMN\_Km\_PA} + \frac{NaAD}{NMNAT1\_NMN\_Km\_PB}}$$

$$\mathbf{NMNAT1\_NaMN} = \frac{NamPT\_compartment * (ETNMNAT * NMNAT1\_NaMN\_scaling * \left(\frac{NMNAT1\_NaMN\_kcat\_A * NaMN}{NMNAT1\_NaMN\_Km\_A} - \frac{NMNAT1\_NAMN\_kcat\_PA * NaAD}{NMNAT1\_NaMN\_Km\_PA}\right)}{1 + \frac{NaMN}{NMNAT1\_NaMN\_Km\_A} + \frac{NMN}{NMNAT1\_NaMN\_Km\_B} + \frac{NaAD}{NMNAT1\_NaMN\_Km\_PA} + \frac{NAD}{NMNAT1\_NaMN\_Km\_PB}}$$

$$\mathbf{NADS} = \frac{NamPT\_compartment * NADS\_E\_T * NADS\_turnover * NaAD * ATP * NADS\_scaling}{(NADS\_Km + NaAD}$$

$$\mathbf{NT5\_NMN} = \frac{NamPT\_compartment * NT5\_NMN\_ET * NT5\_NMN\_scaling * NT5\_NMN\_kcat * NMN}{NT5\_NMN\_Km + NMN}$$

$$\mathbf{PNP\_NR} = \frac{NamPT\_compartment * PNP\_NR\_E\_T * PNP\_NR\_turnover * NR * Pi * PNP\_NR\_scaling}{PNP\_NR\_Km + NR}$$

NNMT = $$\frac{NamPT\_compartment * NNMT\_ET * NNMT\_scaling * NNMT\_Kcat * SAM * NAM}{Kma * (Kmb + NAM) * (1 + \frac{methyl\_NAM}{NNMTki}) + SAM * Kmb + SAM * NAM}$$

Nam_efflux =

$$(NamPT\_compartment * celldivision\_rate\_NamPT\_compartment * NAM)$$

NT5_NaMN =

$$\frac{NamPT\_compartment * NT5\_NaMN\_ET * NT5\_NaMN\_scaling * NT5\_NaMN\_kcat * NaMN}{NT5\_NaMN\_Km + NaMN}$$

SIRT =

$$\frac{NamPT\_compartment * SIRT\_ET * SIRT\_scaling * SIRT_{Kcat} * NAD * H3_{ac}}{((SIRT\_Km + NAD) * (1 + \frac{NAM}{SIRT\_Ki}))}$$

NAD_consumption_without_Nam_inhibition =

$$NamPT\_compartment * NAD\_consumption\_without\_Nam\_inhibition\_ET * * \frac{NAD\_consumption\_without\_Nam\_inhibition\_scaling * NAD\_consumption\_without\_Nam\_inhibition\_kcat * NAD}{NAD\_consumption\_without\_Nam\_inhibition\_Km + NAD}$$

NADA =

$$\frac{NamPT\_compartment * NADA\_ET * NADA\_scaling * NADA_{Kcat} * NAM}{NADA_{Km} + NAM + \frac{NADA\_Km * NA}{NADA\_Ki}}$$

NAMimport =

$$(NamPT\_compartment * (Nam\_transporter * Nam\_ex - Nam\_transporter * NAM))$$

NAMPT =

$$\frac{NamPT\_compartment * ((NAMPT\_ET * (NAMPT\_scaling * (Kcat\_Namprt) * NAM * \left(0.8 + 0.2 * \frac{pAMPK}{15}\right)}{(Km\_NamPRT) + NAM + (Km\_NamPRT) * \frac{NAD}{NAMPT\_Ki)}}$$

NAR_efflux =

$$NamPT\_compartment * celldivision\_rate\_NamPT\_compartment * NAR$$

NA_efflux =

$$NamPT\_compartment * celldivision\_rate\_NamPT\_compartment * NA$$

NAD_binding =

$$NamPT\_compartment * (NAD\_binding\_k1 * NAD - NAD\_binding\_k2 * NADbound)$$

NRK1_NaMN = $$\frac{NamPT\_compartment * NRK1\_NaMN\_ET * NRK1\_NaMN\_scaling * NRK1\_NaMN\_kcat * NAR}{NRK1\_NaMN\_Km + NAR}$$

PNP_NAR = $$\frac{NamPT\_compartment * PNP\_NAR\_E\_T * PNP\_NAR\_turnover * NAR * Pi * PNP\_NAR\_scaling}{PNP\_NAR\_Km + NAR}$$

NR_efflux = $$NamPT\_compartment * celldivision\_rate\_NamPT\_compartment * NR$$

NRK1_NMN = $$\frac{NamPT\_compartment * NRK1\_NMN\_ET * NRK1\_NMN\_kcat * NRK1\_NMN\_scaling * NR}{(NRK1\_NMN\_Km + NR)}$$

Table A1. Parameter values for the metabolic signaling pathway model described in Chapter 2, and used in the above model equations.

Rate parameter names	**Values**
compartment_Cell	1
par_IRS_phos_by_Amino_Acids	0.0331672 (min^-1)
par_AMPK_T172_phos_by_Amino_Acids	17.6284 (min^-1)
par_mTORC2_S2481_phos_by_Amino_Acids	0.0268658 (min^-1)
par_IR_beta_phos_by_Insulin	0.0203796 (min^-1)
par_IR_beta_pY1146_dephos	0.493514 (min^-1)
par_IR_beta_ready	323.611 (min^-1)
par_IRS_phos_by_IR_beta_pY1146	2.11894 (min^-1)
par_IRS_p_phos_by_p70_S6K_pT229_pT389	0.3388 (min^-1)
par_IRS_phos_by_p70_S6K_pT229_pT389	0.08637 (min^-1)

par_IRS_pS636_turnover	25 (min^-1)
par_AMPK_T172_phos	0.490602 (min^-1)
par_AMPK_pT172_dephos	165.704 (min^-1)
par_Akt_S473_phos_by_mTORC2_pS2481_first	0.0000131992 (min^-1)
par_Akt_S473_phos_by_mTORC2_pS2481_second	0.159093 (min^-1)
par_Akt_T308_phos_by_PI3K_p_PDK1_first	7.47437 (min^-1)
par_Akt_T308_phos_by_PI3K_p_PDK1_second	7.47345 (min^-1)
par_Akt_pT308_dephos_first	88.9654 (min^-1)
par_Akt_pT308_dephos_second	88.9639 (min^-1)
par_Akt_pS473_dephos_first	0.376999 (min^-1)
par_Akt_pS473_dephos_second	0.380005 (min^-1)
par_TSC1_TSC2_S1387_phos_by_AMPK_pT172	0.00175772 (min^-1)
par_TSC1_TSC2_T1462_phos_by_Akt_pT308	1.52417 (min^-1)
par_TSC1_TSC2_pS1387_dephos	0.25319 (min^-1)
par_TSC1_TSC2_pT1462_dephos	147.239 (min^-1)
par_mTORC1_pS2448_dephos_by_TSC1_TSC2	0.00869774 (min^-1)
par_mTORC1_S2448_activation_by_Amino_Acids	0.0156992 (min^-1)
par_mTORC2_pS2481_dephos	1.42511 (min^-1)
par_mTORC2_S2481_phos_by_PI3K_variant_p	0.120736 (min^-1)
par_p70_S6K_T229_phos_by_PI3K_p_PDK1_first	0.0133521 (min^-1)
par_p70_S6K_T229_phos_by_PI3K_p_PDK1_second	1.00E-06
par_p70_S6K_T389_phos_by_mTORC1_pS2448_first	0.00261 (min^-1)

par_p70_S6K_T389_phos_by_mTORC1_pS2448_second	0.11072089 (min^-1)
par_p70_S6K_pT229_dephos_first	1.00E-06
par_p70_S6K_pT229_dephos_second	0.159201353 (min^-1)
par_p70_S6K_pT389_dephos_first	1.10036056 (min^-1)
par_p70_S6K_pT389_dephos_second	1.1021526 (min^-1)
par_PRAS40_S183_phos_by_mTORC1_pS2448_first	0.15881 (min^-1)
par_PRAS40_S183_phos_by_mTORC1_pS2448_second	0.0683009 (min^-1)
par_PRAS40_T246_phos_by_Akt_pT308_first	0.279344 (min^-1)
par_PRAS40_T246_phos_by_Akt_pT308_second	0.279401 (min^-1)
par_PRAS40_pS183_dephos_first	1.8706 (min^-1)
par_PRAS40_pS183_dephos_second	1.88453 (min^-1)
par_PRAS40_pT246_dephos_first	11.8759 (min^-1)
par_PRAS40_pT246_dephos_second	11.876 (min^-1)
par_PI3K_p_PDK1_dephos	0.18913343 (min^-1)
par_PI3K_PDK1_phos_by_IRS_p	0.0001872267 (min^-1)
par_PI3K_variant_p_dephos	0.108074886 (min^-1)
par_PI3K_variant_phos_by_IR_beta_pY1146	0.000549027801(min^-1)
par_scale_IR_beta_pY1146_obs	1
par_scale_IRS_pS636_obs	1
par_scale_AMPK_pT172_obs	1

par_scale_Akt_pT308_obs	1
par_scale_Akt_pS473_obs	1
par_scale_TSC1_TSC2_pS1387_obs	1
par_scale_mTOR_pS2448_obs	1
par_scale_mTOR_pS2481_obs	1
par_scale_p70_S6K_pT229_obs	1
par_scale_p70_S6K_pT389_obs	1
par_scale_PRAS40_pT246_obs	1
par_scale_PRAS40_pS183_obs	1
kUKAP	0.000163
ksirt	5*2.0e7 1/s
kAKT	0.5 (min^-1)
kAMPK	0.5 (min^-1)
kSIRTFOXO	0.1 (min^-1)
AVG_CBP	0.1 mM
Vopgc	0.000046(mM)
Vspgc	0.000142 (mM)
kAPGC	0.007578 (mM)
Vdpgc	0.000388 (mM)
kdpgc	0.003299 (mM)
kdn	0.0012 (min^-1)
k10	0.000166 ((nM*min)^-1)
kULKd	0.00169 ((nM*min)^-1)
KULKM	0.000158 ((nM*min)^-1)
argeninie vmax	0.5470 mmol.min^-1
mTORC1_L_vmax	1.5 mol.min^-1.
leucine_a	100
Km_NamPRT	0.005 mM
Kcat_NamPRT	0.462 (min^-1)

ETNMNAT	10
Initial_for_cell_devision_all	2.80E-05
NAPRT_E_T	10
NAPRT_turnover	3.3
NAPRT_scaling	0.001
NAPRT_Km	0.00015 mM
NMNAT1_NMN_scaling	0.001
NMNAT1_NMN_kcat_A	32281 (min^-1)
NMNAT1_NMN_Km_A	0.0223 mM
NMNAT1_NMN_kcat_PA	77401 (min^-1)
NMNAT1_NMN_Km_PA	0.059 mM
NMNAT1_NMN_Km_B	0.0677 mM
NMNAT1_NMN_Km_PB	0.502 mM
NMNAT1_NaMN_scaling	0.001
NMNAT1_NaMN_kcat_A	25741 (min^-1)
NMNAT1_NaMN_Km_A	0.0677 mM
NMNAT1_NaMN_kcat_PA	62281 (min^-1)
NMNAT1_NaMN_Km_PA	0.502 mM
NMNAT1_NaMN_Km_B	22.3 mM
NMNAT1_NaMN_Km_PB	0.059 mM

NADS_E_T	10
NADS_turnover	21
NADS_scaling	0.001
NADS_Km	0.19 mM
NT5_NMN_ET	10
NT5_NMN_scaling	0.001
NT5_NMN_kcat	301 (min^-1)
NT5_NMN_Km	5 mM
PNP_NR_E_T	10
PNP_NR_turnover	40
PNP_NR_scaling	0.001
PNP_NR_Km	1.48 mM
NNMT_ET	10
NNMT_scaling	0.001
NNMT_Kcat	4861 (min^-1)
NNMT_Ki	0.06 mM
Kma	0.0018 mM
Kmb	0.4 mM
NT5_NaMN_ET	10
NT5_NaMN_scaling	0.001
NT5_NaMN_kcat	1681 (min^-1)

NT5_NaMN_Km	3.5 mM
SIRT_ET	10
SIRT_scaling	0.001
SIRT_Kcat	40.21 (min^-1)
SIRT_Km	0.029 mM
SIRT_Ki	0.06 mM
NAD_consumption_without_Nam_inhibition_ET	10
NAD_consumption_without_Nam_inhibition_scaling	0.001
NAD_consumption_without_Nam_inhibition_kcat	1 (min^-1)
NAD_consumption_without_Nam_inhibition_Km	1 mM
NADA_ET	0
NADA_scaling	0.001
NADA_Kcat	41.4 (min^-1)
NADA_Km	0.009 mM
NADA_Ki	0.1 mM
NAMPT_ET	400
NAMPT_scaling	0.001
NAMPT_Ki	0.0021 mM
NAD_binding_k1	6000 (min^-1)
NAD_binding_k2	600 (min^-1)
NRK1_NaMN_ET	10
NRK1_NaMN_scaling	0.001

NRK1_NaMN_kcat	13.8 (min^-1)
NRK1_NaMN_Km	0.0034 mM
PNP_NAR_E_T	10
PNP_NAR_turnover	40
PNP_NAR_scaling	0.001
PNP_NAR_Km	1.48 mM
NRK1_NMN_ET	10
NRK1_NMN_scaling	0.001
NRK1_NMN_kcat	13.8 (min^-1)
NRK1_NMN_Km	0.0034 mM
v	0.00001 mM/s
Cytosol	1 L
NamPT_compartment	0.001 L
celldivision_rate_NamPT_compartment	0.0017 mM/min
Gln	1 mM
DNA_damage	1 mM
DNA_ADPR	1 mM
H3_ac	1 mM
H3_deac	1 mM
Glu	1 mM
Pi	1 mM
methyl_NAM	0.01 mM
H2O	1 mM
PPi	0.012 mM
AMP	1 mM
ADP	1 mM

SAM	0.08 mM
SAH	1 mM
PRPP	1 mM
ATP	1 mM
scaling factor_AA	100

A.2 Model equations and parameters for circadian clock model

Below is a complete list of equations used in the metabolic signaling pathway model described in Chapter 4. Model parameters are given in Table A2.

$$\frac{d[\text{per}]}{dt} = -\boldsymbol{dm\_per} * [\boldsymbol{per}] + \left(\frac{\boldsymbol{Vmax\_per} * \left(1 + \boldsymbol{fold\_per} * \left(\frac{[\boldsymbol{CB}]}{\boldsymbol{Ka\_per\_cb} * (1 + \boldsymbol{Act\_SIRT})}\right)^{\boldsymbol{hill\_per\_cb}}\right)}{1 + \left(\frac{[\boldsymbol{CB}]}{\boldsymbol{Ka\_per\_cb} * (1 + \boldsymbol{Act\_SIRT})}\right)^{\boldsymbol{hill\_per\_cb}} * \left(1 + \left(\frac{[\boldsymbol{PC}]}{\boldsymbol{Ki\_per\_pc}}\right)^{\boldsymbol{hill\_per\_pc}}\right)} \right)$$

$$\frac{d[\text{cry}]}{dt} = -\boldsymbol{dm\_cry} * [\text{cry}] + \left(\frac{\boldsymbol{Vmax\_cry} * \left(1 + \boldsymbol{fold\_cry} * \left(\frac{[\text{CB}]}{\boldsymbol{Ka\_cry\_cb} * (1 + \text{Act\_SIRT})}\right)^{\boldsymbol{hill\_cry\_cb}}\right)}{1 + \left(\frac{[\text{CB}]}{\boldsymbol{Ka\_cry\_cb} * (1 + \text{Act\_SIRT})}\right)^{\boldsymbol{hill\_cry\_cb}} * \left(1 + \left(\frac{[\text{PC}]}{\boldsymbol{Ki\_cry\_pc}}\right)^{\boldsymbol{hill\_cry\_pc}}\right)} * \frac{1}{1 + \left(\frac{[\text{Prot\_rev}]}{\boldsymbol{Ki\_cry\_rev}}\right)^{\boldsymbol{hill\_cry\_rev}}} \right)$$

$$\frac{d[\text{rev}]}{dt} = -\boldsymbol{dm\_rev} * [\text{rev}] + \left(\frac{\boldsymbol{Vmax\_rev} * \left(1 + \boldsymbol{fold\_rev} * \left(\frac{[\text{CB}]}{\boldsymbol{Ka\_rev\_cb} * (1 + \text{Act\_SIRT})}\right)^{\boldsymbol{hill\_rev\_cb}}\right)}{1 + \left(\frac{[\text{CB}]}{\boldsymbol{Ka\_rev\_cb} * (1 + \text{Act\_SIRT})}\right)^{\boldsymbol{hill\_rev\_cb}} * \left(1 + \left(\frac{[\text{PC}]}{\boldsymbol{Ki\_rev\_pc}}\right)^{\boldsymbol{hill\_rev\_pc}}\right)} \right)$$

$$\frac{d[\text{ror}]}{dt} = -\boldsymbol{dm\_ror} * [\text{ror}] + \left(\frac{\boldsymbol{Vmax\_ror} * \left(1 + \boldsymbol{fold\_ror} * \left(\frac{[\text{CB}]}{\boldsymbol{Ka\_ror\_cb} * (1 + \text{Act\_SIRT})}\right)^{\boldsymbol{hill\_ror\_pc}}\right)}{1 + \left(\frac{[\text{CB}]}{\boldsymbol{Ka\_ror\_pc} * (1 + \text{Act\_SIRT})}\right)^{\boldsymbol{hill\_ror\_cb}} * \left(1 + \left(\frac{[\text{PC}]}{\boldsymbol{Ki\_ror\_pc}}\right)^{\boldsymbol{hill\_ror\_pc}}\right)} \right)$$

$$\frac{d[\text{bmal}]}{dt} = -\boldsymbol{dm\_bmal} * [\text{bmal}] + \left(\frac{\boldsymbol{Vmax\_bmal} * \left(\mathbf{1} + \boldsymbol{fold\_bmal} * (\mathbf{1} + \text{Act\_PGC1a}) * \left(\frac{[\text{Prot\_ror}]}{\boldsymbol{Ka\_bmal\_ror}} \right)^{\boldsymbol{hill\_bmal\_ror}} \right)}{\mathbf{1} + \left(\frac{[\text{Prot\_rev}]}{\boldsymbol{Ki\_bmal\_rev}} \right)^{\boldsymbol{hill\_bmal\_rev}} + \left(\frac{[\text{Prot\_ror}]}{\boldsymbol{Ka\_bmal\_ror}} \right)^{\boldsymbol{hill\_bmal\_ror}}} \right)$$

$$\frac{d[\text{Prot\_per}]}{dt} = -\boldsymbol{dp\_per} * (\mathbf{1} + \boldsymbol{m\_per\_sirt} * \text{Act\_SIRT} + \boldsymbol{m\_per\_ampk} * \text{Act\_AMPK}) * [\text{Prot\_per}] + \boldsymbol{kp\_per} * [\text{per}] - (\boldsymbol{kass\_pc} * [\text{Prot\_cry}] * [\text{Prot\_per}] - \boldsymbol{kdiss\_pc} * [\text{PC}])$$

$$\frac{d[\text{Prot\_cry}]}{dt} = -\boldsymbol{dp\_cry} * (\mathbf{1} + \boldsymbol{m\_cry\_ampk} * \boldsymbol{Act\_AMPK}) * [\text{Prot\_cry}] + \boldsymbol{kp\_per} * [\text{cry}] - (\boldsymbol{kass\_pc} * [\text{Prot\_cry}] * [\text{Prot\_per}] - \boldsymbol{kdiss\_pc} * [\boldsymbol{PC}])$$

$$\frac{d[\text{Prot\_rev}]}{dt} = -\boldsymbol{dp\_rev} * [\text{Prot\_rev}] + \boldsymbol{kp\_rev} * [\text{rev}]$$

$$\frac{d[\text{Prot\_ror}]}{dt} = -\boldsymbol{dp\_ror} * [\text{Prot\_ror}] + \boldsymbol{kp\_ror} * [\text{ror}]$$

$$\frac{d[\text{Prot\_bmal}]}{dt} = -\boldsymbol{dp\_bmal}[\text{Prot\_bmal}] + \boldsymbol{kp\_bmal} * [\text{bmal}] - (\boldsymbol{kass\_cb} * [\text{Prot\_bmal}] - \boldsymbol{kdiss_{cb}} * [\text{CB}]) + (\boldsymbol{par\_mTORC1\_bmal} * [\boldsymbol{Prot\_bmal}] * [\boldsymbol{mTORC1}])$$

$$\frac{d[\text{PC}]}{dt} = +(\boldsymbol{kass\_pc} * [\text{Prot\_cry}] * [\text{Prot\_per}] - \boldsymbol{kdiss\_pc} * [\text{PC}]) - \boldsymbol{dp\_pc} * [\text{PC}]$$

$$\frac{d[\text{CB}]}{dt} = +(\boldsymbol{kass\_cb} * [\text{Prot\_bmal}] - \boldsymbol{kdiss\_cb} * [\text{CB}]) - \boldsymbol{dp\_cb} * [\text{CB}] - (\boldsymbol{par\_mTORC1\_cb} * [\boldsymbol{CB}] * [\boldsymbol{mTORC1}])$$

$$\frac{d[\text{nampt}]}{dt} = -\boldsymbol{dm\_nampt} * [\text{nampt}] + \left(\frac{\boldsymbol{Vmax\_nampt} * \left(\mathbf{1} + \boldsymbol{fold\_nampt} * \left(\frac{[\text{CB}]}{\boldsymbol{Ka\_nampt\_cb} * (\mathbf{1} + \text{Act\_SIRT})} \right)^{\boldsymbol{hill\_nampt\_cb}} \right)}{\mathbf{1} + \left(\frac{[\text{CB}]}{\boldsymbol{Ka\_nampt\_cb} * (\mathbf{1} + \text{Act\_SIRT})} \right)^{\boldsymbol{hill\_nampt\_cb}} * \left(\mathbf{1} + \left(\frac{[\text{PC}]}{\boldsymbol{Ki\_nampt\_pc}} \right)^{\boldsymbol{hill\_nampt\_pc}} \right)} \right)$$

$$\frac{d[\text{Prot\_nampt}]}{dt} = -\frac{\boldsymbol{dp\_nampt} * [\text{Prot\_nampt}]}{\mathbf{1} + \boldsymbol{m\_nampt\_ampk} * \text{Act\_AMPK}} + \boldsymbol{kp\_nampt} * [\text{nampt}]$$

$$\frac{d[\text{NAD}]}{dt} = -\left(\frac{\boldsymbol{d\_nad} * ([\text{NAD}] - \boldsymbol{NAD\_basal})}{\boldsymbol{Knad} + [\text{NAD}] - \boldsymbol{NAD\_basal}}\right) + \left(\frac{\boldsymbol{Vmax\_nad} * [\text{Prot\_nampt}] * ([\text{NAD}] - \boldsymbol{NAD\_basal})}{\boldsymbol{Knam} + \boldsymbol{NAD\_tot} - [\text{NAD}]}\right)$$

$$\frac{d[\text{dbp}]}{dt} = -\boldsymbol{dm\_dbp} * [\boldsymbol{dbp}] + \left(\frac{\boldsymbol{Vmax\_dbp} * \left(\mathbf{1} + \boldsymbol{fold\_dbp} * \left(\frac{[\text{CB}]}{\boldsymbol{Ka\_dbp\_cb} * (\mathbf{1} + \text{Act\_SIRT})}\right)^{\boldsymbol{hill\_dbp\_cb}}\right)}{\mathbf{1} + \left(\frac{[\text{CB}]}{\boldsymbol{Ka\_dbp\_cb} * (\mathbf{1} + \text{Act\_SIRT})}\right)^{\boldsymbol{hill\_dbp\_cb}} * \left(\mathbf{1} + \left(\frac{[\text{PC}]}{\boldsymbol{Ki\_dbp\_pc}}\right)^{\boldsymbol{hill\_dbp\_pc}}\right)}\right)$$

$$\textbf{Act\_SIRT} = \frac{\boldsymbol{Csirt} * \boldsymbol{Vsirt} * [\text{NAD}]}{\boldsymbol{Ksirt} + [\text{NAD}]}$$

$$\textbf{Act\_PGC1a} = \frac{\boldsymbol{Cpgc1} * \boldsymbol{Vpg} * \text{Act\_AMPK} * \text{Act\_SIRT} * \text{Prot\_TGC1a}}{\mathbf{1} + \frac{\text{Act\_AMPK}}{\boldsymbol{Kpg1}} * \left(\mathbf{1} + \frac{\text{Act\_SIRT}}{\boldsymbol{Kpg2}}\right)}$$

Table A2. Parameter values for the metabolic circadian clock model described in Chapter 4, and used in the above model equations.

Symbol	Description	Value
par_bmal_mTORC1	Inhibitory effect of BMAL1 on mTORC1	0.0118
par_per_mTORC1	Inhibitory effect of PER2 on mTORC1	0.0104
par_mTORC1_bmal	Activating effect of mTORC1 on BMAL1	0.0104
par_mTORC1_cb	Inhibitory effect of mTORC1 on CLOCK-BMAL1	0.0261
kp_bmal	Translation rate constant from Bmal1 mRNA to BMAL1 protein	0.5405
dp_bmal	Degradation rate of BMAL1 protein	0.2252
$kass\_cb$	Association rate constant of CLOCK-BMAL! complex	0.0151
$kdiss\_cb$	Disassociation rate constant of CLOCK-BMAL! complex	0.0066
d_cb	Degradation rate of CLOCK-BMAL1	0.0849
kp_per	Translation rate constant from Per2 mRNA to PER2 protein	3.9968
dp_per	Degradation rate of PER2 protein	56.1535
dm_per	Degradation rate of Per2 mRNA	0.3005
$Vmax\_per$	Generation rate constant of Per1 mRNA	0.8032
kp_cry	Translation rate constant from Cry1 mRNA to CRY1 protein	14.0871

dp_cry	Degradation rate of CRY1 protein	0.6536
$kass\_pc$	Association rate constant of PER-CRY complex	13.2884
$kdiss\_pc$	disassociation rate constant of PER-CRY complex	0.0261
kp_rev	Translation rate constant from Rev-Erb mRNA to REV-ERB protein	0.0641
kp_ror	Translation rate constant from Ror mRNA to ROR protein	0.3677